



# GRAĐEVINSKI MATERIJALI I KONSTRUKCIJE

# BUILDING MATERIALS AND STRUCTURES

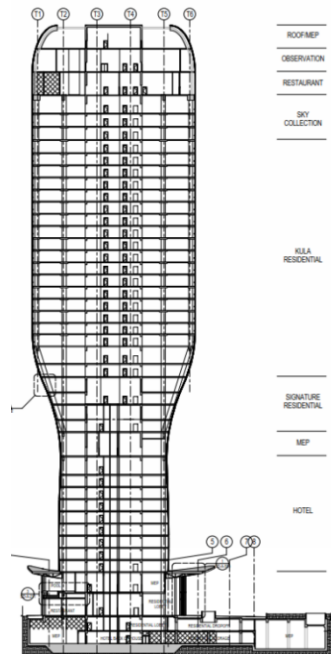
Volume 64  
August 2021  
ISSN 2217-8139 (Print)  
ISSN 2335-0229 (Online)  
UDK: 06.055.2:62-  
03+620.1+624.001.5(49  
7.1)=861

# 4

---

Society for Materials and Structures Testing of Serbia  
University of Belgrade Faculty of Civil Engineering  
Association of Structural Engineers of Serbia

---



**CONTENTS**

T. Isaković , M. Gams, A. Janevski, Z. Rakićević, A. Bogdanović, G. Jekić, K. Kolozvari, J. Wallace, M. Fischinger <b>Shake table test of RC walls' coupling provided by slabs</b> <b>Original scientific paper</b> .....	225
Jelena Dobrić, Nina Gluhović, Zlatko Marković, Dragan Buđevac <b>Stability design criteria for closely spaced built-up stainless steel columns</b> <b>Original scientific paper</b> .....	235
Sangeetha Palanivelu, Dhinakaran Moorthy, Gobinaath Subramani, Jeevan Raj Dhayanithi <b>Strength enhancement of cold-formed steel tubular column using GFRP strip subjected to axial compression</b> <b>Preliminary report</b> .....	251
Bojidar Yanev <b>Supply and Demand in Engineering and Management</b> <b>Original scientific paper</b> .....	261
Nemanja Miljković, Mladen Milićević, Svetlana Ristić, Darko Popović, Vanja Alendar <b>Kula Belgrade – Part 1 - Specific topics of structural design</b> <b>Technical paper</b> .....	269
Instructions for authors .....	283

**EDITORIAL BOARD**

**Editor-in-Chief**

Professor **Snežana Marinković**  
University of Belgrade, Faculty of Civil Engineering, Institute  
for Materials and Structures, Belgrade, Serbia  
e-mail: [sneska@imk.grf.bg.ac.rs](mailto:sneska@imk.grf.bg.ac.rs)

**Deputy Editor-in-Chief**

Professor **Mirjana Malešev**  
University of Novi Sad, Faculty of Technical Sciences,  
Department of Civil Engineering, Novi Sad, Serbia  
e-mail: [miram@uns.ac.rs](mailto:miram@uns.ac.rs)

**Members**

Professor **Jose M. Adam**  
ICITECH, Universitat Politècnica de Valencia, Valencia,  
Spain

Dr **Ksenija Janković**  
Institute for Testing Materials – Institute IMS, Belgrade,  
Serbia

Professor Emerita **Dubravka Bjegović**  
University of Zagreb, Faculty of Civil Engineering,  
Department of materials, Zagreb, Croatia

Professor Academician **Yatchko P. Ivanov**  
Bulgarian Academy of Sciences, Institute of Mechanics,  
Sofia, Bulgaria

Professor **Tatjana Isaković**  
University of Ljubljana, Faculty of Civil and Geodetic  
Engineering, Ljubljana, Slovenia

Professor **Michael Forde**  
University of Edinburgh, Institute for Infrastructure and  
Environment, School of Engineering, Edinburgh, United  
Kingdom

Professor **Vlastimir Radonjanin**  
University of Novi Sad, Faculty of Technical Sciences,  
Department of Civil Engineering, Novi Sad, Serbia

**Predrag L. Popovic**  
Vice President, Wiss, Janney, Elstner Associates, Inc.,  
Northbrook, Illinois, USA

Professor **Zlatko Marković**  
University of Belgrade, Faculty of Civil Engineering,  
Institute for Materials and Structures, Belgrade, Serbia

Professor **Vladan Kuzmanović**  
University of Belgrade, Faculty of Civil Engineering,  
Belgrade, Serbia

Professor Emeritus **Valeriu A. Stoian**  
University Politehnica of Timisoara, Department of Civil  
Engineering, Research Center for Construction  
Rehabilitation, Timisoara, Romania

Secretary:

**Slavica Živković**, Master of Economics  
Society for Materials and Structures Testing of Serbia, 11000 Belgrade, Kneza Milosa 9  
Telephone: 381 11/3242-589; e-mail: [office@dimk.rs](mailto:office@dimk.rs), web sajt: [www.dimk.rs](http://www.dimk.rs)

English editing:

Professor **Jelisaveta Šafranč**, University of Novi Sad, Faculty of Technical Sciences, Novi Sad, Serbia

Technical support:

**Stoja Todorović**, e-mail: [saska@imk.grf.bg.ac.rs](mailto:saska@imk.grf.bg.ac.rs)

Dr **Vilma Ducman**  
Head of Laboratory for Cements, Mortars and  
Ceramics, Slovenian National Building and Civil  
Engineering Institute, Ljubljana, Slovenia

Assistant Professor **Ildiko Merta**  
TU Wien, Faculty of Civil Engineering, Institute of  
Material Technology, Building Physics, and Building  
Ecology, Vienna, Austria

Associate Professor **Ivan Ignjatović**  
University of Belgrade, Faculty of Civil Engineering,  
Institute for Materials and Structures, Belgrade, Serbia

Professor **Meri Cvetkovska**  
University "St. Kiril and Metodij", Faculty of Civil  
Engineering, Skopje, Macedonia

Dr **Anamaria Feier**  
University Politehnica of Timisoara, Department for  
Materials and Manufacturing Engineering, Timisoara,  
Romania

Associate Professor **Jelena Dobrić**  
University of Belgrade, Faculty of Civil Engineering,  
Institute for Materials and Structures, Belgrade, Serbia

Dr **Vladimir Gocevski**  
Hydro-Quebec, Mécanique, structures et architecture,  
Ingénierie de production, Montréal (Québec), Canada

Dr **Nikola Tošić**  
MSCA Individual Fellow, Civil and Environmental  
Engineering Department, Universitat Politècnica de  
Catalunya (UPC), Barcelona, Spain

Assistant Professor **Ehsan Noroozinejad Farsangi**  
Earthquake Engineering Department, Graduate  
University of Advanced Technology, Iran

## Aims and scope

Building Materials and Structures aims at providing an international forum for communication and dissemination of innovative research and application in the field of building materials and structures. Journal publishes papers on the characterization of building materials properties, their technologies and modeling. In the area of structural engineering Journal publishes papers dealing with new developments in application of structural mechanics principles and digital technologies for the analysis and design of structures, as well as on the application and skillful use of novel building materials and technologies.

The scope of Building Materials and Structures encompasses, but is not restricted to, the following areas: conventional and non-conventional building materials, recycled materials, smart materials such as nanomaterials and bio-inspired materials, infrastructure engineering, earthquake engineering, wind engineering, fire engineering, blast engineering, structural reliability and integrity, life cycle assessment, structural optimization, structural health monitoring, digital design methods, data-driven analysis methods, experimental methods, performance-based design, innovative construction technologies, and value engineering.

<b>Publishers</b>	Society for Materials and Structures Testing of Serbia, Belgrade, Serbia, veb sajt: <a href="http://www.dimk.rs">www.dimk.rs</a> University of Belgrade Faculty of Civil Engineering, Belgrade, Serbia, <a href="http://www.grf.bg.ac.rs">www.grf.bg.ac.rs</a> Association of Structural Engineers of Serbia, Belgrade, Serbia, <a href="http://dgks.grf.bg.ac.rs">dgks.grf.bg.ac.rs</a>
<b>Print</b>	Razvojno istraživački centar grafičkog inženjerstva, Belgrade, Serbia
<b>Edition</b>	quarterly
<b>Peer reviewed journal</b>	
<b>Journal homepage</b>	<a href="http://www.dimk.rs">www.dimk.rs</a>
<b>Cover</b>	<b>Kula Belgrade– render (left), vertical section (middle), progress of works in Oct 2021 (right), from <i>Kula Belgrade – Part 1 - Specific topics of structural design</i> by Nemanja Miljković, Mladen Milićević, Svetlana Ristić, Darko Popović, Vanja Alendar</b>
<b>Financial support</b>	Ministry of Education, Science and Technological Development of Republic of Serbia University of Belgrade Faculty of Civil Engineering Institute for testing of materials-IMS Institute, Belgrade Faculty of Technical Sciences, University of Novi Sad, Department of Civil Engineering Serbian Chamber of Engineers

CIP - Каталогизacija u publikaciji  
Narodna biblioteka Srbije, Beograd

620.1

**GRAĐEVINSKI materijali i konstrukcije** = Building materials and structures / editor-in-chief Snežana Marinković  
. - God. 54, br. 3 (2011)- . - Belgrade : Society for Materials and Structures Testing of Serbia : University of Belgrade, Faculty of Civil Engineering : Association of Structural Engineers of Serbia, 2011- (Belgrade : Razvojno istraživački centar grafičkog inženjerstva). - 30 cm

Tromesečno. - Je nastavak: Materijali i konstrukcije  
= ISSN 0543-0798. - Drugo izdanje na drugom medijumu:  
Građevinski materijali i konstrukcije (Online) = ISSN 2335-0229  
ISSN 2217-8139 = Građevinski materijali i konstrukcije  
COBISS.SR-ID 188695820



## Shake table test of RC walls' coupling provided by slabs

T. Isaković<sup>\*1)</sup>, M. Gams<sup>1)</sup>, A. Janevski<sup>1)</sup>, Z. Rakićević<sup>2)</sup>, A. Bogdanović<sup>2)</sup>, G. Jekić<sup>2)</sup>, K. Kolozvari<sup>3)</sup>, J. Wallace<sup>4)</sup>, M. Fischinger<sup>1)</sup>

<sup>1)</sup> University of Ljubljana, Faculty of Civil and Geodetic Engineering, Ljubljana, Slovenija

<sup>2)</sup> Institute of Earthquake Engineering and Engineering Seismology IZIS, Skopje, North Macedonia

<sup>3)</sup> California State University, Fullerton, USA

<sup>4)</sup> University of California, Los Angeles, USA

### Article history

Received: 25 October 2021

Received in revised form:

12 November 2021

Accepted: 20 November 2021

Available online: 30 December 2021

### Keywords

RC coupled walls,  
Shake table test,  
Floor-to-piers interaction,  
Large scale experiment

### ABSTRACT

When designed to the seismic load effects, reinforced concrete walls connected by slabs without coupling beams are usually considered cantilever walls. Several recent studies indicated that slabs themselves could provide strong coupling in some cases, and the walls could respond differently from cantilever walls. To study the slab-to-wall piers interaction, a shake table test of the half-scale three-story specimen was conducted within HORIZON 2020 SERA-TA project. The specimen consisted of four rectangular walls linked by three slabs. It was subjected to a series of seismic excitations of increasing intensity. In the last three tests, the nonlinear response of the slabs and wall piers was observed.

At the strong seismic excitations, one pier was subjected to strong tensile, while the adjacent pier was subjected to strong compression forces. The crack pattern of piers was asymmetric and different from the cross-shaped damage pattern, typical for cantilever walls.

The coupling of wall piers provided by slabs was considerably stronger than it was expected. The share of the overturning moment resisted by the frame action induced by the slabs was more than 50%. All slabs were fully activated and significantly damaged. Their damage was primarily flexural. The effective width of slabs was equal to their total width.

## 1 Introduction

During the seismic design of RC walls connected only by slabs (without coupling beams), experienced engineers typically consider them as cantilever walls. The slabs are considered rigid diaphragms. Their bending and shear stiffness are neglected, assuming they are small compared to the wall's stiffness. It is also assumed that the slab's flexural capacity is small compared to the bending capacity of the wall.

Following the previous assumptions, a hinged connection between piers and slabs are considered in the numerical model. The response mechanism of such a model to a horizontal load is shown in Figure 1a. The wall piers having the same properties are subjected to equal bending moments. There are no axial forces in piers due to the horizontal load.

However, in some cases, such a numerical model is not accurate enough, and the assumptions used to formulate it are less acceptable. The stiffness of the slabs is inversely proportional to the third power of the opening's width between piers. The stiffness of the walls is inversely proportional to the third power of the wall height. In some

cases, the opening length is significantly smaller than the height of the walls (e.g. in the prototype of the tested specimen, the opening length is 1 m and the height of the wall is 9 m – see Section 2). Consequently, the ratio of the slab's stiffness and the stiffness of the wall piers is significantly larger than it is typically assumed in the traditional models. Moreover, the bending capacity of the slabs can also be considerably larger than it is generally expected and cannot be neglected. It depends on the effective width of the slabs, which is in some cases significantly larger than that assumed in the traditional design (this will be demonstrated later in the text).

Following the previous observations, it can be concluded that the slabs can provide significantly stronger coupling of wall piers than it is typically expected. When the stronger coupling is provided, the response of the piers and the entire building (see Figure 1b) is significantly different from the response of an assembly of the cantilever walls. Since the bending capacity of slabs is not negligible, the corresponding shear forces induce the additional axial forces to wall piers.

\* Corresponding author:

E-mail address: [tatjana.isakovic@fgg.uni-lj.si](mailto:tatjana.isakovic@fgg.uni-lj.si)

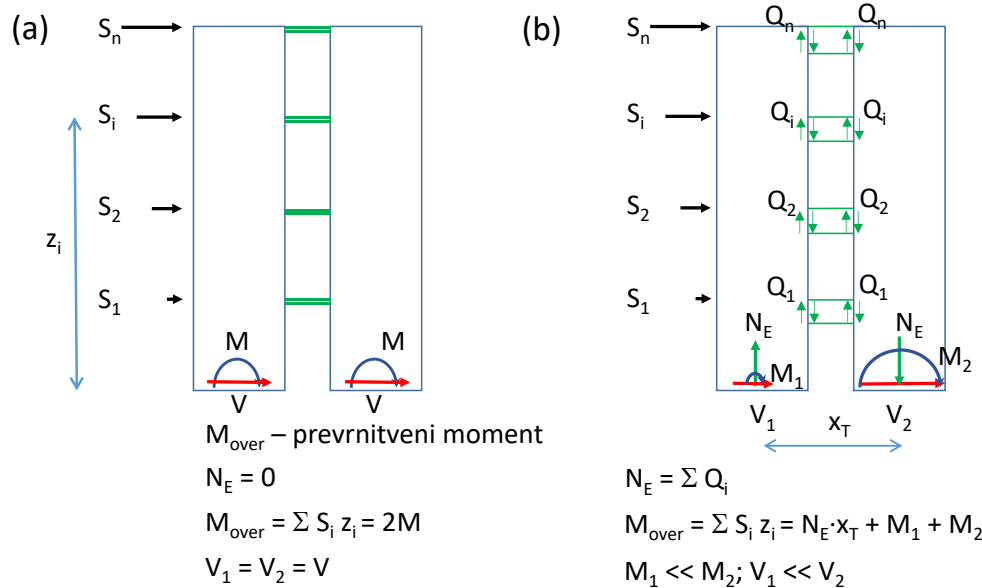


Figure 1. Resisting mechanisms: a) cantilever walls (very weak coupling), b) coupled walls (significant coupling of wall piers)

These forces cause the change of the stiffness as well as the strength of piers. The stiffness and strength of pier subjected to tensile seismic forces can be considerably smaller than the stiffness and the strength of piers subjected to compression. Due to stiffness changes, significant redistributions of demand between piers could occur in the nonlinear range. When these redistributions are disregarded in the design, considerable damage and even failure of piers can occur.

Experiments (e.g. [1], [2], [3]) proved that the forces in piers subjected to compression could be even doubled compared to the results of the elastic analysis. Therefore, even the sophisticated elastic shell numerical models, the use of which is rapidly increasing in practice, cannot be the solution to the problem.

Previous observations were confirmed during the earthquakes in Chile (2010) and New Zealand (2010, 2011) ([4], [5], [6]). The damage was particularly severe in higher buildings, where the buckling and the rupture of the longitudinal boundary reinforcement and the shear damage of piers were observed. One of the reasons for such damage is the inability of elastic models to consider the variable interaction between piers and floors.

Similar conclusions were obtained at UL FGG based on the shake table experiment of a typical European coupled wall (Figure 2). This wall consisted of two non-planar wall piers ("T" shaped piers) connected by five slabs and five diagonally reinforced beams [1]. It was found that due to the interaction between beams and slabs, the bending strength of floors can be considerably larger than expected (determined using standard procedures). Consequently, the wall piers were considerably more coupled than it was predicted. The strong coupling resulted in brittle shear failure of wall piers.

The traditional assumption that the slab alone (without beams) cannot provide considerable coupling of wall piers

has been recently called into question by several experiments and analytical studies (e.g. [7], [8]). In [7] (Figure 3), it was shown that even very thin slabs without beams could provide significant coupling of wall piers. The response of a seven-story rectangular wall was tested. It was connected to the perpendicular stabilizing wall only by slabs to avoid their interaction. To additionally minimize the coupling effect, slabs were slotted at the connection with the walls. They were only 5 cm thick at the slot (see Figure 3b). Considerable shear forces were generated along the whole length of the slots, resulting in the substantial increase of the axial force in the tested wall. The bending moments and shear forces in the wall were also increased due to the induced axial forces.

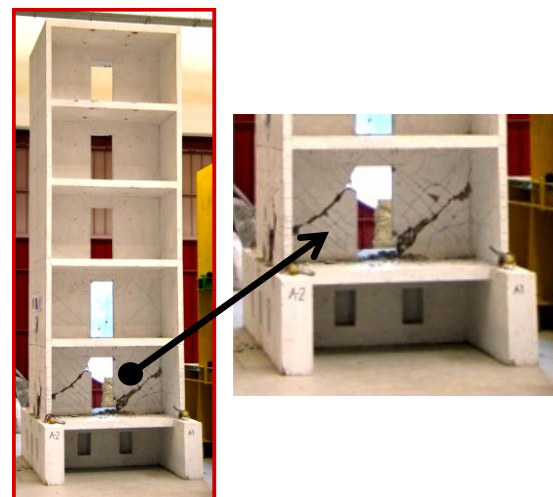


Figure 2. The brittle failure of the non-planar coupled walls tested at the shaking table

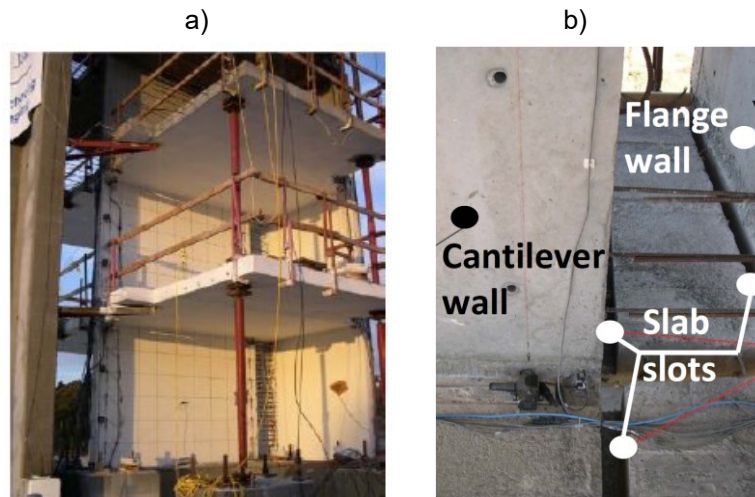


Figure 3. Cantilever RC wall tested at shake table at UCSD:  
 a) the wall and "gravity columns", used to support the slab and provide stability in the direction perpendicular to the wall plane  
 b) the slab slots (courtesy Panagiotou MM et al. [7])

The conclusions of this study demonstrate the essential subject of the research presented in this paper. The assumption that slabs due to the relatively small moment of inertia cannot significantly couple the wall piers and that connections between piers and floors can be represented by hinges with zero bending moments is inadequate for certain wall configurations. In such cases, the connections should be represented by plastic hinges, where the moment capacity depends on the slab's flexural strength. The bending moment corresponding to the flexural strength of the slab can be significant in all cases where the considerable effective width of the slab is activated. The shear forces in the slab corresponding to the flexural strength of the slab induce the variable axial forces in piers and can qualitatively change the response of the wall piers and the entire structure.

## 2 Description of the specimen, excitations and instrumentation

### 2.1 The geometry of the specimen

A shake table experiment of the half-scale three-story specimen consisting of four RC walls connected only by slabs (without any beams) was conducted (see Figures 4 and 5). To get as realistic as possible information about the slabs-to-walls interaction, the maximum possible size of the specimen was selected, considering the limitations of the shake table regarding the overturning moment (about 500 kNm). Scale factors considered in the design of the specimen are summarized in Table 1.

The main goal of the experiment was to obtain information about the varying floor-to-wall interaction at different levels of the response, particularly in the nonlinear range. Thus, the proper balance between the realistic size (strength) of the structural elements and the limitations of the shake table had to be found. The selected height of the walls' cross-section (75 cm) enabled the yielding of the walls when they were subjected to the maximum possible intensity of the seismic load limited by the performances of the shake table. At the same time, this dimension was realistic enough considering the dimensions of walls in practice. The

thickness of the walls (10 cm) was selected considering the typical thickness of structural walls in Slovenian design practice (20 cm). The aspect ratio of the walls' cross-section was 7.5. The aspect ratio of the wall (height of the wall/ height of the cross-section) was 6. The clear distance between walls piers (see Figure 5) was 50 cm, which corresponds to the 100 cm opening in the prototype (e.g. the opening for the doors).



Figure 4. The tested specimen

The size of the slabs (3 m x 3 m) was defined following the typical tributary area for walls in RC wall buildings in Slovenia (6 m x 6 m). The thickness of the specimen's slabs (8 cm) was defined considering the typical thickness of the slab in the prototype buildings (16 cm)

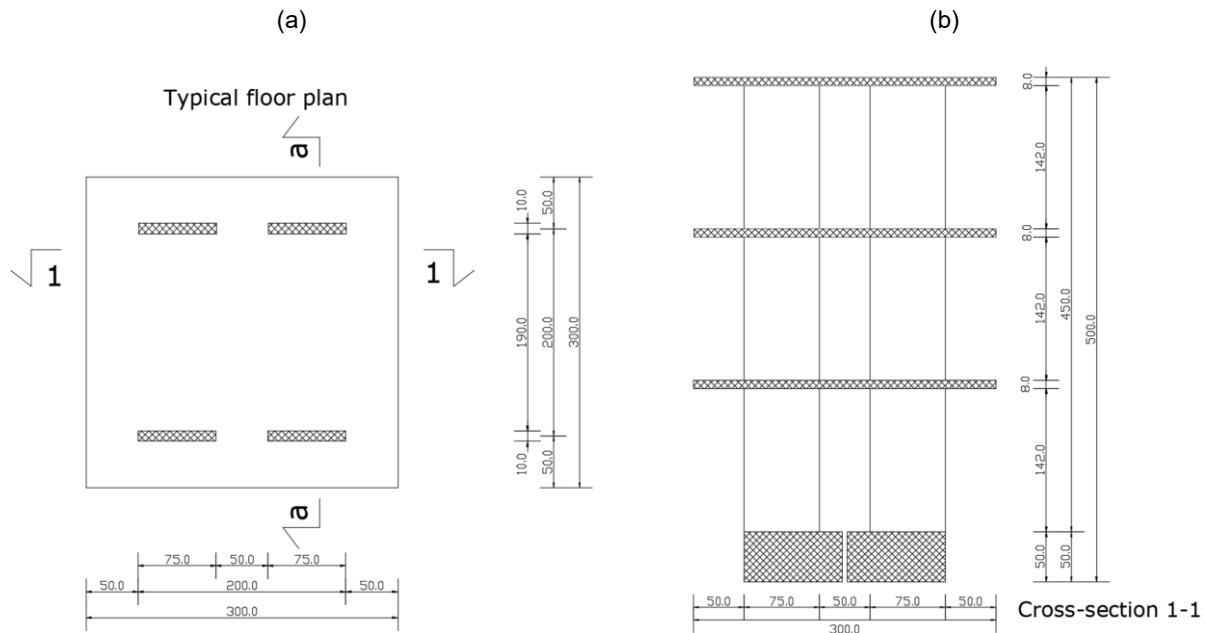


Figure 5. The specimen's dimensions and geometry: (a) floor plan, (b) side view

Table 1. Scale factors

Variable	Scale Factor Prototype/Model	Value of the Scale Factor
Length	$S_L$	2
Area	$S_L^2$	4
Volume	$S_L^3$	8
Moment of inertia	$S_L^4$	16
Mass	$S_M$	10
Stress	$S_\sigma$	1
Strain	$I$	1
Modulus of elasticity	$I$	1
Force	$S_L^2$	4
Moment	$S_L^3$	8
Acceleration	$S_\sigma S_L^2 / S_M$	$1 \cdot 4 / 10 = 0.4$
Time	$\sqrt{S_M / S_L / S_\sigma}$	$\sqrt{(10 / 1 / 2)} = 2.24$

The total mass of the specimen without foundations was 8.2 t. In general, in most of the shake table tests, additional masses are typically provided to obtain the realistic demand. Therefore, steel ingots are often installed at the slabs. In the studied case, this was not an option since the ingots affected the main properties of the floors (strength and stiffness), which made a crucial influence on their interaction with wall piers. Instead of the added masses, the time and the accelerations were properly scaled (see Table 1) to obtain the realistic demand.

## 2.2 Material properties and the reinforcement

The strength of the used concrete was on average 26 MPa and 27.5 MPa for walls and slabs, respectively.

In walls, the minimum flexural (longitudinal) reinforcement was provided. Initially, it was planned to use 12 ribbed bars of diameter 6 mm. Since only the brittle bars of such diameter were available on the market, the walls were finally reinforced by 12 ductile plain bars of diameter 8 mm (see Figure 6a). The yielding and ultimate stress of the corresponding steel was 300 MPa and 420 MPa, respectively. The shear reinforcement  $\phi 6$  mm/7.5 cm was provided over the entire height of the walls.

The slabs were reinforced by two reinforcing meshes Q-131, providing  $1.31 \text{ cm}^2/\text{m}$  for the top and the bottom reinforcing layers (see Figure 6b). The yielding and the ultimate stress of the corresponding steel were 500 MPa and 560 MPa, respectively.

Shake table test of RC walls' coupling provided by slabs

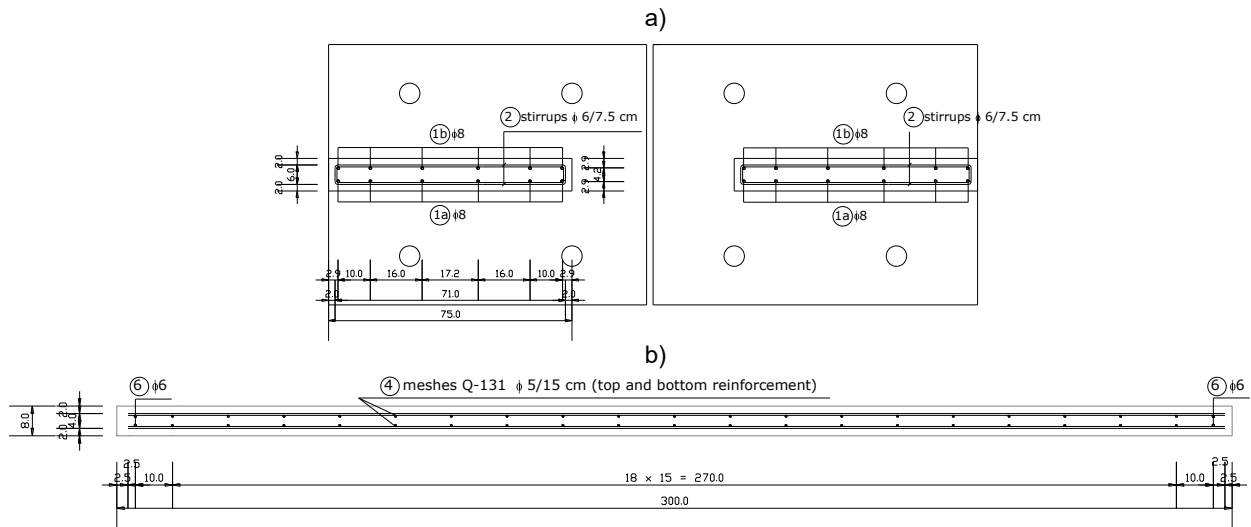


Figure 6. The reinforcement of a) walls and b) slabs

2.3 Seismic excitation

The shake table was excited by an artificial accelerogram (see Figure 7a), which was generated by modifying accelerogram Petrovac N-S, registered during the 1979 Montenegro earthquake. This accelerogram was modified to match the EC8 acceleration spectrum corresponding to soil

site type A and 2% damping. The 2% damping was considered since, in most experiments, viscous damping is typically smaller than in actual buildings due to the lack of different sources of damping (e.g. partition walls, etc.). The target accelerogram and the accelerogram applied during the tests and the corresponding acceleration spectra are presented in Figure 7a and 7b, respectively.

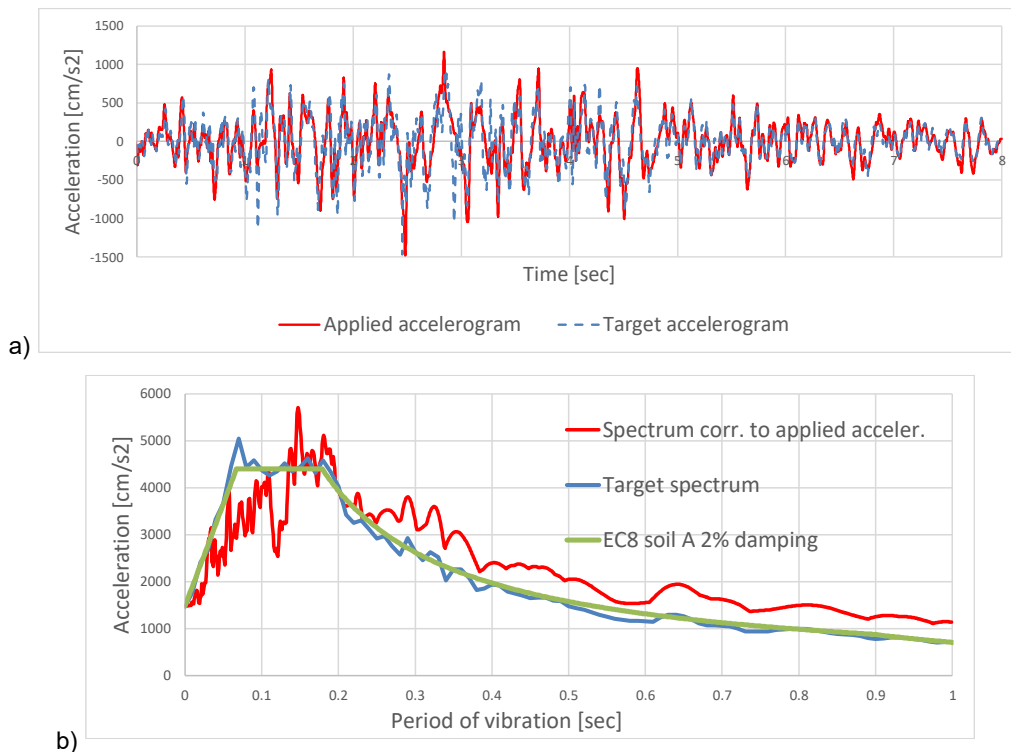


Figure 7. Seismic excitation: a) target and applied accelerogram, b) corresponding acceleration spectra for PGA = 1,5 g (Note: The time and accelerations are scaled considering the scale factors from Table 1).

A series of uniaxial tests were performed, with gradually increasing intensity of the seismic excitation in the direction of walls (N-S – see Figure 8). All runs are summarized in Table 2. The testing was concluded when the displacement capacity of the shake table was exhausted (12 cm). In

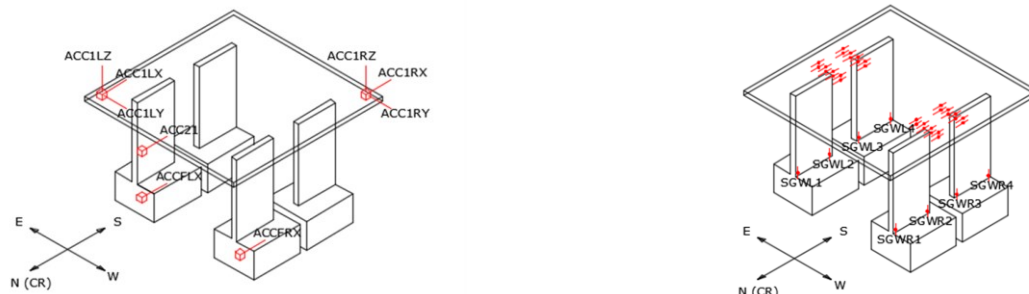
between the tests, the periods/frequencies of the structure were measured. The measured values were 0.14 sec, 0.20 sec, 0.32 sec, and 0.32 sec before the first test R010, after R060(2), after R150(1), and after R150(2), respectively.

Table 2. The list of the performed tests

Test	Maximum acceleration at the shake table	Period of vibration
R010	0.1 g	0.14 s (before the test)
R020	0.2 g	
R030	0.3 g	
R050	0.5 g	
R060(1)	0.6 g	
R060(2)	0.6 g	0.20 s (after the test)
R080	0.8 g	
R090	0.9 g	
R120	1.2 g	
R150(1)	1.5 g	0.32 s (after the test)
R150(2)	1.5 g	0.32 s (after the test)

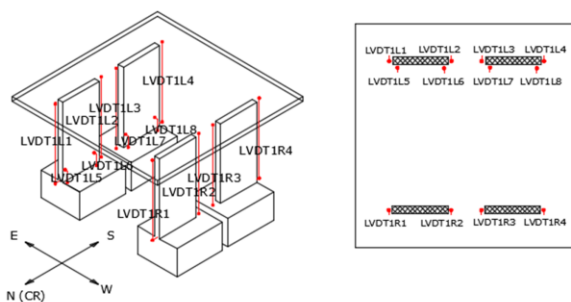
2.4 Instrumentation

The instrumentation is summarized in Figure 8.



a) Accelerometers were installed at all slabs and at the foundation level (only the scheme of the first story is presented)

c) Strain gauges were used to measure deformations in all slabs and at the bottom of walls (only the first story is presented)



b) LVDT'S were used to measure relative vertical displacements (deformations) along all stories and at the bottom of the walls (only the first story is presented)

d) Optical measurements of deformations were performed at outer faces of the bottom story of all walls



Figure 8. An overview of the instrumentation

3 Response of the tested specimen

3.1 Observed response

The response of the tested building was essentially elastic up to the test R120. The first cracks were observed at the bottom of the wall piers and in the 1<sup>st</sup> story slab near the joints with the walls after the test R030. When the seismic intensity was increased, the cracks also appeared in the second and the third slab. The cracks in the slabs were first

limited to the area near the joints with the walls. When the seismic intensity was increased, they were gradually expanded to the whole width of the slabs between the two rows of wall piers (see Figure 9). The cracks were clearly visible at the top and the bottom surfaces of the slabs.

The damage in the wall piers was initiated at the very bottom cross-section near the foundations. Later on, additional cracks were gradually formed up to approximately 100 cm from the foundation level (see Figure 10a). The cracks were initiated at the outer edges of each wall pier.

When the seismic intensity was increased, they extended toward the inner edges (see Figure 10a). The crack pattern was considerably different from the cross-shaped damage pattern, typical for cantilever walls (compare the crack patterns, presented in Figures 10a and 10b).

In test R120, the response of the building entered the nonlinear range. The cracks were spread over the entire width of the slab in between the two rows of the wall piers (see Figure 9). The width of the cracks in the slabs was considerably increased. The yielding of the reinforcement in the slabs was achieved. The effective width of slabs was equal to their total width. The flexural strength of slabs was fully activated, generating considerable axial forces in wall piers (see Figure 1b). The frame action caused by the slabs was considerable (see also the discussion in section 3.3).

The response of two wall piers located at the same side of the specimen was considerably different. This is evident in

Figure 11a, where the two piers' response (obtained with optical measurements) is presented. In the left pier, where the tensile axial force was generated, the considerable cracks were formed approximately up to 1m from the foundation level (see the orange areas surrounded by the red circle, which indicate cracks). In the right wall pier, which was subjected to compression, the damage was located mostly at the bottom of the wall.

In the last two tests (R150(1) and R150(2)), where the nonlinear deformations were noticeable, the differences in the response of two piers were visible to the naked eye. The considerable rocking of the wall subjected to the tension was observed. In the last test, the buckling of the longitudinal reinforcement at the outer edge of one of the piers was observed (see Figure 11b), indicating that this pier was subjected to relatively large compression stresses.

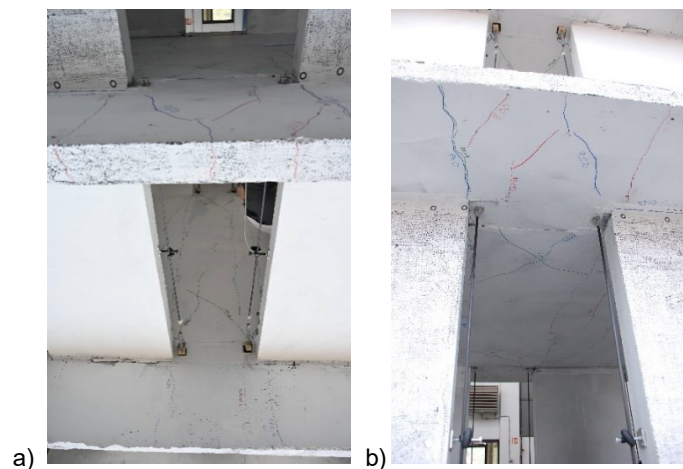


Figure 9. Cracks were formed a) at the top and b) at the bottom surfaces of the slabs, all over their width between two rows of wall piers

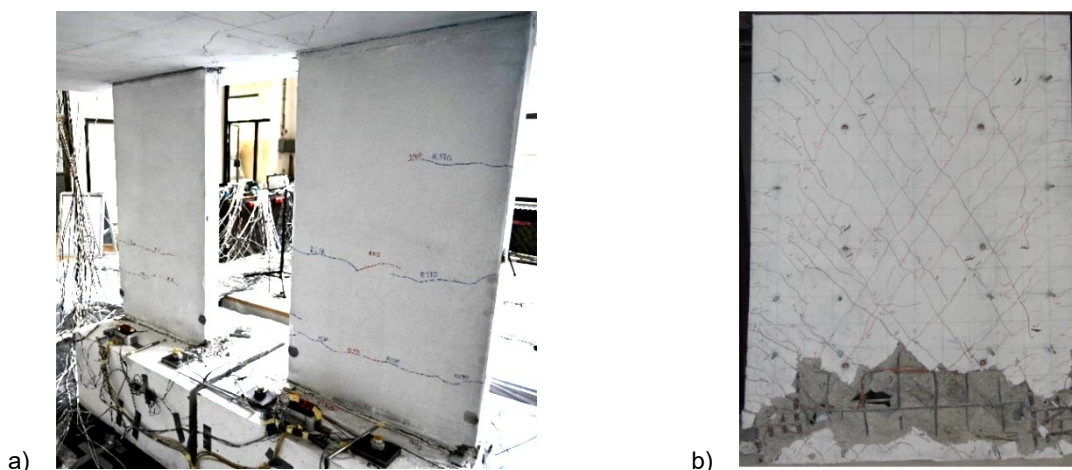


Figure 10. a) Cracks, which were observed in the wall piers,

b) Crack pattern typical for cantilever walls (courtesy of Tran and Wallace [9])

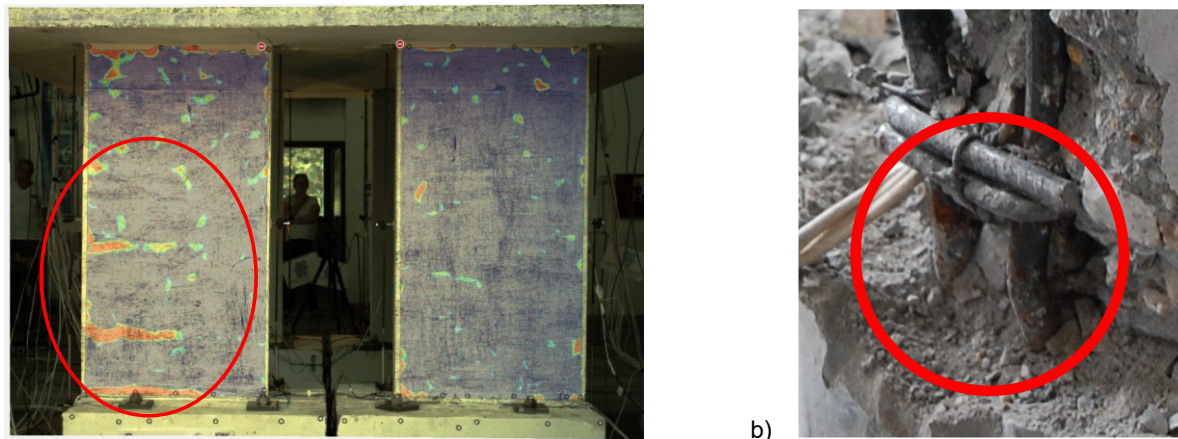


Figure 11. a) Response of two piers was considerably different, b) Buckling of the longitudinal bars was observed in the outer edge of one pier

### 3.2 Global parameters of the response

The envelopes of horizontal story accelerations, the envelopes of horizontal displacements and the envelopes of story drifts in the direction of the seismic excitation (N-S see Figure 8) are presented in Figure 12. The presented accelerations are the average values of the accelerations measured at two stations (see Figure 8a) at each slab. The hysteretic response throughout all tests, expressed in terms of displacements and the base shear, is presented in Figure 13. The base shear is estimated from the measured average story accelerations.

The response of the tested building was essentially elastic up to the test R120. In this test, one peak acceleration of 1.2g was registered at the shaking table. The majority of strong peaks had an intensity of 0.8g. This corresponds to the peak ground acceleration of 0.32g in the prototype structure. Note, however, that the response of structures subjected to different real accelerograms can enter the nonlinear range also at smaller peak ground accelerations. The level of yielding also depends on the geometry of the building. In higher and narrower structures (e.g. concrete cores), yielding can occur at the lower seismic intensities.

This is the topic of ongoing extensive parametric study at UL FGG.

Maximum acceleration of 3.4g was registered at the top of the building at test R150(2). It corresponds to the acceleration excitation of the shake table of 1.5g. Note, however, that seismic excitation of 1.5g was applied only in one single time step (see Figure 7a). Most of the local maximums corresponded to the acceleration excitation of about 1g. This corresponds to an acceleration of 0.4g in the prototype structure (see Table 1).

During the last test, R150(2), the maximum displacement of 53 mm was obtained at the top of the building in both directions (N-S and S-N). This value corresponds to a 1.1% drift. The displacement envelope was almost linear, and the story drifts almost constant in all stories (see Figures 12b and 12c). This is an additional indication that the response was different from that typical for cantilever walls.

The top displacement to base-shear relationship, presented in Figure 13c, confirms the visual observations from the experiment that the structure entered the nonlinear range in the test R120. The gradually decreasing stiffness of the structure (see Figure 13 a-c) is in good agreement with the measured increasing periods of vibrations (see section 2.3).

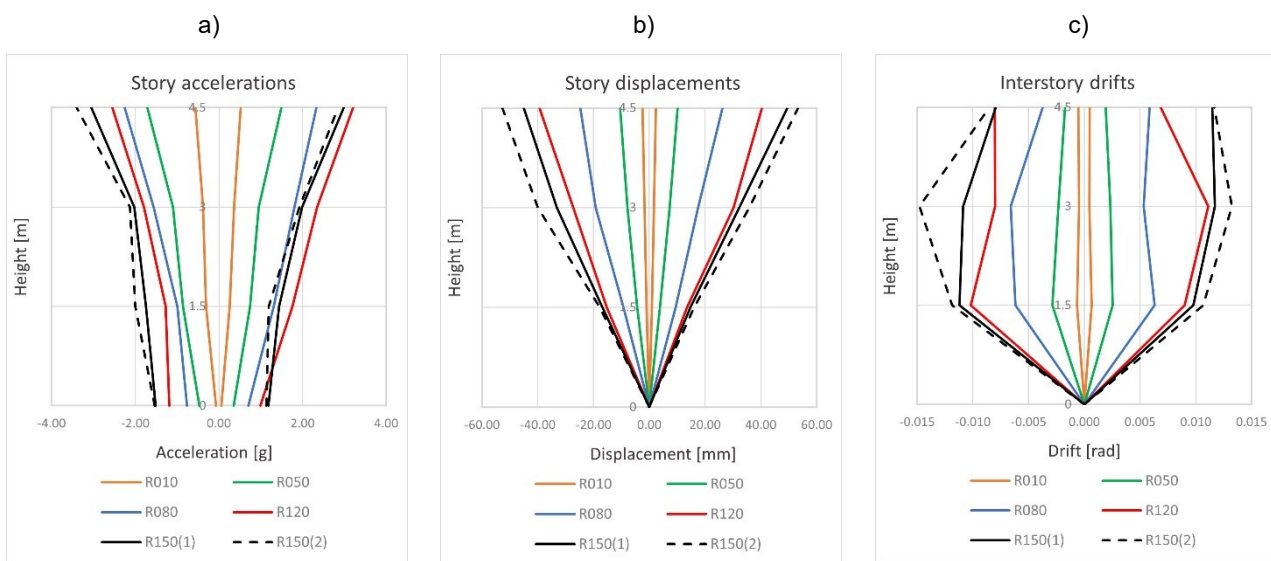


Figure 12. Envelopes of a) horizontal story accelerations, b) horizontal story displacements, c) story drifts in the direction of excitation

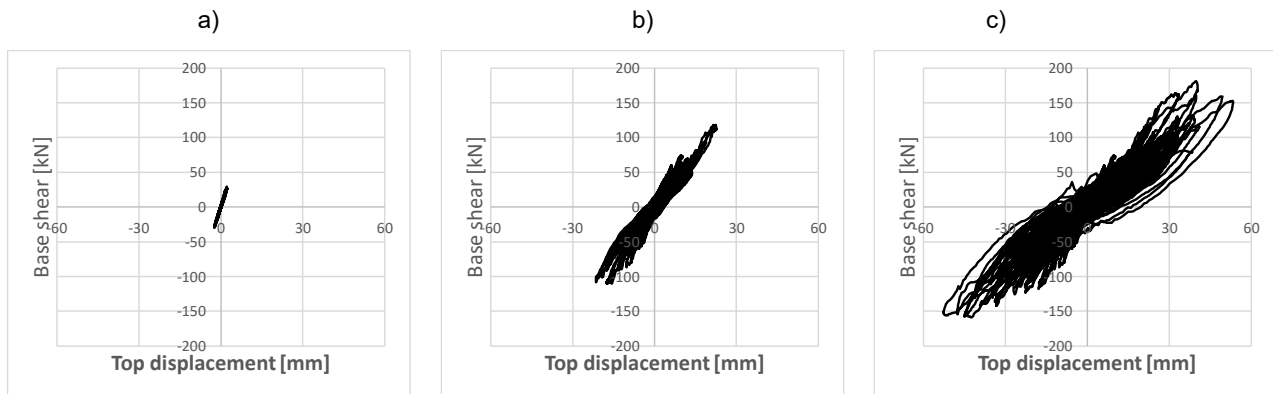


Figure 13. Hysteretic response at three different stages of testing: a) after R010, b) after R060(2), and c) after the last test R150(2)

### 3.3 Estimated level of coupling

The coupling level was estimated considering the ratio of the overturning moment resisted by the flexural response of piers and the shear resisted by the frame action of slabs (moment due to the axial forces in walls resulting from the accumulated shear in slabs – see Section 1).

The coupling level was analyzed considering the response of the two wall piers at the east side of the tested building (see Figure 8), which was damaged more than the west part (due to the construction imperfections, certain torsion was activated, causing some differences in the response of the east and west side of the specimen). The representative example of this analysis is provided in the following paragraphs, considering one of the peak excitations during the last test, R150(2). In this test, the yielding of wall piers was observed, and their flexural capacity was achieved.

The overturning moment was estimated based on the inertial forces, calculated at all stories from the accelerations measured at the east side of slabs (see Figure 8a) and the tributary mass (half of the mass of the tested specimen). The bending moments at the foundations level caused by these forces were summed to obtain the total overturning moment.

At the beginning of the analysis, the axial forces in piers were unknown. Thus, their flexural capacity was estimated considering the axial force caused by the gravity load  $N_g = 20$  kN per wall pier. Both piers' corresponding total flexural capacity was  $M_{FC} = 140$  kNm (70 kNm per wall pier).

The overturning moment  $M_{over}$  was 290 kNm. Considering the flexural capacity of piers ( $M_{FC} = 140$  kNm), the part of the overturning moment resisted by the frame action was defined as  $M_{FA} = 290 - 140 = 150$  kNm.

To obtain the axial forces  $N_E$  in wall piers caused by the seismic excitation,  $M_{FA}$  was divided by the axial distance of wall piers (1.25m). In this way,  $N_E$  was estimated to be 120 kN. In one wall pier, this force was tensile in the other compressive (see Figure 1b).

In the next step,  $N_E$  and  $N_g$  were summed to obtain the total axial forces in piers (due to the gravity and the seismic load). In the pier subjected to tension, the axial force was  $N_t = 100$  kN (tensile force). In pier subjected to compression, the axial force was  $N_c = 140$  kN (compressive force).

The flexural capacity of each pier at axial load  $N_t$  and  $N_c$  was calculated to be 30 kNm and 105 kNm, in the pier subjected to tension and compression, respectively. Thus, the total flexural capacity of both piers was  $M_{FC} = 135$  kNm.

Consequently, the value of the overturning moment, resisted by the frame action, amounted to:

$$M_{FA} = M_{over} - M_{FC} = 290 - 135 = 155 \text{ kNm} \quad (1)$$

$$M_{FC}/M_{over} = 155/290 = 0.53 \quad (2)$$

Note that despite considerable changes of the axial forces in wall piers and considerable changes of their flexural capacity (compared to that corresponding to  $N_g$ ), the total flexural capacity of both piers was only slightly changed. This is not surprising, considering that the flexural capacity of the piers is changing proportionally to the changes of the axial force. In pier subjected to tension, the flexural capacity was reduced. At the same time, the flexural capacity in the pier subjected to compression was increased for the approximately same amount.

In the analyzed case, the part of the overturning moment resisted by the frame action was 53 % of the total overturning moment  $M_{over}$  (see Equation 2). Note that in Eurocode 8, the coupled walls are defined as walls where the frame action contributes more than 25 % of the total overturning moment. Considering this definition, the analyzed structure should be designed following the rules for buildings with coupled walls.

As mentioned before (see Section 1), the studied walls are typically designed as cantilever walls, neglecting the frame action induced by slabs. In the studied case, this would considerably underestimate the compression stresses and shear forces in the piers subjected to compression. This could lead to brittle failure of the wall and the damage, which is similar to that observed in the recent earthquakes (e.g. buckling of the longitudinal bars, which was observed in the presented experiments).

## 4 Conclusions

The half-scale shake table tests of the three-story RC coupled wall building were conducted to study the slab-to-wall interaction. The specimen consisted of four rectangular walls connected only by the slabs.

A numerical model consisting of four cantilever walls connected with a rigid diaphragm would be typically used for the seismic analysis of such structures. In this way, the flexural stiffness and the strength of slabs are neglected, assuming that they are small compared to those of wall piers and insignificantly affect the response of the whole structure. This further means that it is assumed that slabs without beams cannot considerably couple wall piers.

In the experiment, contrary to this generally accepted approach, the considerable coupling of relatively flexible wall piers was provided only by slabs. The flexural capacity of slabs at the plastic hinges near the wall piers was large enough to provide strong frame action. The ratio of the overturning moment resisted by the frame action was larger than 50 %. In Eurocode 8, the upper value of this effect defining the cantilever wall systems is half of that observed in the experiment (25 %).

All slabs were fully activated. They were considerably cracked over the entire width between two rows of piers. The response of the wall piers was substantially different from that typical for the cantilever walls. The considerable rocking was observed in the piers subjected to relatively large tension induced by the frame action. In piers subjected to compression, the buckling of the longitudinal bars occurred due to the relatively large compressive stresses also caused by the frame action of the slab.

The presented experiment confirmed the indications of some other experiments found in the literature that for certain building configurations, only the slabs without beams can provide considerable coupling of wall piers. In such cases, the typical design, based on the assumptions that the walls respond as cantilever walls, can significantly underestimate the demand in piers. This can further lead either to brittle shear failure of walls or to their failure caused by the buckling of the longitudinal bars induced by significant compression stresses, which were underestimated in the design.

#### Acknowledgements

The project leading to this paper received funding from the European Union's Horizon 2020 research and innovation programme under grant agreement No 730900.

#### References

- [1] M. Fischinger, P. Kante, T. Isaković, Shake-table response of a coupled RC wall with thin T-shaped piers, *Jour. of Struc. Eng.* 143:5, (2017) 1-16.
- [2] A.R. Santhakumar, The ductility of coupled shear walls. Dissertation, University of Canterbury, (1974).
- [3] R. Alvarez, J.I. Restrepo, M. Panagiotou, R.A. Santhakumar, Truss Model for analysis of reinforced concrete coupled structural walls, *Bulletin of Earthquake Engineering*: 17: 6419–6436, (2019).
- [4] L.M. Massone, Fundamental Principles of the Reinforced Concrete Design Code Changes in Chile Following the Mw 8.8 Earthquake in 2010, *Engineering Structures*, vol. 56, (2013), pp. 1335-1345.
- [5] Boroschek R et al., Lessons from the 2010 Chile earthquake for performance based design and code development, *Performance-based seismic engineering: vision for an earthquake resilient society*, Dordrecht: Springer, (2014), pp 143 – 157.
- [6] K.J. Elwood et al., Performance-Based Issues from the 22 February 2011 Christchurch Earthquake, *Performance-based seismic engineering: vision for an earthquake resilient society*. Dordrecht: Springer, (2014), pp 159 – 175.
- [7] M.M. Panagiotou et al., Shake-Table Test of a Full-Scale 7-Story Building Slice. Phase I: Rectangular Wall, *Jour. of Struc. Eng.*, 137: 6, (2011).
- [8] T. Nagae, K. Tahara, T. Matsumori, H. Shiohara, T. Kabeyasawa, S. Kono, M. Nishiyama, J. Wallace, W. Ghannoum, J. Moehle, R. Sause, W. Keller, Z. Tuna Z, Design and Instrumentation of the 2010 E-Defense Four-Story Reinforced Concrete and Post-Tensioned Concrete Buildings, PEER Report 2011/104, Pacific Earthquake Engineering Research, Berkeley, USA, (2011).
- [9] T.A. Tran, J.W. Wallace, Cyclic Testing of Moderate-Aspect-Ratio Reinforced Concrete Structural Walls, *ACI Structural Journal* 112(6)(2015), pp.653-665.



## Stability design criteria for closely spaced built-up stainless steel columns

Jelena Dobrić<sup>\*1)</sup>, Nina Gluhović<sup>1)</sup>, Zlatko Marković<sup>1)</sup>, Dragan Buđevac<sup>1)</sup><sup>1)</sup> University of Belgrade, Faculty of Civil Engineering, Bulevar kralja Aleksandra 73, 11000 Belgrade, Serbia

### Article history

Received: 16 October 2021

Received in revised form:

27 November 2021

Accepted: 30 November 2021

Available online: 30 December 2021

### Keywords

Stainless steel;  
Built-up member;  
Flexural buckling;  
Parametric study;  
Design method;  
Shear stiffness

### ABSTRACT

This paper aims to develop design recommendations for closely spaced built-up stainless steel columns, based on findings gained in performed research at the University of Belgrade. The research focuses on pin-ended built-up columns formed from two press-braked channel chords oriented back-to-back and addresses their flexural buckling capacity about the minor axis. The impact of overall and local chord slenderness, interconnection stiffness, geometric imperfections and material nonlinearity is evaluated. In order to fully exploit their structural performance, two separate approaches for the design of built-up columns with welded or bolted interconnections are defined that include different formulas for shear stiffness.

### Highlights:

1. FE parametric studies including overall and chord slenderness and interconnection type.
2. Assessment of sensitivity to geometric imperfections.
3. Development of a design method for closely spaced built-up columns.
4. Reliability analysis of proposed design method.

## 1 Introduction

The use of cold-formed steel members with open cross-sections in built-up assemblies extends their application to light framing systems, wall bearing systems, trusses, latticed transmission towers and communication structures. If these structures are in a specific, aggressive or urban area, different stainless steel alloys may be utilized owing to their excellent corrosion resistance, ease of maintenance, good toughness, high fire resistance, pleasing appearance and general environmental benefits. Built-up members with chords in contact or closely spaced and connected through packing plates by bolts or welds usually have a more efficient structural response under compression compared to hot-rolled or welded single members at similar cost.

The built-up columns made of symmetrically placed individual channels or angle sections are more stable in torsional or torsional-flexural buckling than their individual, integral members. Furthermore, cross-sectional distortions, residual stresses and heat-affected zones in the vicinity of welds may be considerably minimized by the discontinuous welding process. The structural response of built-up column is more complex than that of a comparable solid column considering the reduced shear rigidity of built-up section with discrete interconnections. Effects of longitudinal shear, caused by the interaction between the contact areas of the individual chords, may affect the overall behaviour and reduce the flexural buckling resistance of the built-up member. The effects of shear on bending deflection may

significantly vary depending on the interconnectivity along the chords. In contrast to welded interconnections, the hole clearance in bolted interconnections can result in a more substantial longitudinal slip between the chords and, consequently, leads to additional flexibility of the built-up column. Thus, the longitudinal shear in built-up columns has to be evaluated and accounted for in the development of a suitable design procedure.

Over the past two decades, significant attention has been paid to aspects of the potential use of stainless steel in construction. Experimental work has focused on stainless steel structural elements of tubular and hollow cross-section. The number of investigations on open stainless steel sections is much smaller and none of them address closely spaced built-up structural elements. The experimental and theoretical observations on carbon steel built-up columns serve as a basis for a better understanding of the behaviour of the equivalent columns made from stainless steel. Bleich (1952) [1] developed a simplified analytical criterion based on an energy approach to determine the modified slenderness ratio of pin-ended battened columns. Zandonini [2] tested two series of compressed closely spaced built-up members consisting of two back-to-back channels with welded and snug-tight bolted interconnections. The end connections of all specimens were constructed by means of preloaded bolts.

<sup>\*</sup> Corresponding author:E-mail address: [jelena@imk.grf.bg.ac.rs](mailto:jelena@imk.grf.bg.ac.rs)

Astaneh et al. [3] performed tests on two back-to-back angles with welded, snug-tight and preloaded bolted interconnections. Using the data from these investigations [2], [3] as the basis, Zahn and Haaijer [4] recognized the effect of interconnection stiffness on the overall behaviour of closely spaced built-up columns and developed two different empirical formulations of the modified slenderness ratio for columns with snug-tight bolted interconnections and with welded or preloaded bolted interconnections. The developed empirical equations were introduced into the first edition of the AISC LRFD Specification [5]. The adopted design procedure involves modifying the general method for the design of axially compressed solid columns by replacing the modified (equivalent) overall slenderness ratio of a built-up member instead of the fully effective slenderness.

Based on Bleich's work [1], Aslani and Goel [6] proposed a new analytical formula which includes a section separation ratio  $\alpha$  to determine shear stiffness provided by interconnections, and verified it by their own experimental data for welded back-to-back hot-rolled angle members. This analytical formula replaced Zahn and Haaijer's equation [4] for columns with welded or preloaded bolted interconnections in the AISC LRFD Specification [5] and was also adopted in the Specification for Structural Steel Buildings ANSI/AISC 360-05 [7]. Based on the new test database, Sato and Uang [8] developed simplified equations for the modified slenderness ratio by employing a  $K$ -shear factor which has different values depending on the shape of the built-up cross-section. These equations, valid for built-up columns with either welded or preloaded bolted interconnections, are established in the design procedure of the previous [9] and latest version of the American Specification ANSI/AISC 360-16 [10]. Sherman and Yura [11] showed that preventing longitudinal slip in the end interconnections has a beneficial effect on the overall behaviour of built-up members. They also proposed an equation for determining the shear transfer force in the end interconnections to prevent slip between individual chords. As per section E6 of ANSI/AISC 360-16 [10] the end connections of built-up columns must be constructed by means of welds or preloaded bolts. If the ends of the built-up column are connected by welds, the weld length should not be less than the maximum dimension of the built-up cross-section; if the ends of the built-up column are connected by bolts, their longitudinal spacing should not be larger than four times the bolt diameter over a distance that is equal to 1.5 times the maximum dimension of the built-up cross-section. It should be pointed out that ANSI/AISC 360-16 [10] requires that the slenderness ratio of each of individual chords should not exceed 75% of the governing slenderness ratio of the built-up member.

EN 1993-1-4 [12] does not provide explicit rules for determining the flexural-buckling resistance of stainless steel closely spaced built-up members. Clause 5.4.1 states that the design provisions for carbon steel columns given in EN 1993-1-1 [13] may be applied to stainless steel columns. EN 1993-1-1 [13] has different analytical method for the design of compressed built-up members in comparison with ANSI/AISC 360-16 [10]. Clause 6.4 offers a simplified design procedure that is primarily intended for uniform battened or laced built-up columns with pin-ended boundary conditions. Essentially, the method replaces the discrete structure of a built-up column with an equivalent continuous column taking into account second order theory and smearing shear stiffness through properties of the bracing members. In order to restrict the influence of shear deformations or displacements between the connected chords, it is required

that the number of the modules between the restraints of chords is not smaller than three.

Clause 6.4.4 also provides the rules for closely spaced built-up members. Provided that the conditions given in Table 6.9 [13] related to the maximum spacing between interconnections are met, the closely spaced built-up member may be designed as a single member by ignoring shear deformations. Otherwise, the provisions for battened members given in clause 6.4.3 should be applied. Contrary to ANSI/AISC 360-16 [10], the Eurocode 3 design approach [13] for closely spaced built-up columns does not address the influence of the interconnection shear stiffness on the column resistance. Additionally, there are no specific recommendations in terms of construction details for interconnections.

This paper aims to fill the gaps caused by the lack of research in the field of stainless steel built-up columns and propose new design criteria for these types of structural elements. The investigation focuses on pin-ended built-up columns formed from two press-braked channel chords oriented back-to-back to form a non-slender I-section, addressing their flexural buckling capacity about the built-up axis. The paper presents FE (Finite Element) parametric studies based on a comprehensive experiment and FE simulation presented in detail in papers [14], [15], [16] and intended to extend the gathered experimental and numerical outcomes to a wider range of geometric variations affecting the compressive capacity of built-up columns including overall or chord failure modes. The investigation is concentrated on the most commonly used austenitic stainless steel grade EN 1.4301 (X5CrNi18-10). The FE results are used to develop two separate approaches for determining the flexural-buckling resistance of hinged supported built-up columns whose chords are directly connected by means of snug-tight bolts (in EN 1993-1-8 [17] denoted as shear bolt connection category A) or by welds. The design model is compatible with rules given in EN 1993-1-4 [12], EN 1993-1-1 [13] and is based on Bleich's work [1].

## 2 FE parametric studies

### 2.1 Description of influencing parameters

Extensive FEPSs (Finite Element Parametric Studies) are conducted with reference to a wide-ranging set of overall and local chord slenderness and interconnection type in order to meet different performance levels of structural behaviour and to establish a calculation model for the design buckling resistance  $N_{b,Rd}$  of the compressed built-up columns with hinged ends. A quasi-static analysis is made with the Abaqus software package [18]. The parametric studies cover the FE models of tested built-up columns that have been calibrated and validated against flexural-buckling tests [15], [16].

The CFSS (Cold-Formed Stainless Steel) built-up columns consist of two press-braked channel chords placed back-to-back and directly and discontinuously interconnected by means of either groove welds or bolts (see Figure 1). The nominal dimensions of the channel section are 100 x 40 x 4 mm with an internal corner radius of 8 mm. The cross-section is classified as class 3 [14] according to EN 1993-1-4 [12]. The nominal length of welded interconnections is 100 mm. The bolted interconnections are designed with six M8 bolts grade 8.8 in the arrangement shown in Figure 1. The distance between end bolts in the longitudinal direction is 100 mm. The diameter of holes in the web of the cross-section is 9 mm and a 1 mm bolt hole clearance is provided.

Table 1. Parameters and ranges considered in the main FEPS for columns with bolted interconnections

Designation of the FE model	Parameters					Ratio $\lambda_{ch}/\lambda$
	Nominal length $L$ (mm)	Slenderness ratio of built-up column $\lambda = L/i$	Number of modules between interconnections	Maximum distance between interconnections of chords $a$ (mm)	Maximum chord slenderness ratio $\lambda_{ch} = a/i_{min}$	
U31b-2	500	30.7	2	185	15.3	0.50
U49b-3	800	49.2	3	225	18.7	0.38
U49b-2	800	49.2	2	335	27.8	0.57
U62b-3	1000	61.5	3	290	24.0	0.39
U62b-2	1000	61.5	2	435	36.1	0.59
U92b-3	1500	92.2	3	460	38.1	0.41
U92b-2	1500	92.2	2	685	56.8	0.62
U123b-3	2000	123.0	3	625	51.8	0.42
U123b-2	2000	123.0	2	935	77.5	0.63
U154b-4	2500	153.7	4	595	49.3	0.32
U154b-3	2500	153.7	3	790	65.5	0.43
U154b-2	2500	153.7	2	1185	98.2	0.64
U184b-5	3000	184.5	5	575	47.7	0.26
U184b-4	3000	184.5	4	720	59.7	0.32
U184b-3	3000	184.5	3	960	79.6	0.43
U184b-2	3000	184.5	2	1435	119.0	0.64
U215b-5	3500	215.2	5	675	56.0	0.26
U215b-4	3500	215.2	4	845	70.1	0.33
U215b-3	3500	215.2	3	1125	93.3	0.43
U215b-2	3500	215.2	2	1685	139.7	0.65
U246b-6	4000	246.0	6	645	53.5	0.22
U246b-5	4000	246.0	5	775	64.3	0.26
U246b-4	4000	246.0	4	970	80.4	0.33
U246b-3	4000	246.0	3	1290	107.0	0.43
U246b-2	4000	246.0	2	1935	160.4	0.65

Table 2. Parameters and ranges considered in the main FEPS for columns with welded interconnections

Designation of the FE model	Parameters					Ratio $\lambda_{ch}/\lambda$
	Nominal length $L$ (mm)	Slenderness ratio of built-up column $\lambda = L/i$	Number of modules between interconnections	Maximum distance between interconnections of chords $a$ (mm)	Maximum chord slenderness ratio $\lambda_{ch} = a/i_{min}$	
U31w-2	500	30.7	2	200	16.6	0.54
U49w-3	800	49.2	3	240	19.9	0.40
U49w-2	800	49.2	2	350	29.0	0.59
U62w-3	1000	61.5	3	300	24.9	0.40
U62w-2	1000	61.5	2	450	37.3	0.61
U92w-3	1500	92.2	3	470	38.1	0.41
U92w-2	1500	92.2	2	700	56.8	0.62
U123w-3	2000	123.0	3	632.5	51.8	0.42
U123w-2	2000	123.0	2	950	77.5	0.63
U154w-4	2500	153.7	4	600	49.3	0.32
U154w-3	2500	153.7	3	800	65.5	0.43
U154w-2	2500	153.7	2	1200	98.2	0.64
U184w-5	3000	184.5	5	580	47.7	0.26
U184w-4	3000	184.5	4	725	59.7	0.32
U184w-3	3000	184.5	3	970	79.6	0.43
U184w-2	3000	184.5	2	1450	119.0	0.64
U215w-5	3500	215.2	5	680	56.0	0.26
U215w-4	3500	215.2	4	850	70.1	0.33
U215w-3	3500	215.2	3	1135	93.3	0.43
U215w-2	3500	215.2	2	1700	139.7	0.65
U246w-6	4000	246.0	6	650	53.5	0.22
U246w-5	4000	246.0	5	780	64.3	0.26
U246w-4	4000	246.0	4	975	80.4	0.33
U246w-3	4000	246.0	3	1300	107.0	0.43
U246w-2	4000	246.0	2	1950	160.4	0.65

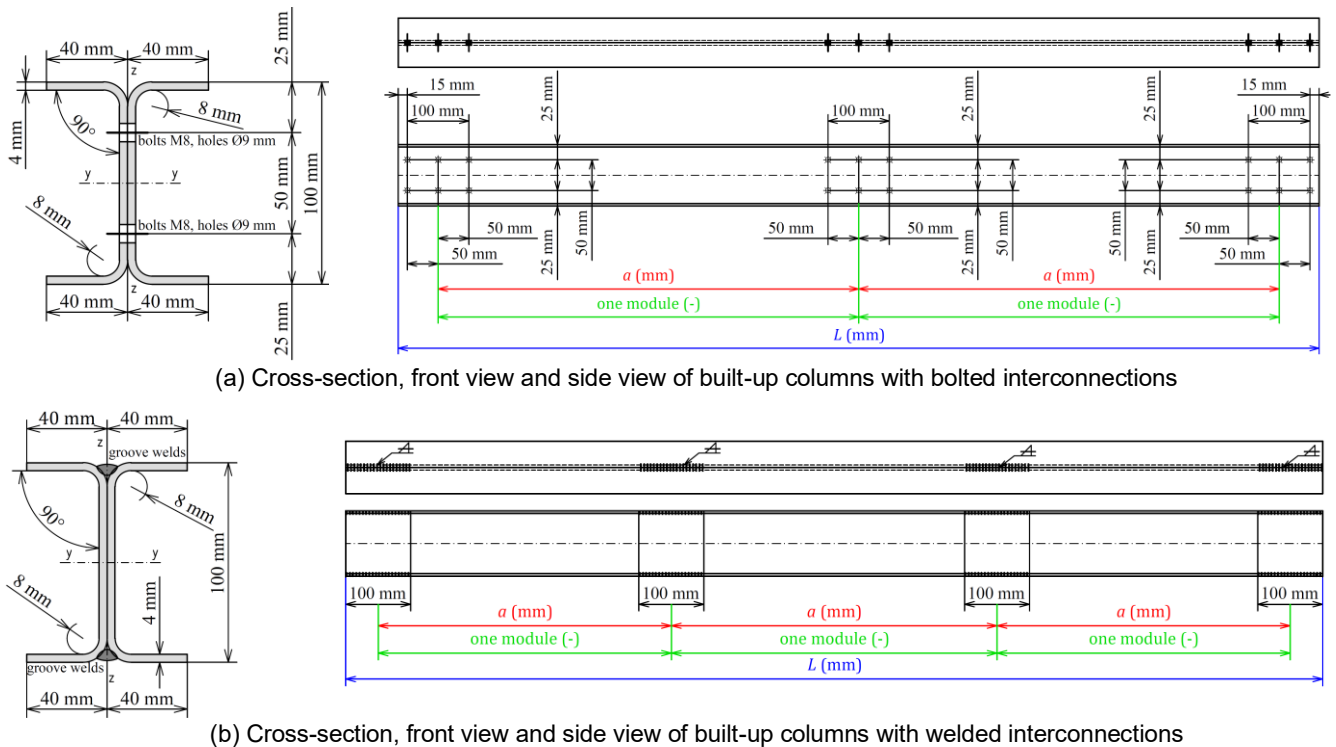


Figure 1. Nominal geometry and parameter designation of built-up columns in FEPSs

The length of both interconnection types is selected to correspond to the maximum dimension of the built-up cross-section. Both ends of each FE model are flat and perpendicular to its longitudinal axis.

FEPSs were divided into two parts: the main parametric study and the imperfection sensitivity study, in which the influences of various parameters on the column compressive resistance were analysed. The main FEPS focuses on a wide range of overall and local chord slenderness ratios as listed in Table 1 and Table 2 for columns with bolted and welded interconnections, respectively. The considered parameters were column length  $L$  and spacing between interconnections  $a$ . In Table 1 and Table 2,  $\lambda$  is the overall slenderness ratio of the entire section about the built-up member axis (equal to column length-to-radius of gyration of the built-up section about the buckling axis—minor principal axis), whereas  $\lambda_{ch}$  is chord slenderness ratio equal to spacing between interconnections-to-minimum radius of gyration of an individual chord. The chord slenderness ratios of built-up columns were varied by changing the number of modules between interconnections, where one module represents one regular spacing between two adjacent interconnections (see Figure 1). The analysed range of overall slenderness ratios from 31 to 246 (the corresponding range of non-dimensional slenderness ratio  $\bar{\lambda}$  is 0.38 to 3.07) may be used for different structural applications under static conditions of compressed built-up members. The spacing between interconnections is limited such that the slenderness of the individual chords does not exceed 65% of the overall built-up slenderness. This is strongly associated with the findings of the experimental research of Dobrić et al. [15], where, for interconnection spacings thus adopted, the governing buckling mode of all built-up specimens was governed by the overall flexural buckling about the minor principal axis of the

built-up section. The designations of the FE models in Table 1 and Table 2 are in accordance with the labelling system of tested specimens as explained in a previous paper [15]: the first letter indicates the shape of the chords' cross-section "U", the subsequent number indicates the overall slenderness of the column, and the final letter "b" or "w" indicates the weld or bolt interconnection. The number in the third position represents the number of modules between interconnections.

The imperfection sensitivity study was performed to thoroughly assess possibilities for potential buckling failures of individual chord members affected by the shape and magnitude of their initial out-of-straightness imperfections. The study encompasses the geometric imperfections of individual chords in the shape of a sine wave between interconnections in the plane perpendicular to their minor principal axis (imperfection shapes IS2 and IS3), considering two variabilities in the amplitude of  $\delta_0 = L/1000$  and a permissible fabrication tolerance of  $\delta_0 = L/750$  specified in EN 1090-2 [19], as shown in Figure 2. It was assumed that these imperfections can lead to premature failure of individual chords before the built-up column as a whole becomes unstable. Therefore, this study focused only on built-up columns with interconnections at the ends and at mid-height, for which the chord slenderness ratio-to-overall slenderness ratio is approximately 65%. A range of intermediate and high overall slenderness of 92, 184 and 246 was considered. The structural behaviour of built-up columns, affected by imperfection shapes IS2 and IS3, is examined through a comparison with the behaviour of equivalent columns affected by the imperfection shape IS1, shown in Figure 3, which is used as an input parameter in the main FEPS.

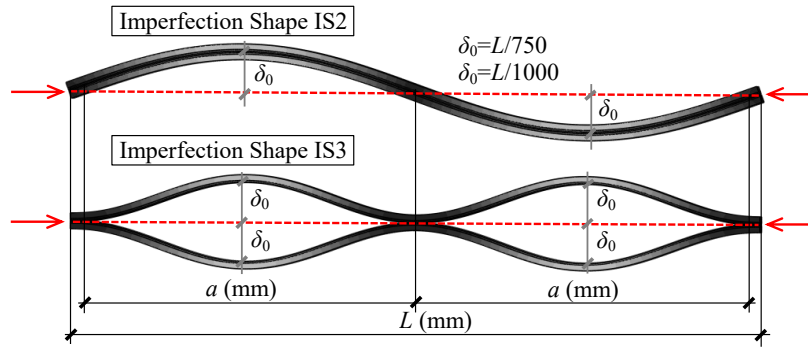


Figure 2. Overall geometric imperfections of built-up columns with two modules used in the imperfection sensitivity study

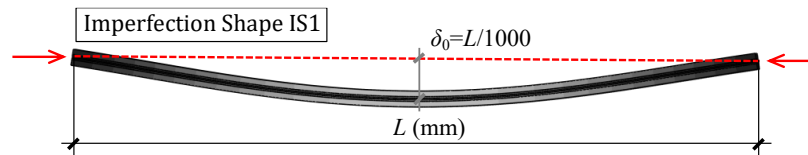


Figure 3. Overall geometric imperfections used in the main FEPS

Moreover, in order to validate the FE model used for the parametric studies, it is important to incorporate the unique set of most important parameters affecting the structural behaviour of a built-up column that leads to good agreement between tests [15] and FE results [16]. These are: material nonlinearity, strain hardening effects, residual stresses and annealing effects in the vicinity of welded interconnections, and bolt slipping in bolted interconnections.

Comprehensive FE simulations of the flexural-buckling tests are presented in detail in [16]. The mechanical properties obtained from the flat and corner longitudinal tensile coupon tests [14] were incorporated into the flat and corner parts of the press-braked chord section of FE models. In order to account for the reduction in strength properties in the vicinity of welds affected by the partial annealing of the material throughout the Heat Affected Zone (HAZ), the third material model was applied in the HAZ and welds [16], where a modified Ramberg–Osgood material model according to Arrayago et al. [20] was used to develop the stress–strain curve. Nominal values of key mechanical properties for annealed stainless steel EN 1.4301 (ASCE 304) were used according to Annex B of SE/ASCE 8-02 [21]. Table 3 summarises the key material properties adopted for each of the three considered material models. The yield strength  $f_y$  is taken as the 0.2 % proof strength, the ultimate tensile strength  $f_u$ , the strain corresponding to the ultimate tensile strength  $\epsilon_u$  and the strain hardening parameters  $n$  and  $m$ , are in accordance with the two-stage Ramberg–Osgood material model [20].

Plasticity with isotropic hardening was used for all parts of the section with an initial modulus of elasticity of  $E = 200$  GPa, and Poisson’s ratio of  $\nu = 0.3$ . Nominal stress–strain curves were transformed to true stress–strain curves for input in the Abaqus plasticity model [18].

The individual chords were modelled as S4R shell elements with reduced integration and with a size of 6 mm. The hexahedral solid elements C3D8R, 6 x 6 mm in size, were used to form the mesh of the welded interconnections. Contact conditions between the chords and the welds were defined by tie constraints at the joining surfaces. The attachment tool in the Abaqus software package [18] which involves attachment points was utilized to model the bolts in a nominal arrangement between chords. The bolts were modelled using the Cartesian mesh-independent connector type with a linear elastic stiffness of 50 kN/mm. This value was calibrated against test data obtained on specimens with bolted interconnections [16]. The rotational stiffness of connector was not considered. The degrees of freedom of the bolt were coupled to the adjacent nodes by distributing the coupling system between the connector point and its corresponding surface on the chord’s web. The corresponding nodes on the chords’ webs within the radius of 5 mm around the reference point were kinematically constrained by means of two rigid bodies connected by a spring element. The surface-to-surface general contact interaction was selected in the modelling approach in order to take into account the interactions between individual chords. The hard contact formulation of normal behaviour and the penalty friction formulation of tangential behaviour were used. A friction coefficient of 0.35 was assumed for all contact surfaces.

The cross-section points at the column’s ends were kinematically constrained to the central upper and lower reference points which were assigned hinged boundary conditions. Displacement control was used to apply the compressive load; a vertical displacement of 10 mm was applied to the upper reference point.

Table 3. Key material properties adopted in the FE models

Position	$f_y$ (N/mm <sup>2</sup> )	$f_u$ (N/mm <sup>2</sup> )	$\epsilon_u$ (%)	Strain hardening parameters	
				$n$	$m$
Flat parts	307	634	53	6.3	2.2
Corner parts	458	680	37	4.9	2.5
Welds and HAZ	207	571	64	8.3	2.0

The distribution of residual stresses in a fabricated austenitic stainless steel I-section, proposed by Gardner and Cruise [22], was adopted in the regions of welded interconnections. The residual stresses were incorporated into the models as initial model conditions through predefined fields. Maximum tensile residual stresses of  $1.3 \cdot f_y = 399 \text{ N/mm}^2$  were set in the vicinity of welds, where  $f_y = 307 \text{ N/mm}^2$  is experimentally obtained yield strength of the basic flat sheet material [14]. The residual stresses are in self-equilibrium in the cross-section with maximum compressive residual stresses of  $94 \text{ N/mm}^2$ . Discontinuous welding of individual chords caused variable cross-sections along the column. Thus, a stable equilibrium in the longitudinal direction was obtained in an initial analysis step prior to applying the compression load to the FE model. The residual stresses induced by the manufacturing process were not included in the FE models due to their minimal influence on the member compressive resistance [23]. The FE analysis included an eigenvalue Linear Buckling Analysis (LBA) and a nonlinear buckling analysis. The eigenvalue LBA was employed in order to permit numerical Geometrically and Materially Nonlinear Analysis with Imperfections (GMNIA). Superposition of initial imperfections in the shape of the lowest overall buckling mode with an amplitude of  $\delta_0 = L/1000$  (labelled in Figure 3 as imperfection shape IS1) and the lowest local (cross-section) buckling mode with an amplitude of  $\omega_0$  is assigned to all FE models. The amplitudes of local geometric imperfection  $\omega_0$  were determined by means of the modified Dawson and Walker model [24], as given by Eq.(1), where  $t$  is the thickness of the plate,  $f_y$  is the yield strength of basic flat sheet material and  $\sigma_{cr,min}$  is the minimum critical buckling stress of all the plate elements of the cross-section:

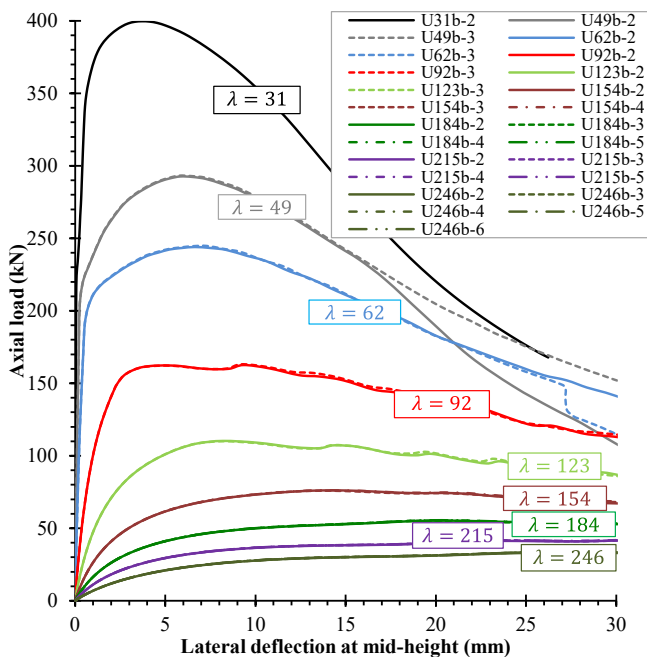
$$\varpi_0 = 0.036t(f_y/\sigma_{cr,min}) \quad (1)$$

This expression has been found to have good agreement between the tests and FE results for stainless steel channel stub columns [14] and slender built-up columns with chord in contacts [16]. The adopted approach in imperfection modelling is based on scientific investigation [23] covering structural behaviour of cold-formed stainless steel columns.

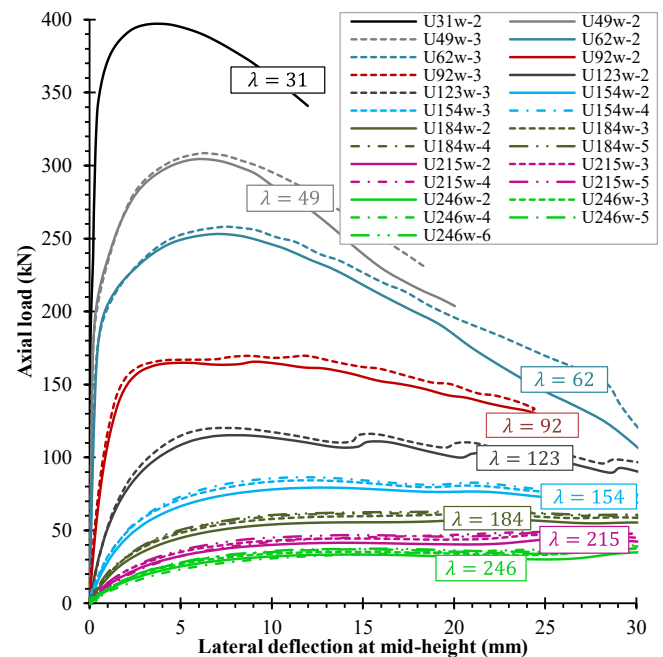
A GMNIA was performed to obtain the ultimate loads and potential failure modes of CFSS built-up columns. The large displacements, pronounced non-linear material behaviour and complex contact conditions often lead to an inability to solve instability problems with standard implicit static numerical solvers. Hence, the FEPSs were performed as quasi-static using the dynamic explicit solver in the Abaqus software package [18], thus, successfully overcoming the usual convergence issues.

### 3 Discussion of results

Key numerical results of the main FEPS presented in diagrammatic form as load–lateral deflection curves in the buckling plane are shown in Figure 4, both for built-up columns with bolted and welded interconnections. Figure 5 compares the buckling capacities of equivalent built-up columns with different interconnection types, with the same overall slenderness ratio and the same number of modules between interconnections. As a result of the imperfection sensitivity study, the load–lateral deflection curves generated for columns affected by imperfection shapes IS1, IS2 and IS3 are presented and compared in Figure 6. The value of ultimate buckling load  $N_{b,u}$  is also shown on the corresponding curve. Moreover, Figure 7 compares the different buckling responses of the selected built-up column U184w-2 caused by variations in the shape of overall geometric imperfections, but without change the amplitude value of  $L/1000$ . A brief analysis of the results of FEPSs is presented as follows:



(a) Built-up columns with bolted interconnections



(b) Built-up columns with welded interconnections

Figure 4. Load–lateral deflection curves at mid-height of FE models – main FEPS

1) The failure mode of each FE model is overall flexural buckling about the minor axis of the built-up section without any local-overall interactions. The structural integrity of the built-up section is maintained in the ultimate limit state: the premature failure of the individual chord members does not occur;

2) The initial overall geometric imperfection when modelled as a sine wave with an amplitude of  $L/1000$  at the column's mid-height has an important effect on the buckling resistance of built-up columns in the intermediate and high slenderness range from  $\lambda = 123$  to  $\lambda = 246$ . The residual stresses and reduction of enhanced strength properties of the material in the corner regions in the vicinity of welds significantly affect the column behaviour in the low slenderness range up to  $\lambda = 92$ ;

3) The FE models with bolted interconnections of the same overall slenderness and with different chord slenderness ratios have almost identical buckling and post-buckling structural behaviour (see coincidences of load-lateral deflection curves in Figure 4a). By increasing the number of interconnections, the buckling loads of the columns remain unchanged with a small deviation up to 3.6% for high slenderness ( $\lambda = 215$ ). This is due to the fact that the built-up column with bolted interconnections is less rigid and more susceptible to initial imperfections than the column with welded interconnections. It should be noted that in the tests [15], an increase of column compressive capacity of 24% was recorded in the high slenderness domain ( $\lambda = 184$ ) by changing the number of modules from two to three. However, the measured geometric imperfections of tested specimens have considerably lower magnitudes and different distribution patterns compared with modelled geometric imperfections of the FE models;

4) In contrast to the previous finding, the FE models with welded interconnections of the same overall slenderness showed an increase of the compressive resistance with an increasing number of modules between interconnections (see Figure 4b). Increasing the number of interconnections from two to five increases the column resistance by 16% in the high slenderness domain ( $\lambda = 215$ ). However, this increase is limited to 1.3% for the low slenderness ( $\lambda = 49$ ) due to the effects of the welding process. In addition, for the variation of the number of modules from two to three in the high slenderness range ( $\lambda = 184$ ), the increase of column buckling resistance was 10% in the tests [15], whereas in the main FEPS is only 6%;

5) As indicated in Figure 5, the FE models with welded interconnections exhibit a better structural response than FE models with bolted interconnections, over almost the entire slenderness range, except for low slenderness  $\lambda = 31$ . This

finding is strongly influenced by the higher shear stiffness of welded interconnections compared with bolted interconnections. The lowest structural response of the welded column with slenderness  $\lambda = 31$  is associated with the effects of residual stresses and partial annealing in the HAZ. In the case of columns with interconnections at their ends and at mid-height, the ratio of welded column resistance-to-bolted column resistance ( $N_{b,u,weld}/N_{b,u,bold}$ ) is almost constant and amounts to approximately 1.04 in the slenderness range  $\lambda = 123$  to 246, and approximately 1.03 in the slenderness range  $\lambda = 49$  to 92. Decreasing of the chord slenderness ratio in the overall slenderness range  $\lambda = 123$  to 246 resulted in a gradual growth of compressive resistance as the improved composite action of chords within the welded built-up section leads to a more favourable buckling response. For the maximum number of modules, used in the high slenderness range, the buckling resistance of the columns with welded interconnections is approximately 17% higher relative to the equivalent columns with bolted interconnections. As shown in Figure 5b, the FE model U246-6 and FE model U 215-5 have approximately same values of the ratio  $N_{b,u,weld}/N_{b,u,bold}$ . Hence, in comparison with columns with slenderness  $\lambda = 215$ , the slenderest columns ( $\lambda = 246$ ) are less sensitive to the benefits of the higher stiffness of the welded interconnections. This leads to the conclusion that the beneficial effects of higher number of interconnections between chords of built-up columns on their ultimate resistances increase with increasing the overall column slenderness.

However, it should be noted that the ratio  $N_{b,u,weld}/N_{b,u,bold} \approx 1,10$  is approximately same for equivalent FE models with three modules between interconnections in the intermediate and high slenderness range  $\lambda = 123$  to 246;

6) The shape and amplitude of the initial overall geometric imperfections are crucial predictors of the critical failure mode, because their changes significantly affect the buckling response of a built-up column (see Figure 6). As expected, the compressed built-up members are most sensitive to the sine wave shape of initial geometric imperfections with an amplitude of  $L/1000$  at mid-height (labelled as IS1). The distribution and magnitude of initial imperfections of individual chords, represented as a sine wave between interconnections (denoted as IS2 and IS3), do not contribute to the premature failure of individual chords. Furthermore, these imperfection shapes ensure higher initial stiffness and compressive resistance of built-up columns and may lead to an inelastic buckling response in the intermediate slenderness range. It can be seen from Fig. 3 that the direction lines of applied compression loads deviate from mid-length of individual chords between adjacent inter-

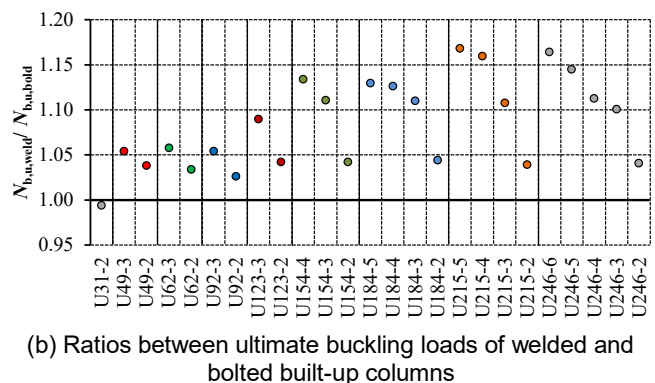
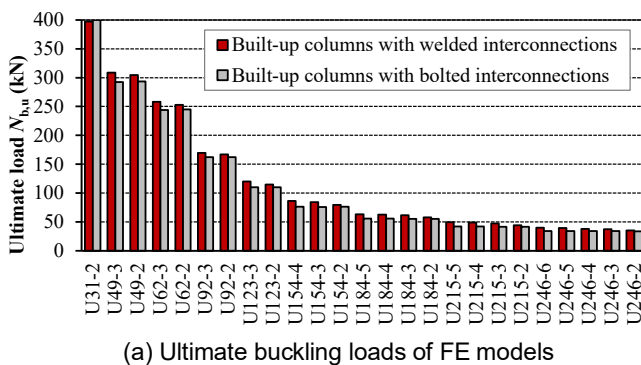


Figure 5. Comparison of ultimate buckling loads of FE models – main FEPS

connections. However, they pass through the built-up section at the column's mid-height both for IS2 and IS3, which has an impact on the overall buckling behaviour of the columns. Besides, in the case of IS3, the individual chords are specifically geometrically positioned within the built-up section, which affects the overall flexural stiffness of the built-up columns. Moreover, the analysed shapes of imperfections IS2 and IS3 do not represent the critical, lowest buckling modes of built-up columns that were computed by linearized eigenvalue analyses.

There are specific simultaneous effects of imperfection amplitude and imperfection shape IS3 both on welded and bolted built-up columns with high slenderness. It can be seen in Figure 6b, Figure 6c, Figure 6e and Figure 6f that the built-up column acts as a more stable system for a higher amplitude of  $\delta_0 = L/750$  rather than for a lower amplitude of  $\delta_0 = L/1000$  when considering imperfection shape IS3. Additionally, for the same shape IS3, the columns with welded interconnections have a much greater effectiveness in the high slenderness range both for  $\lambda = 184$  and  $246$  than the equivalent bolted columns, while their compressive resistances are almost equal in the intermediate slenderness range ( $\lambda = 92$ ).

The influence of the variation in initial out-of-straightness on the ultimate response of the built-up columns is also

highlighted through the variation in distribution of longitudinal stresses and internal forces generated at the failure state of the selected FE model U184w-2, as shown in Figure 7. The internal forces and moments are calculated for the column cross-sections at mid-height and at mid-distances between interconnections. It can be clearly seen from Figure 7 that the considered imperfection shapes do not change the critical failure mode of the built-up column which occurs by overall buckling about the minor axis. The location of the critical cross-section under the maximum bending moment is near the mid-height of column affected by either IS1 or IS3. However, the critical cross-section of column affected by the asymmetric curvature of imperfection shape IS2 is located approximately at mid-distance between the interconnections. For bending about the minor axis, the longitudinal stresses vary linearly through the both flanges with the maximum compressive stresses of  $\sigma_{11,max} = 191 \text{ N/mm}^2$  to  $\sigma_{11,max} = 200 \text{ N/mm}^2$  occurring at the edge fibres on the one side of the buckled column. Contrary to the column affected by either IS2 or IS3 for which the entire critical cross-section is under compressive stresses (see Figure 7b and Figure 7c), the tensile longitudinal stresses occurring on the convex side of the deflected column influenced by IS1 can be seen in Figure 7a.

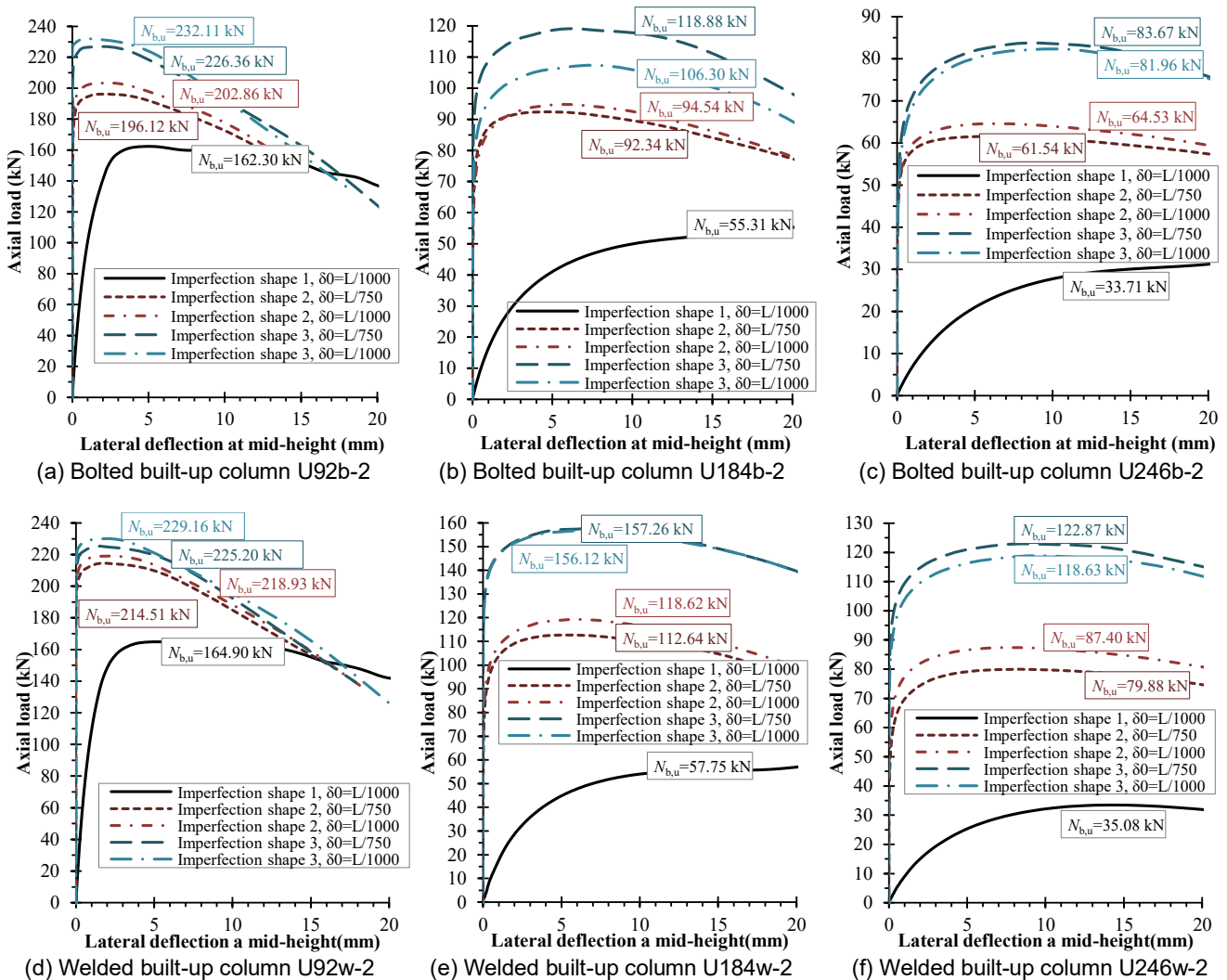


Figure 6. Load-lateral deflection curves at mid height of FE models – imperfection sensitivity study

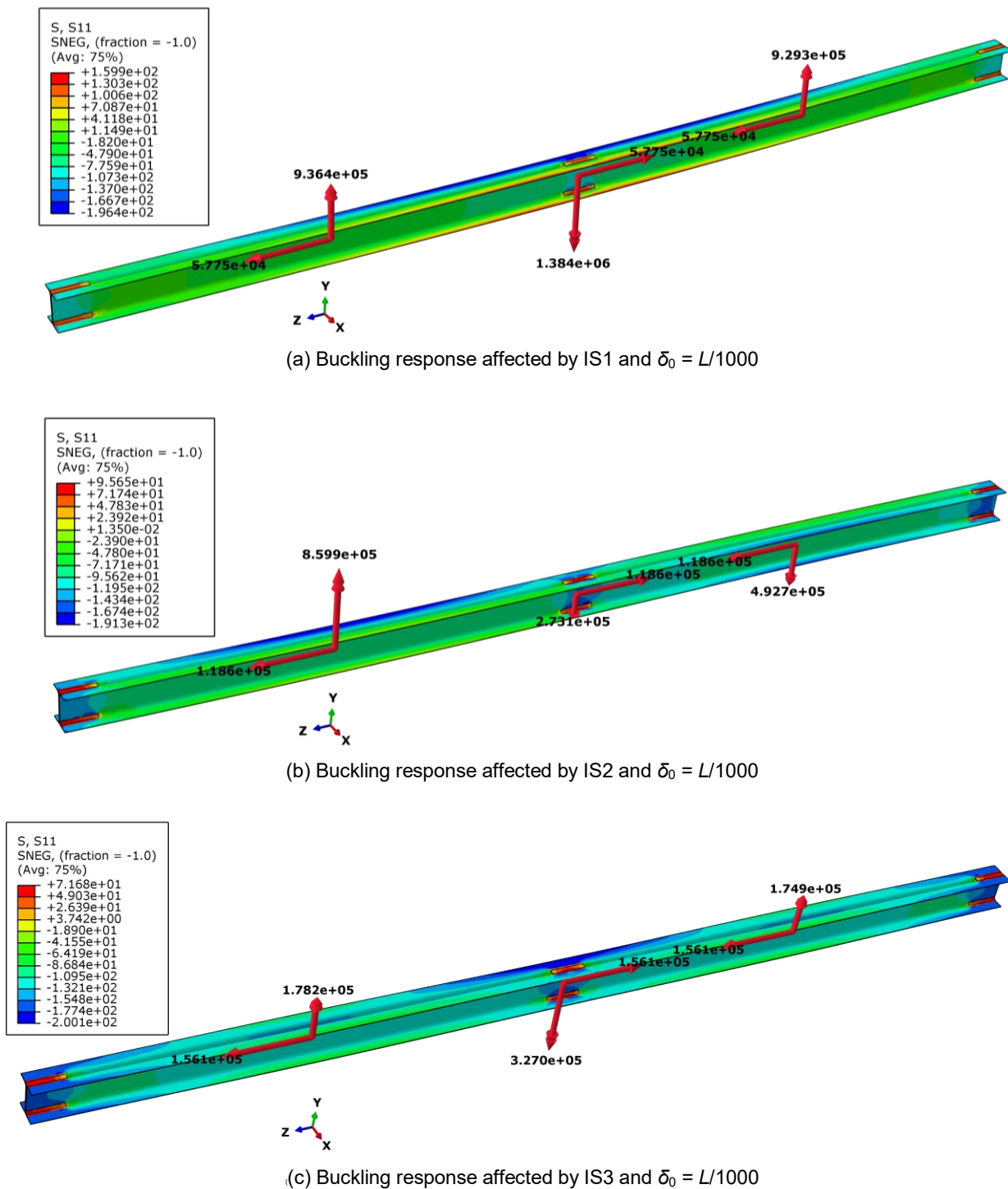


Figure 7. The axial stresses and internal forces of FE model U184w-2 at the ultimate load level

Quantification of the increase of column resistance by changing the shape and amplitude of the geometric imperfection, presented in Table 4, is provided through comparisons of ultimate buckling loads of built-up columns affected by IS2 and IS3 and amplitudes  $\delta_0 = L/1000$  and  $\delta_0 = L/750$  with those of built-up columns affected by imperfection shape IS1 and an amplitude of  $\delta_0 = L/1000$ . As indicated in

Table 4, the increase of ultimate buckling loads varies significantly from 92% to 250% for imperfections shape IS3 and from 67% to 128% for IS2 in the high slenderness range, while the increase of ultimate loads in the intermediate slenderness range is lower: from 37% to 43% for IS3 and from 21% to 33% for IS2.

Table 4. Quantification of the increase of buckling loads by changing geometric imperfections.

Column	Amplitude	$N_{b,u}^{IS3,\delta_0} / N_{b,u}^{IS1,L/1000}$	
		Imperfection shape IS3	Imperfection shape IS2
U92b-2	$\delta_0 = L/1000$	1.43	1.25
	$\delta_0 = L/750$	1.39	1.21
U92w-2	$\delta_0 = L/1000$	1.39	1.33
	$\delta_0 = L/750$	1.37	1.30
U184b-2	$\delta_0 = L/1000$	1.92	1.71
	$\delta_0 = L/750$	2.15	1.67
U184w-2	$\delta_0 = L/1000$	2.70	2.05
	$\delta_0 = L/750$	2.72	1.95
U246b-2	$\delta_0 = L/1000$	2.43	1.91
	$\delta_0 = L/750$	2.48	1.83
U246w-2	$\delta_0 = L/1000$	3.38	2.49
	$\delta_0 = L/750$	3.50	2.28

#### 4 Design proposal

The development of the method leading to the establishment of design resistance expressions for CFSS closely spaced built-up members under compression based on the column buckling tests [15] and the results of main FEPS are presented in section 4.2. The proposed design procedure focuses on built-up columns formed from two press-braked channel chords oriented back-to-to back that are in direct contact. The basic material is austenitic alloy of stainless steel grade EN 1.4301.

##### 4.1 Analytical criterions for the design of built-up columns

Using the energy method, Bleich [1] provided analytical solutions for elastic flexural buckling of simply supported latticed and battened built-up columns. The solutions are based on the condition that the strain energy due to deflection is equal to the work done by the external axial compression load, indicating the transition from the stable configuration to the unstable form of the elastic system. In the case of battened columns, the elastic strain energy consists of the energy due to overall bending of a built-up member, energy due to the local bending of individual chords and the energy due to the local bending of the bracing elements. Solving the energy condition [1] results in the critical buckling load of battened built-up columns  $N_{cr,V}$ :

$$N_{cr,V} = \frac{\pi^2 EI}{(kL)^2} = \frac{\pi^2 EI}{\left(1 + \frac{\pi^2 I_0}{24I_{ch}} \left(\frac{a}{L}\right)^2 + \frac{\pi^2 EI_0}{L^2} \frac{ah_0}{12EI_b}\right) L^2} \quad (2)$$

where  $k$  is the buckling length factor for battened built-up columns, given by Eq. (3):

$$k = \sqrt{1 + \frac{\pi^2 I_0}{24I_{ch}} \left(\frac{a}{L}\right)^2 + \frac{\pi^2 EI_0}{L^2} \frac{ah_0}{12EI_b}} \quad (3)$$

The buckling length factor  $k$  accounts for detrimental shear distortion effects caused by amplification of overall lateral deflections of the column and additional deflections of the column segments between battens. Equation (2) can also be written as:

$$N_{cr,V} = \frac{1}{\frac{L^2}{\pi^2 EI} + \frac{a^2}{24EI_{ch}} \left[\frac{I_0}{I} + \frac{2I_{ch}h_0}{I_b a} \frac{I_0}{I}\right]} \quad (4)$$

In foregoing equations,  $L$  is the column length,  $a$  is the distance between mid-points of interconnections,  $h_0$  is the distance between the chord centroids,  $A_{ch}$  is the cross-sectional area of one chord,  $I_{ch}$  is the second moment of area of a single chord about the minor principal axis parallel to the axis of buckling,  $I_0$  is the second moment of area of the built-up section about the buckling axis (neglecting the second moment of area of individual chords about their own minor principal axis),  $I_b$  is the in-plane second moment of area of one-batten members and  $I$  is the total second moment of area of a built-up member with respect to the principal axis perpendicular to the plane of buckling. The following notations for critical force  $N_{cr}$  and shear stiffness  $S_v$  may be introduced:

$$N_{cr} = \frac{\pi^2 EI}{L^2} \quad (5)$$

$$S_v = \frac{24EI_{ch}}{a^2 \left[\frac{I_0}{I} + \frac{2I_{ch}h_0}{I_b a} \frac{I_0}{I}\right]} \quad (6)$$

Therefore, Eq. (4) can be reformulated as follows:

$$N_{cr,V} = \frac{1}{\frac{1}{N_{cr}} + \frac{1}{S_v}} \quad (7)$$

In order to simplify Eq.(6), Bleich [1] neglected the influence of the second moment of area of individual chords  $I_{ch}$  with regard to the term  $I_0 = 2A_{ch}(h_0/2)^2$  when calculating the total second moment of area of a built-up column  $I$ , by approximating the ratio  $I_0/I$  as equal to unity. This leads to

$$S_v = \frac{24EI_{ch}}{a^2 \left[1 + \frac{2I_{ch}h_0}{I_b a}\right]} \quad (8)$$

However, the outcomes gained in the investigation of Aslani and Goel [6] show that Bleich's simplified approximation, given by Eq.(8), may result in significant errors in the prediction of buckling resistance, particularly in the case of battened columns with a relatively small distance between individual chords or closely spaced built-up columns. It was shown that the  $I_0/I$  ratio decreases as the distance between centroids of chords becomes smaller. On the other hand, based on the test data of Zandonini [2], Zahn and Haaijer [4] demonstrated that built-up columns with snug-tight bolted interconnections are more susceptible to shear deformations. The Eurocode 3 design procedure takes

into account these aspects: Eq.(8) corresponds to the expression on the left-hand side of the conditional equation for shear stiffness of a battened column, defined in clause 6.4.3 of EN 1993-1-1 [13], which is given as follows:

$$S_v = \frac{24EI_{ch}}{a^2 \left[ 1 + \frac{2I_{ch}h_0}{I_b a} \right]} \leq \frac{2\pi^2 EI_{ch}}{a^2} \quad (9)$$

Expressions for shear stiffness  $S_v$  given by Eqs (6), (8) and (9) take into account the flexural stiffness of the individual chords and battened members that is strongly associated with overall shear deformations.

The expression for critical load  $N_{cr}$  given by Eq.(5) takes into account the flexural stiffness of the built-up column with a stiff bracing system that is strongly associated with overall bending deformations. The total second moment of area of the built-up member  $I$  in Eq.(5) is taken as:

$$I = 0.5h_0^2 A_{ch} + 2I_{ch} \quad (10)$$

It should be noted that Eq. (5) deviates from the expression for effective critical load  $N_{cr,eff}$  stated in clause 6.4.1 of EN 1993-1-1 [13] given by Eq.(11), in terms of the second moment of area of the battened built-up column, as follows:

$$N_{cr,eff} = \frac{\pi^2 EI_{eff}}{L^2} \quad (11)$$

where:

$$I_{eff} = 0.5h_0^2 A_{ch} + 2\mu I_{ch} \quad (12)$$

In Eq.(12),  $I_{eff}$  is the effective second moment of area of a battened built-up member and  $\mu$  is the efficiency factor which is contained in the above stated formula representing the contribution of the chords' moments of inertia to the overall bending stiffness of the battened column. The efficiency factor  $\mu$  ranges between 0 and 1.0 and depends on the overall slenderness of the built-up column.

#### 4.2 Proposed design method

The proposed procedure for the design of closely spaced built-up CFSS columns modifies the general method for the design of axially compressed stainless steel conventional (solid) columns stated in clause 5.4.2 of EN 1993-1-4 [12]. The procedure introduces an empirical equation for the equivalent (modified) non-dimensional slenderness ratio of a built-up member  $\bar{\lambda}_{eq}$  instead of the geometric non-dimensional slenderness ratio of a solid member  $\bar{\lambda}$ , to reflect influences of shear deformations on the column strength. The analytic buckling curve is based on the Perry-Robertson equations and the linear expression for the imperfection parameter  $\eta = \alpha(\bar{\lambda}_{eq} - \bar{\lambda}_0)$ . The influences of geometric imperfections, residual stresses and load eccentricity on the predicted flexural-buckling resistance is implicitly accounted for by employing an imperfection factor  $\alpha$  associated with the appropriate buckling curve depending on the cross-section shape and manufacturing process. Two curves are specified in EN 1993-1-4 [12] for flexural buckling: for cold-formed sections ( $\alpha = 0.49$ ,  $\bar{\lambda}_0 = 0.4$ ) and for welded sections ( $\alpha = 0.76$ ,  $\bar{\lambda}_0 = 0.2$ ). However, by based on research findings conducted over the last decade, the fourth edition of the Design Manual for Structural Stainless Steel [25] has revised

the buckling curves and adopted the more conservative curve  $d$  for cold-formed channel sections made from austenitic stainless steel. Hence, considering basic material and type of chord section, the imperfection factor  $\alpha = 0.76$  in conjunction with a non-dimensional limiting slenderness  $\bar{\lambda}_0 = 0.2$  is used in this method both for welded and bolted CFSS built-up members. Several minor modifications of the design procedure stated in EN 1993-1-1 [13] are made for the purpose of its applicability to a buckling check of closely spaced and directly interconnected CFSS built-up columns:

1) The expression for critical buckling load  $N_{cr,v}$  given by Eq.(7) is utilized;

2) The efficiency factor  $\mu$  is set equal to unity when calculating the effective second moments of area  $I_{eff}$  in Eq.(11). Hence, Eqs. (5) and (10) are used in the calculation method;

3) The second term within the denominator brackets is excluded from the expression for shear stiffness  $S_v$  in Eq. (9) because of the absence of the battens within the built-up cross-section with chords in contact. However, in order to satisfy the condition in Eq. (9) the expression on the right-hand side of this equation should be used. This gives:

$$S_v = \frac{2\pi^2 EI_{ch}}{a^2} \quad (13)$$

Eq.(13) is intended to predict the flexural-buckling resistance of CFSS built-up columns with bolted interconnections;

4) Using key findings from Aslani and Goel [6], Bleich's exact solution given by Eq. (6) is employed in an attempt to introduce the beneficial impact of shear stiffness of welded interconnections in design procedure. However, the second term within the denominator brackets in Eq. (6) should be excluded, which leads to:

$$S_v = \frac{24EI_{ch} I}{a^2 I_0} \quad (14)$$

Thus Eq. (14) is used to predict the flexural-buckling resistance of CFSS closely spaced built-up columns with welded interconnections. The flowchart in Figure 8 gives an overview of the proposed design method.

#### 4.3 Range of application

The procedure covers the following conditions:

- the cross-section is cold-formed from austenitic stainless steel;
- the cross-section is classified as class 3;
- the individual chords are interconnected by means of bolts or by welds;
- bolted interconnections should be designed as Category A: bearing type in accordance with EN 1993-1-8 [17];
- the length of the bolted interconnection is defined by the distance between end bolts in the longitudinal direction (in a line in the direction of load transfer) that is equal to the maximum dimension of the built-up cross-section; the bolts are positioned on the chords' webs in an arrangement that meets requirements specified by EN 1993-1-8 [17]. The internal spacing between centres of bolt holes in both directions is  $5d_0$ , the end distances from the centre of a bolt hole to the adjacent end of a chord's web is  $2d_0$  in the case of end interconnections, where  $d_0$  is the diameter of bolt hole;

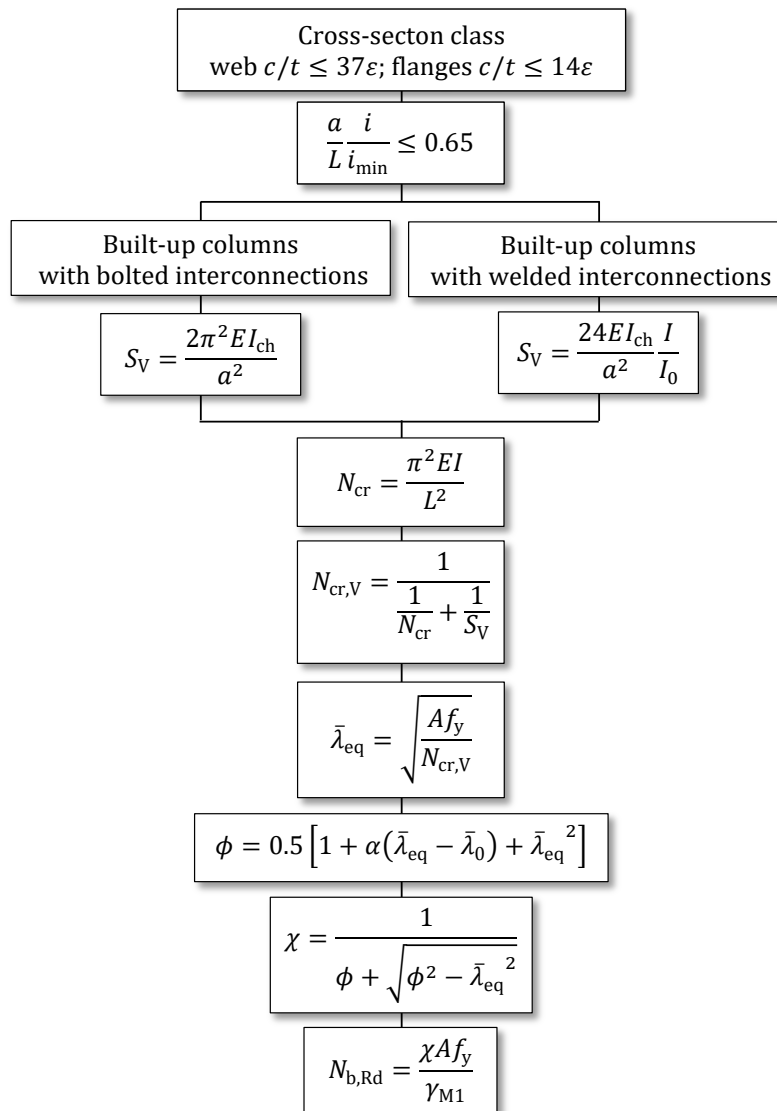


Figure 8. Design method applicable for buckling design checks of CFSS closely spaced built-up columns

- the length of welded interconnection corresponds to the maximum dimension of the built-up cross-section; the welds are placed in the contact regions between both chords' flanges;
- the properties of interconnections are uniform along the column's length;
- the distances between mid-points of interconnections are uniform along the column's length;
- the spacing between interconnections is limited such that the slenderness of the individual chords does not exceed 65% of the overall built-up slenderness about the axis of the built-up cross-section that corresponds to the minor principal axis; the chord slenderness ratio is based on the distance between interconnections  $a$  and a minimum radius of gyration of individual chords  $i_{\min}$ .

#### 4.4 Accuracy assessment of proposed design method

In order to assess the accuracy of the proposed design method, a comparative analysis is performed in which predicted buckling resistances of built-up columns are

compared with generated test [15] and numerical buckling resistances. In the design calculation,  $f_y$  was taken as 307 N/mm<sup>2</sup>, which is the measured strength of flat sheet steel [14] and a partial safety factor of  $\gamma_{M1}$  was taken as 1.0. The comparisons are presented in Figure 9 and a summary of the obtained results is presented in Table 5.

The mean test-to-predicted buckling load ratio  $N_{b,u, \text{test}}/N_{b,u, \text{pred}}$  is 1.87 and the Coefficient of Variation (CoV) is 6.3% for the columns with bolted interconnections. The mean value of  $N_{b,u, \text{test}}/N_{b,u, \text{pred}}$  is 1.66 and CoV is 9.0% for the columns with welded interconnections. In the case of FE data, the mean numerical-to-predicted buckling load ratio  $N_{b,u, \text{FE}}/N_{b,u, \text{pred}}$  is 1.16 and the CoV is 8.3% for the columns with bolted interconnections, while the mean value of  $N_{b,u, \text{FE}}/N_{b,u, \text{pred}}$  is 1.16 and the CoV is 2.3% for the columns with welded interconnections. Considering both test and FE results, the mean value of the  $N_{b,u}/N_{b,u, \text{pred}}$  ratio is 1.37 and the CoV is 30% for columns with bolted interconnections, while the mean value of the  $N_{b,u}/N_{b,u, \text{pred}}$  ratio is 1.35 and the CoV is 20% for the columns with welded interconnections.

The significant distinctions between test and FE data are strongly associated with a discrepancy in the shapes and magnitudes of initial geometric imperfections of specimens in the test [15] and columns in the main FEPS, respectively. The measured imperfection amplitudes of specimens in the corresponding buckling plane are  $L/3432$  to  $L/24000$  [15]. Besides, the shapes of measured imperfections do not

reflect the lowest overall buckling mode of tested built-up columns. As for the geometric imperfections in the main FEPS, they were taken as sinusoidal shapes with an amplitude of  $L/1000$  at columns' mid-height representing the critical (lowest) buckling modes of all FE models in order to obtain lowest buckling resistances.

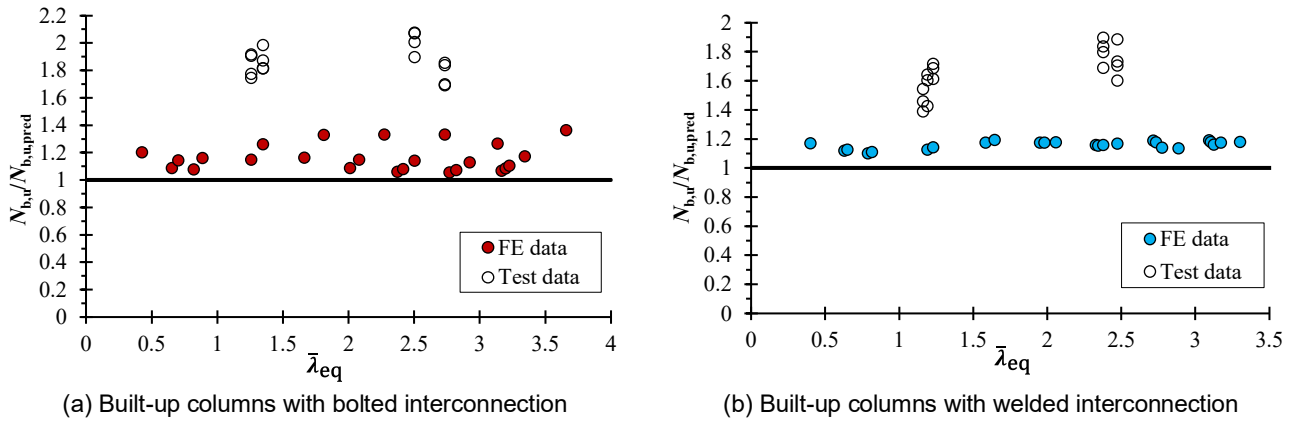


Figure 9. Comparison between design resistance predictions and test and FE results

Table 5. Comparison between design resistance predictions and test and FE results

Dataset	Built-up columns with bolted interconnection			Built-up columns with welded interconnection		
	No. of test data/FE data	$N_{b,u}/N_{b,u,pred}$ Mean	CoV	No. of test data/FE data	$N_{b,u}/N_{b,u,pred}$ Mean	CoV
Test data	16	1.87	0.063	17	1.66	0.090
FE data	25	1.16	0.083	25	1.16	0.023
Test +FE data	41	1.37	0.300	42	1.35	0.200

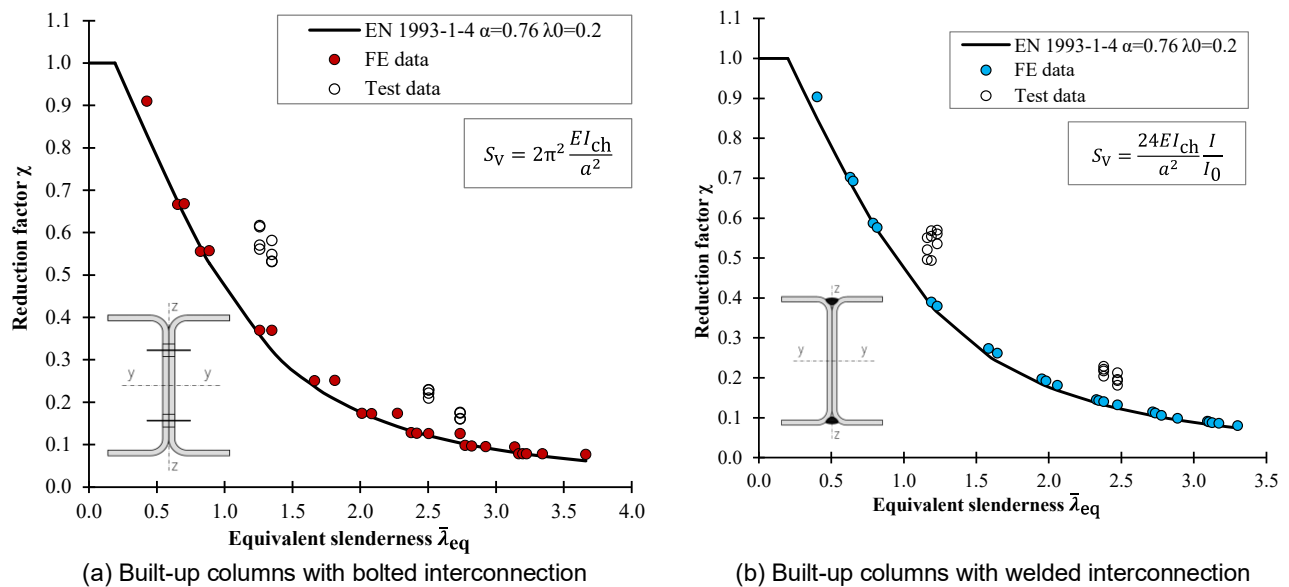


Figure 10. Comparison between normalised test and FE results and buckling curve d

Graphical comparisons between the predicted design resistances presented by the buckling curve *d* and the normalised FE and test compressive resistances of CFSS built-up columns are also provided in Figure 10. The FE and test ultimate loads are normalised by dividing by the squash load and are plotted against the column equivalent slenderness ratio. The normalised FE and test results are based on the enhanced average yield strength of the cross-section [14], which eliminates the influence of the enhanced material strength in corner regions of press-braked section from the buckling curve. The comparisons show that the FE results of the main parametric study closely follow the buckling curve pattern, and confirm the applicability of the proposed design approach both for CFSS built-up compressed members with bolted and welded interconnections.

### 5 Reliability analysis

In order to evaluate the reliability of the proposed design method and identify the value of the partial factor for member resistance  $\gamma_{M1}$ , a statistical analysis based on provisions stated in Annex D of EN1990 [26] was performed. The points, representing pairs of corresponding test ( $N_{b,u,test}$ ) and FE ( $N_{b,u,FE}$ ) data, and design data ( $N_{b,u,pred}$ ), are plotted in Figure 11.

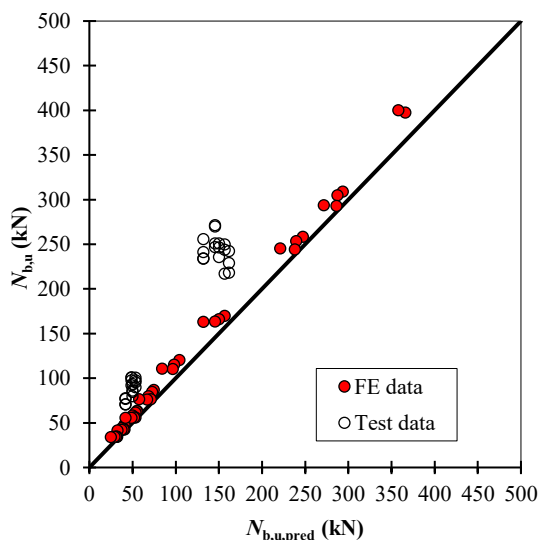


Figure 11. Comparison of test and FE resistance with design resistance predictions

The diagram shown in Figure 11 indicates the expected trend line of FE data regarding to line  $\theta = \pi/4$  for stainless steel alloys. However, the test results show a scatter in comparison with numerical results. Thus, to obtain an economical design resistance function, the generated results are split into two subsets with respect to FE and test results, as per clause D 8.2.2.5 of EN 1990 [26]. Table 6 lists the key statistical parameters for comparisons between predicted design resistances and test and numerical data, respectively. These are:

Table 6. Summary of reliability analysis of proposed design method based on test and FE results

Section type	Material	Dataset	No. of test data / FE data	$k_{d,na}$	$b$	$V_{\delta}$	$V_r$	$\gamma_{M1}$
Closely spaced built-up section	Austenitic stainless steel	Test data	33	3.041	1.693	0.100	0.122	1.18
		FE data	50	3.048	1.141	0.060	0.090	1.09

- the design (ultimate limit state) fractile factor,  $k_{d,n}$ ,
- the correction factor represented is the average test or FE resistance-to-design model resistance ratio based on a least squares best fit to the slope of all data,  $b$ ,
- the CoV of the test and FE data relative to the design model resistance,  $V_{\delta}$ ,
- the combined CoV incorporating both model and basic variable uncertainties,  $V_r$
- the partial factor for member resistance,  $\gamma_{M1}$ .

For the yield strength, an over-strength value of 1.3 and a CoV of 0.06 for austenitic stainless steel are used, as recommended by Afshan et al. [27].

It can be seen from Table 6 that the obtained partial safety factor for the proposed design method, based on FE data, is lower than the codified value of 1.10 in EN 1993-1-4 [12]. However, when only the test data are considered, the partial safety factor  $\gamma_{M1}$  is higher than 1.10; this is due to the variation and scattering of the test data obtained from experiments [15]. This indicates a need for further tests in this range, in order to generate a larger database for more precise statistical analysis.

### 6 Conclusions

A comprehensive investigation of the structural behaviour of CFSS closely spaced built-up members under pure compression, including literature review, test [14], [15], qualitative [16] and quantitative numerical studies, was carried out with the aim of acquiring a valuable database that enabled the development of an accurate and reliable design method. The following conclusions are drawn from this investigation:

1. The structural response of a built-up column is affected by a wide range of influencing parameters which determine the interaction level between individual chord members and the shear forces in the interconnections. The type of interconnections, the number of interconnections and initial overall geometric imperfections have an important effect on a column's buckling resistance. However, the influence of the type and number of interconnections significantly vary depending on column slenderness and the distribution and magnitude of the imperfections. Based on results of the main FEPS in which the effects of overall and local chord slenderness and interconnection stiffness have been investigated, the initial overall geometric imperfection of a sine wave with an amplitude of  $L/1000$  affects the ultimate buckling resistance of a built-up column of intermediate and high slenderness. The combined weakening effect due to residual stresses and reduction of enhanced material strength properties in the vicinity of welds affects the column's behaviour in the low slenderness domain. The number of interconnections does not affect the compressive resistance of a built-up column with bolted interconnections: by decreasing the chord slenderness ratio, the ultimate buckling load remains approximately unchanged within the whole analysed slenderness range, with deviations up to 3.6%. This is caused by the flexibility of bolted interconnections and slipping effects in the bolt hole clearance which contributes to higher shear deformations.

Decreasing the chord slenderness ratio results in a gradual increase of compressive resistance of the built-up column with welded interconnections up to 16% in the high slenderness range, and up to 1.3% in the low slenderness range. The built-up column with welded interconnections exhibits better structural response than those with bolted interconnections in almost the whole slenderness range. The ultimate buckling loads of welded built-up columns are 3 to 17% higher compared with columns with bolted interconnections;

2. Based on the imperfection sensitivity study, the shape of initial imperfections significantly affects the column buckling resistance. For considered values of the individual chord slenderness-to-the overall built-up slenderness ratios, up to the value of 0.65, the imperfection shape of individual chords represented as a sine wave between interconnections does not lead to the premature failure of individual chords of built-up columns with two modules between interconnections. Furthermore, such shapes of initial out-of-straightness ensure higher initial stiffness and compressive capacity of the built-up column. In comparison with the compressive capacity of built-up columns affected by a bow imperfection and an amplitude of  $L/1000$ , the increase of ultimate buckling loads varies from 21% up to 250% over the analysed slenderness range;

3. The FE results generated in the main parametric study and test data have been used to develop and validate a simple method for the design of pin-ended CFSS built-up columns whose chords are oriented back-to-back and directly connected by bolts or welds, by focusing on semi-compact cross-sections. The proposed design procedure involves two different formulas for shear stiffness, separately provided for built-up columns with bolted interconnections and built-up columns with welded interconnections. The flexural-buckling resistance is determined by considering the buckling curve  $d$  in conjunction with a non-dimensional limiting slenderness  $\bar{\lambda}_0 = 0.2$ . The proposed design method extends limits of the chord slenderness ratio-to-overall slenderness ratio up to 65% for both types of built-up columns;

4. The reliability analysis of the proposed design method performed on 33 test and 50 numerical results indicates that the partial safety factors  $\gamma_{M1}$  are close to the codified value of 1.1 in EN 1993-1-4 [12].

### List of symbols

$A$	cross-sectional area of a built-up column
$A_{ch}$	cross-sectional area of one chord of a built-up column
$a$	distance between mid-points of interconnections (restraints of chords)
CoV	coefficient of variation
$c$	width or depth of a part of a cross section
$d_0$	hole diameter for the bolt
$E$	modulus of elasticity
FE	finite element
$f_y$	yield strength taken as the 0.2 % proof strength $f_{0.2}$
$f_u$	ultimate tensile strength
$h_0$	distance of centroids of chords of a built-up column
$I$	second moment of area of the built-up section, about the buckling axis $I = I_0 + 2I_{ch}$

$I_{ch}$	second moment of area of single chord section about minor principal axis parallel to the buckling axis $I_{ch} = A_{ch} i_{min}^2$
$I_0$	second moment of area of the built-up section about the buckling axis, neglecting the second moment of area of individual chords about their own minor principal axis $I_0 = 2A_{ch}(h_0/2)^2$
$I_{eff}$	effective second moment of area of the built-up column
$I_b$	second moment of area of one batten about the buckling axis
$i$	radius of gyration of the built-up section about the buckling axis (minor principal axis)
$i_{min}$	minimum radius of gyration of single chord members
$k$	buckling length factor
$L$	length of built-up column
$m$	strain hardening parameter
$N_{cr}$	critical force of the built-up column
$N_{cr,eff}$	effective critical force of the built-up column
$N_{cr,V}$	critical buckling load of a built-up column
$N_{b,u}$	ultimate buckling load
$N_{b,u,bolt}$	ultimate buckling load of built-up column with bolted interconnections
$N_{b,u,weld}$	ultimate buckling load of built-up column with welded interconnections
$N_{b,u,test}$	test ultimate buckling load
$N_{b,u,FE}$	FE ultimate buckling load
$N_{b,Rd}$	design buckling resistance
$n$	strain hardening parameter
$S_v$	shear stiffness of a closely spaced built-up column
$t$	relevant thickness
$\alpha$	imperfection factor
$\bar{\delta}_0$	overall imperfection amplitude
$\gamma_{M1}$	partial factor for the resistance of members
$\varepsilon$	coefficient depending on $f_y$ ; $\varepsilon = \sqrt{\frac{235}{f_y} \frac{E}{210000}}$
$\varepsilon_u$	strain corresponding to the ultimate tensile strength
$\eta$	imperfection parameter
$\lambda$	overall column slenderness ratio
$\lambda_{ch}$	chord slenderness ratio
$\bar{\lambda}_0$	non-dimensional limiting slenderness ratio
$\bar{\lambda}$	non-dimensional slenderness ratio
$\bar{\lambda}_{eq}$	equivalent non-dimensional slenderness ratio
$\mu$	efficiency factor
$\nu$	Poisson's ratio
$\phi$	value for determining the reduction factor $\chi$
$\chi$	reduction factor for the relevant buckling mode
$\omega$	local imperfection amplitude

### Acknowledgements

This investigation is supported by the Serbian Ministry of Education, Science and Technological Development through the 200092 project.

### References

- [1] F. Bleich, Buckling Strength of Metal Structures, McGraw-Hill Book Company, 1952.
- [2] R. Zandonini, Stability of Compact Built-Up Struts: Experimental Investigation and Numerical Simulation, Costruzioni Metalliche (1985) 202-204.

- [3] A. Astanteh, S.C. Gael, R. D. Hanson, Cyclic Out-of-Plane Buckling of Double-Angle Bracing, *J. Struct. Eng.*, ASCE, 111(5) (1985) 1135-1153.
- [4] C.J. Zahn, G. Haaijer, Effect of Connector Spacing on Double Angle Compressive Strength, *Eng. J.*, AISC 25(3) (1988) 109–118.
- [5] Load and Resistance Factor Design Specification for Structural Steel Buildings, American Institute of Steel Construction (AISC), INC., Chicago, IL., September 1, 1986.
- [6] F. Aslani, S.C. Goel, An Analytical Criterion for Buckling Strength of Built-up Compression Members, *Eng. J.*, AISC 28 (4) (1991) 159-168.
- [7] Specification for Structural Steel Buildings. An American National Standard ANSI/AISC 360-05, American Institute of Steel Construction (AISC), INC, Chicago, IL., March 9, 2005.
- [8] A. Sato, C.M. Uang, Modified Slenderness Ratio for Built-up Members, *Eng. J.*, AISC (2007) 269–280.
- [9] Specification for Structural Steel Buildings. An American National Standard ANSI/AISC 360-10, American Institute of Steel Construction (AISC), Chicago, IL., June 22, 2010.
- [10] Specification for Structural Steel Buildings. An American National Standard ANSI/AISC 360-16, American Institute of Steel Construction (AISC), Chicago, IL., July 7, 2016.
- [11] D.R. Sherman, J.A. Yura, Bolted double angle compression members, *J. Construct. Steel Res.*, 46 (1–3) (1998) 470–471.
- [12] Eurocode 3: Design of steel structures – part 1-4: General rules – supplementary rules for stainless steels, including amendment A1 (2015), EN 1993-1-4:2006+A1:2015, Brussels, Belgium, CEN 2015.
- [13] Eurocode 3: Design of steel structures – Part 1-1: General rules and rules for buildings EN 1993-1-1, Brussels, Belgium, CEN 2005.
- [14] J. Dobrić, D. Budjevac, Z. Marković, N. Gluhović, Behaviour of stainless steel press-braked channel sections under compression, *J. Constr. Steel Res.* 139 (2017) 236–253.
- [15] J. Dobrić, Z. Marković, D. Budjevac, M. Spremić, N. Fric, Resistance of the cold-formed built-up stainless steel members – Part I: Experiment, *J. Construct. Steel Res.* 145 (2018) 552–572.
- [16] J. Dobrić, M. Pavlović, Z. Marković, D. Buđevac, M. Spremić, Resistance of cold-formed built-up stainless steel members – Part II: Numerical simulation, *J. Construct. Steel Res.* 140 (2018) 247–260.
- [17] Eurocode 3: Design of Steel Structures: Design of joints EN 1993-1-8, Brussels, Belgium, CEN 2005.
- [18] ABAQUS User Manual. Version 6.12. Providence, RI, USA: DS SIMULIA Corp; 2012.
- [19] Execution of steel structures and aluminium structures – Part 2: Technical requirements for steel structures EN 1090-2, Brussels, Belgium, CEN 2008.
- [20] I. Arrayago, E. Real, L. Gardner, Description of stress–strain curves for stainless steel alloys, *Mater. Des.*, 87 (2015) 540–552.
- [21] Specification for the Design of Cold-Formed Stainless Steel Structural Members. ASCE Standard SEI/ASCE 8-02, American Society of Civil Engineers, Reston, VA, 2002.
- [22] L. Gardner, R. Cruise, Modeling of residual stresses in structural stainless steel sections, *J. Struct. Eng.*, ASCE 135 (1) (2009) 42–53.
- [23] L. Gardner, D. A. Nethercot, Numerical modeling of stainless steel structural components a consistent approach, *J. Struct. Eng.*, ASCE 130 (10) (2004) 1586–1601.
- [24] R.G. Dawson, A.C. Walker, Post-buckling of geometrically imperfect plates, *J. Struct. Div. (ASCE)* 98 (1) (1972) 75–94.
- [25] Design Manual for Structural Stainless Steel First Edition, Fourth Edition, The Steel Construction Institute, 2017.
- [26] Eurocode – basis of structural design EN 1990, Brussels, Belgium, CEN 2012.
- [27] S. Afshan, P. Francis, N. R. Baddoo, L. Gardner, Reliability analysis of structural stainless steel design provisions, *J. Construct. Steel Res.*, 114 (2015) 293–304.



## Strength enhancement of cold-formed steel tubular column using GFRP strip subjected to axial compression

Sangeetha Palanivelu<sup>\*1)</sup>, Dhinakaran Moorthy<sup>1)</sup>, Gobinaath Subramani<sup>1)</sup>, Jeevan Raj Dhayanithi<sup>1)</sup>

<sup>1)</sup> Department of Civil Engineering, Sri Sivasubramaniya Nadar College of Engineering, Chennai, Tamil Nadu, India

### Article history

Received: 22 April 2021

Received in revised form:

21 September 2021

Accepted: 15 October 2021

Available online: 30 December 2021

### Keywords

Cold-formed steel,  
tubular column,  
glass fibre strip,  
ANSYS,  
failure mode

### ABSTRACT

The experimental and analytical evaluation of externally reinforced square and circular cold-formed steel tubular columns with GFRP strips is presented in this study. Under axial compression, fourteen tubular columns with pinned support, seven square tubular sections, and seven circular hollow section columns with externally bonded GFRP strips at various points were tested to failure. The GFRP strips improved the load-carrying capacity of the columns according to the trial results. The GFRP strip at the ends and intermediate regions, with a clear spacing of 100 to 150 mm between the strips, has been proven to be the most effective in achieving ultimate strength, especially for column specimens with full wrapping. Wrapping the GFRP strips increases the strength of square and circular columns by 24 % and 5%, respectively, when compared to unwrapped specimens. The percentage gain in strength is 16% when the cross-section is changed from circular to square. Local and overall flexural buckling, respectively, are the failure modes seen in the square and circular sections. The experimental strength and axial deformation were compared to the analytical results, which showed a satisfactory correlation.

### List of symbols

D	Diameter of the circular column“mm”
b	Breadth of the square column“mm”
d	Depth of the square column“mm”
h	height of column “mm”
t	thickness of the section “mm”
s	clear spacing between the fibre strip “mm”
P <sub>ANSYS</sub>	Finite element ultimate load “kN”
P <sub>EXP</sub>	Experimental ultimate load “kN”
Δ <sub>ANSYS</sub>	Finite element axial deformation “mm”
Δ <sub>EXP</sub>	Experimental axial deformation “mm”

### Subscripts

ST	Square Tube
CT	Circular Tube
EW	End Wrap
IW	Intermediate Wrap
FW	Full Wrap
NW	No Wrap
CFST	Cold-Formed Steel Tube
GFRP	Glass Fibre Reinforced Polymer
CFRP	Carbon Fibre Reinforced Polymer
EXP	Experimental
ANSYS	Finite element software

## 1 Introduction

Steel hollow sections are commonly employed as compression members in a variety of engineering constructions, and they can be produced using both hot-rolled and cold-formed methods. Cold pressing techniques are commonly used to create the thin-walled hollow section. Cold-formed steel tubular sections in commercially available shapes and sizes can be employed for the structure, depending on the purpose. The design approach for determining the axial load and elastic buckling stress was established and compared with forty-five test results in research of thin-walled steel square hollow sections with CFRP [1]. The experimental investigation [2] used a finite element model to anticipate the results of sixteen

experiments using five different commercially available adhesives. The lap shear strength between the tube and the fibre [3] was determined by testing very high strength butt-welded circular steel tubes strengthened with CFRP. Experimentally, a series of tests on reinforcing circular hollow steel tube sections with high modulus CFRP sheets with various bond lengths and layer counts were conducted[4]. Design curves for predicting the capacity of short CFRP-reinforced steel tubular columns in axial compression [5]. A state-of-the-art review of FRP-strengthened steel structures identifies existing research on the subject as well as future research on confined columns [6]. Cold-formed steel channel section confined with CFRP strips wrapped over the web and flange subjected to eccentric compression: experimental and analytical results [7]. The application of

\* Corresponding author:

E-mail address: [sangeethap@ssn.edu.in](mailto:sangeethap@ssn.edu.in)

FRP in the strengthening of steel structures is dependent on several factors, including surface preparation for bonding, adhesive selection, flexural and fatigue strength of steel structures, and so on [8]. Using EC3 and AISI specifications, the ultimate strength of CFRP wrapped cold-formed steel lipped channel columns was calculated [9]. Punitha Kumar and R. Senthil [10, 11], Jai-Woo Park et al [12], Amr Shaat and Amir Z.Fam [13], and Masoumeh Karimian et al [14] are only a few of the researchers who have looked into steel column strengthening using CFRP and GFRP. Generally, thin-walled sections show deformation before yielding the cross-section whereas the thick-walled sections show deformation after yielding of the cross-section. It was expected that FRP sheets confined column sides, control the outward buckling but not the inward buckling [15]. The inward and outward buckling failure of the short column are shown in Figure 1.

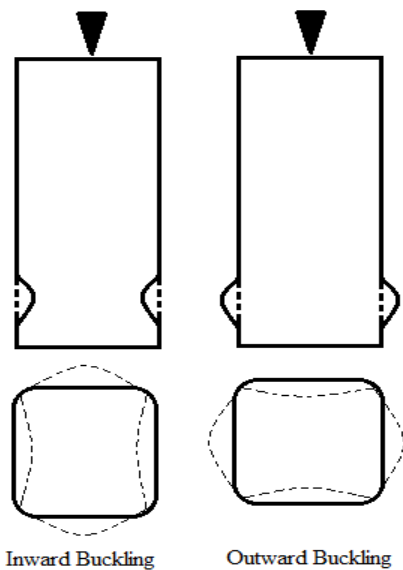


Fig. 1. General failure mode of short column

The behaviour of cold-formed steel tubular columns enhanced with GFRP strips at various positions was reported in this study. The cross section of the tubular column and the position of the GFRP strips were both changed in the investigation. All the columns were tested to

failure under axial compression. The ultimate load-bearing capacity, maximum axial deflection, axial strain, and failure modes were all investigated.

## 2 Experimental program

### 2.1 Fabrication of the column specimen

The specimen was fabricated using cold-formed steel of grade St 34-1079 by IS 1079-2009 specifications. The cold-formed steel square and circular tubular members were cut into lengths of 800 mm using a computerised cutting machine. The slenderness ratio is defined as the ratio between the length of the column to its lateral dimension and it is 10.6 for both square ( $h/d= 800/75$ ) and circular ( $h/D=800/75$ ) cross-section of the tubular member was maintained for comparison. The hollow tubular columns were wrapped with GFRP in the form of strips and tested to failure under axial compression. The coupon test was conducted to study the material properties like yield stress, ultimate stress, modulus of elasticity and elongation of specimen after fracture and they are determined as 267 N/mm<sup>2</sup>, 475 N/mm<sup>2</sup>,  $2.04 \times 10^5$  N/mm<sup>2</sup> and 48 mm respectively. The manufacturer data of GFRP sheets gives that the thickness, tensile strength, tensile modulus, elongation after fracture and mass density thickness are 1 mm, 1724MPa, 76 GPa, 2.8 %, and 2500kg/m<sup>2</sup> respectively. The specimen details and its dimensions are shown in Figure 2 and Table.1.

Before the compression test on column specimens, the outer surface of the CFST columns was cleaned by sandpaper to remove the rust and debris and rough the surface of the column to improve the interlocking property between the steel and the adhesive. For wrapping of GFRP sheet with steel, an epoxy resin Araldite® GY 257 was used. The GFRP strips of wide 100 mm were bonded onto the column specimen and its position is shown in Figure 2. Table.1 also describes measured dimensions of the specimens, the position of the GFRP strip and its clear spacing between the strip. The specimen identification was made as ST – Square Tube, CT – Circular Tube, NW – No Wrap, FW- Full Wrap, IW- Intermediate Wrap and EW- End Wrap. The specification of one specimen from Table. 1, ST – 2IW – EW is the Square tubular section wrapped with two intermediate GFRP strips along with the end strip.

Table 1. Parametres of the CFS wrapped column specimen

Specimen ID	h (mm)	b (mm)	d (mm)	D (mm)	t (mm)	s (mm)	Position of the fiber strip
ST - NW	801	75	75	-	2	-	-
ST – 1IW	802	75	75	-	2	-	Intermediate strip
ST – 2IW	800	75	75	-	2	400	Intermediate strip
ST – EW	802	75	75	-	2	600	End strip
ST – 1IW - EW	801	75	75	-	2	250	Intermediate + End strip
ST – 2IW - EW	803	75	75	-	2	133	Intermediate + End strip
ST – FW	801	75	75	-	2	-	Full strip
CT - NW	802	-	-	75	2	-	-
CT – 1IW	800	-	-	75	2	-	Intermediate strip
CT – 2IW	801	-	-	75	2	400	Intermediate strip
CT – EW	803	-	-	75	2	600	End strip
CT – 1IW - EW	802	-	-	75	2	250	Intermediate + End strip
CT – 2IW - EW	801	-	-	75	2	133	Intermediate + End strip
CT – FW	800	-	-	75	2	-	Full strip

\* h-Height of column, b and d – breadth and depth of the square tube, D- diameter of the circular tube, t-thickness of the cold - formed steel and s - clear spacing between GFRP strip

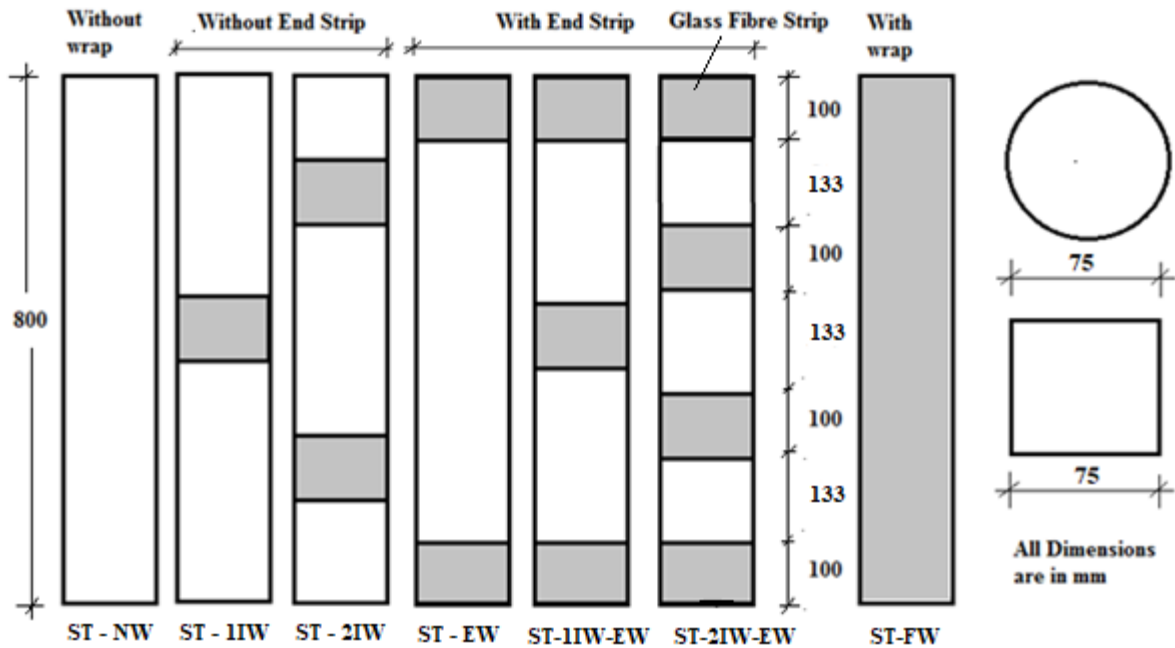


Fig. 2. Details of the CFS wrapped column specimen

## 2.2 Test setup and Instrumentation

All column specimens were tested to failure under axial compression using a Universal Testing Machine (UTM) of capacity 600 kN. The static load was applied at a rate of 0.5 mm/min using hydraulic stroke control [16]. The end of the columns was welded with end plates to achieve pinned support condition. The lateral and axial deflections were measured using two dial gauges having the least count of 0.01 mm. The position of the dial gauges to measure the axial deformation and lateral deformation at mid-height of the

specimen are shown in Figure 3. The longitudinal strain at the mid-height of the specimen was recorded using a 20 mm strain gauge which attached directly to the column specimens either on the steel surface or the fiber surface. The strain values were recorded using a 5-channel strain indicator as shown in Figure 3. The deformation and strain were measured at every 10 kN load interval and all the column specimens were tested until it reaches the maximum load. Figure 3 shows the schematic test setup and experimental test setup.

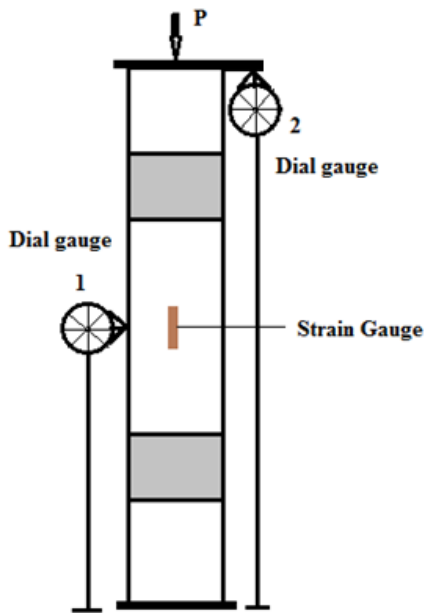




Fig. 3. Test set-up of the CFS wrapped column specimen

### 3 Finite element modelling

#### 3.1 Model description

The 3D FE models of the column specimen with GFRP strip were built using the commercially available software ANSYS. The SOLID 185 and SHELL181 from the element library were used to model the steel tube and GFRP strip respectively[12]. The SHELL element with 6 DOF was used to mesh the specimens. The GFRP wrapped columns were assigned with the material properties obtained from the experimental study to validate the results. To define plastic hardening of the built-up columns, the Von Mises yield surface was used. An axial load was applied at the centre of the top plate, thus load distribution to the specimen, as pressure at the top of the column. The coupling option was

used to connected the nodes between steel and GFRP. Figure 4 shows the mesh model of the square and circular columns with intermediate wrap and end wrap of GFRP.

The pin-end support conditions in terms of displacement and rotation are simulated in the FEA through a reference point both at the top and bottom plate. The translations along x, y and z were constrained against the top end of the plates. The load was applied in increments as sub-steps using Newton-Raphson method from ANSYS library. The overall imperfection was taken as 1/1000 of the overall length of the column, including both the initial bending of the member and initial eccentricity of the loading. For each incremental step of end-shortening, the total reaction at the end is obtained. Using, 'UPGEOM' command in ANSYS, buckling mode was obtained.

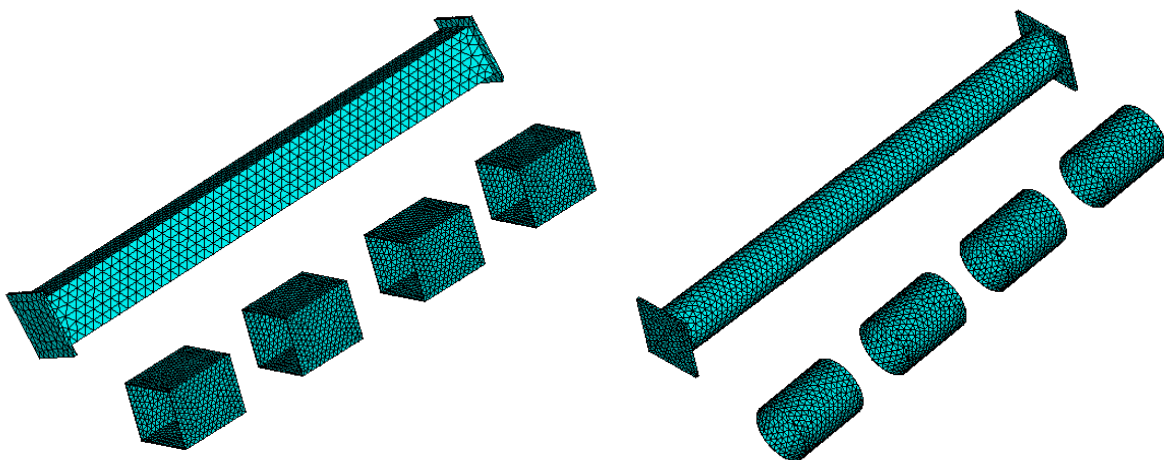


Fig. 4. Mesh model of the column specimen with IW and EW

4 Result and Discussion

4.1 Effect of cross section on GFRP effectiveness

Table 2 gives the experimental results and its comparison. From Table 2, it was found that the strength enhancement of the square and circular tubular columns was 24 % and 5 % respectively as compared to unwrapped columns. The stiffness is the ratio of yield load and corresponding axial deformation, and it was calculated that the stiffness of the circular column was more than the square column with GFRP wrapping. For circular cross-section, the stiffness of the specimens CT – 1 IW, CT – 2 IW, CT – 1 IW – EW, and CT – 2 IW - EW were higher and effective to resist the axial deformation and overall buckling. The Square specimens ST – 2 IW, ST – EW, ST – 2 IW – EW, and ST – FW were able to resist the axial deformation and local buckling, since the stiffness of the specimens is more. Thus the column specimens wrapped with GFRP at intermediate and end portion are effective against local and flexural buckling.

Figure 5 shows the variation of the maximum load-carrying capacity of the square and circular column specimen wrapped with GFRP strip and unwrapped column. Figure 5 shows that axial strength of the square and circular control specimen without wrapping resist the same load but failure mode of the specimen was different. With the change of cross-section from circular to square tubular column, the percentage increase in the ultimate load-carrying capacity was about 16 % for both wrapped and unwrapped columns. The specimens ST-EW and CT-EW wrapped at the end are able to resist more load of 200 kN and 157 kN respectively. The yield point of the column specimens was observed at 70 % of the peak load. The stiffness of the column specimens was calculated by dividing the yields strength. From the ultimate load-carrying capacity of all the specimens, it was found that the specimens with intermediate wrap and combination of end wrap with intermediate wrap were nearly equal to capacity obtained from the specimen which was fully wrapped with GFRP. From this study, it is concluded that optimum spacing between the fiber strip can be 100 mm to 200 mm with end strips to enhance the load carrying capacity of the GFRP wrapped columns.

Table 2. Comparison between the experimental results

Specimen ID	Yield load (P <sub>Y</sub> ) (kN)	Ultimate buckling load (P <sub>U</sub> ) (kN)	Ultimate buckling resistance (F <sub>U</sub> ) (kN/mm <sup>2</sup> )	Axial shortening yield load (Δ <sub>Y</sub> ) (mm)	Axial shortening at ultimate load (Δ <sub>U</sub> ) (mm)	Ratio $\frac{F_U}{F_o}$	Stiffness $\frac{P_Y}{\Delta_Y}$ (kN/mm)
ST - NW	110	155	0.265(F <sub>o</sub> )	1.72	2.87	-	63.95
ST – 1IW	133	190	0.325	1.43	2.97	1.226	76.92
ST – 2IW	133	190	0.325	1.02	2.50	1.226	107.84
ST – EW	140	200	0.342	1.30	3.35	1.290	84.62
ST – 1IW - EW	133	190	0.325	1.63	3.30	1.226	67.48
ST – 2IW - EW	133	190	0.325	0.95	2.35	1.226	115.79
ST – FW	133	190	0.325	1.15	2.60	1.226	95.65
CT - NW	105	150	0.327(F <sub>o</sub> )	2.30	6.40	-	47.83
CT – 1IW	106	152	0.332	0.28	5.00	1.013	400.00
CT – 2IW	109	155	0.338	0.51	5.60	1.033	215.69
CT – EW	110	157	0.342	2.00	6.45	1.047	55.00
CT – 1IW - EW	110	160	0.349	1.00	6.25	1.067	110.00
CT – 2IW - EW	110	160	0.349	0.11	5.80	1.067	1000.00
CT – FW	110	160	0.349	1.36	4.77	1.067	80.88

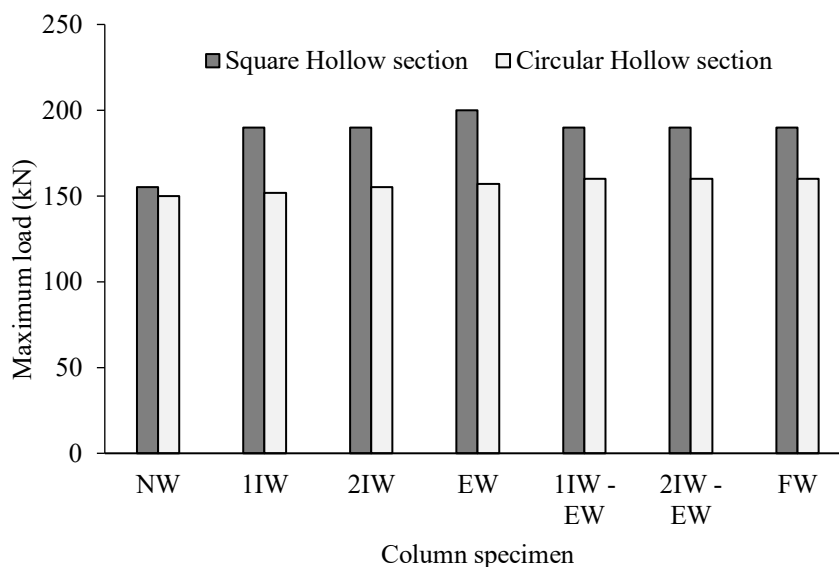


Fig. 5. Comparison between the strength of the square and circular columns wrapped with GFRP

4.2 Load-axial deformation behaviour

The typical axial load-axial deformation characteristics for the column specimens tested are shown in Figures 6&7, which gives the comparison of the square and circular sections with GFRP strips at the end and intermediate position. The axial deformation was recorded from the dial gauge with the least count of 0.01 mm. The curves describe the influence of the fibre strip at the end and intermediate on the axial deformation. The presence of strip at the end and intermediate location reduces the overall buckling of the column specimens. From figure 6, it was found that stiffness of the specimen ST – 2IW – EW was more than the specimen which is fully wrapped specimen ST – FW. The load-axial deformation behaviour of the column specimens differs according to the cross-section and position of the GFRP strip. The slopes of the load-deformation curves, for the square and circular specimen also differ based on the fibre position. It is observed from figure7, specimen CT – 2IW – EW and CT – 1IW – EW are stiffer than the circular column wrapped fully (CT – FW).

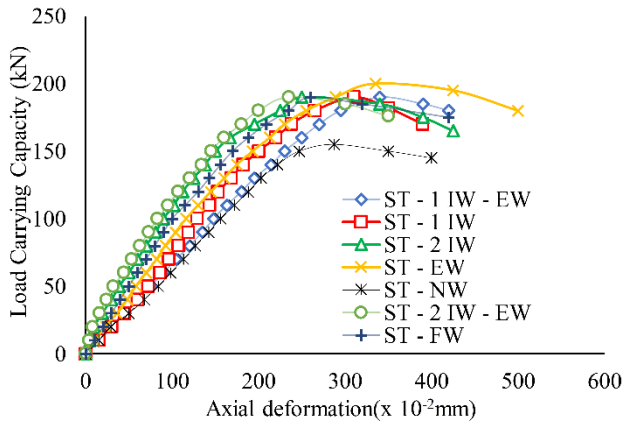


Fig. 6. Load-axial deformation of cold-formed steel square hollow column strengthens with GFRP strip

Figure 8 shows the comparison between experimental and analytical behaviour of the load-deformation behaviour of the circular and square tubular column without GFRP wrapping (CT-NW & ST-NW). From Figure 8, it was observed that the finite element developed using ANSYS was able to predict the load versus axial deformation

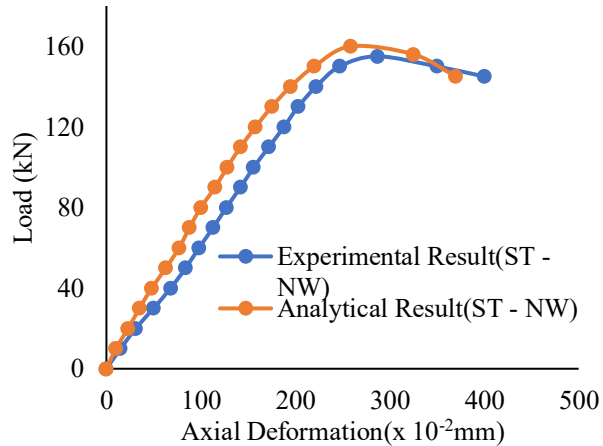
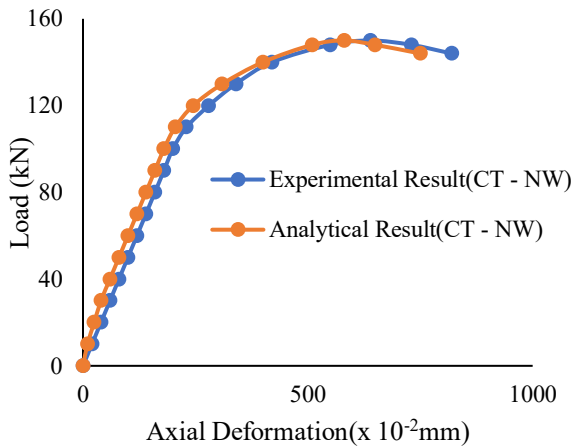


Fig. 8. Comparison between the experimental and analytical load-deformation behaviour (CT-NW & ST-NW)

behaviour of the unconfined column accurately. The FEM model closely predicts the experimental behaviour, thus providing a good correlation against experimental behaviour.

4.3 Load-strain behaviour

The axial load plotted against the axial strain of GFRP strip strengthened column specimens are shown in Figures 9&10 for square and circular cross-section respectively. The strain values were recorded using strain gauge fixed at the mid-height of the specimens. At average strain values of 0.0019, it was observed that all the specimens were initiated to buckle laterally. From Figure10, the strain value decreases for the specimens like CT –FW, CT – 2IW, and CT – EW, thus the confinement pressure of GFRP reduces the strain when compared to the unconfined specimen. The specimen with GFRP sheets confines and provides resistant against both axial and lateral deformation, thereby increasing the resistance against axial deformation of the confined specimen. Once the strain reaches beyond the ultimate tensile strain of the fibre, the specimen mainly fails by GFRP rupture at the end strip both in square and circular cross-section.

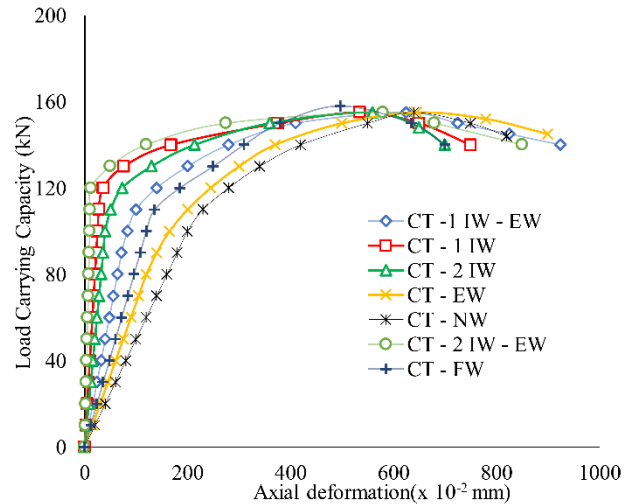


Fig. 7. Load-axial deformation of cold-formed steel circular hollow column strengthens with GFRP strip

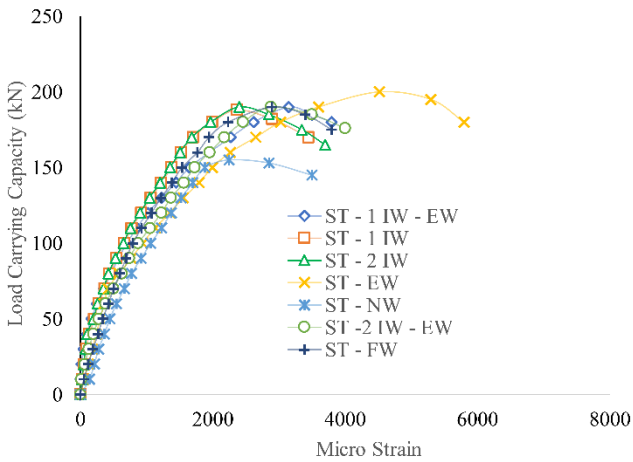


Fig. 9. Load -Micro strain of cold-formed steel square hollow column strengthens with GFRP strip

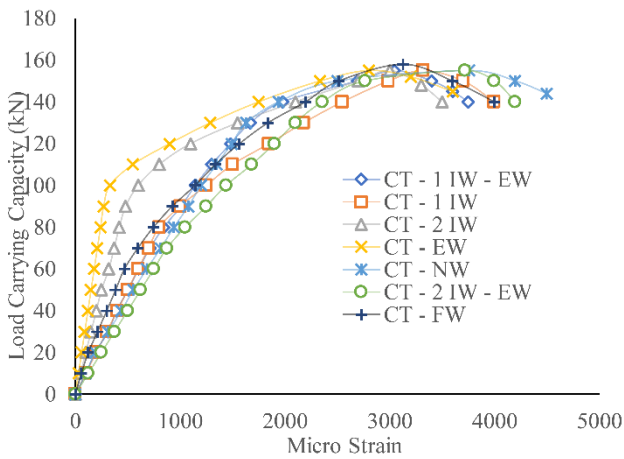


Fig. 10. Load -Micro strain of cold-formed steel circular hollow column strengthens with GFRP strip

#### 4.4 Failure Mode

All the column specimens with different positions of the GFRP strip were tested to failure under compressive load. Figure 11(a) shows the specimens with square cross-section experienced local buckling namely Elephant – foot failure at the top and bottom of the specimens[16]. In this kind of failure, the depth and breadth of the square section became wider. The local buckling in the square cross-section was observed at two opposite faces, buckled inward and buckled outward as mentioned in Figure 1. The specimen ST – NW and ST – FW fails at the base of the specimen by local buckling. For the specimens with end strip of GFRP i.e. ST – EW, and ST – 1IW – EW, failure of the specimen occurred at one-fourth column height as outward buckling. It is also observed from the Figure 11(a) the specimens without end strip, fails at different locations, it mainly depends on the clear spacing between the intermediate strip. Near the corners it was observed that the GFRP delaminated from the steel at the place of buckling [2].

In all GFRP wrapped circular specimens, failure occurred mainly by overall buckling of the specimen and followed by the local buckling in the compression zone near the mid-height of the CT – NW and CT – FW specimen as shown in Figure 11(b). The overall buckling gets reduced in the fully GFRP specimen as compared to the no-wrap specimen, which implies GFRP retard or reduce the failure. The circular column specimen with end strip fails both by flexural and local buckling. The position of the local buckling was at one-fourth height of the specimen for all the specimens wrapped at the end (CT – EW, CT – 1IW – EW and CT – 2IW – EW). The column specimens with intermediate strip alone (CT – 1IW and CT – 2IW) fail both by flexural and local buckling at one-third height of the column and the top on to the compression side. All the specimens confined with GFRP strip were analysed using ANSYS and the deformed shape of the column specimens (experimental and analytical) are shown in Figures 12(a) & 12(b). The analytical results were validated with the test results and good agreement between the experimental and analytical mode were achieved [17].

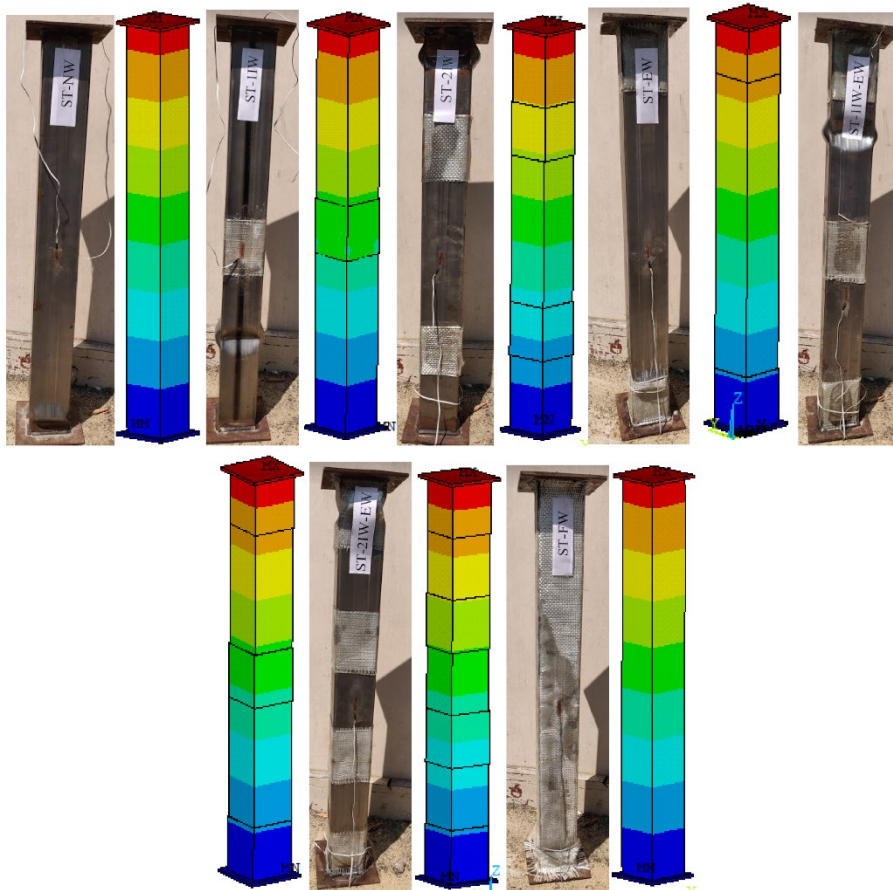


(a)

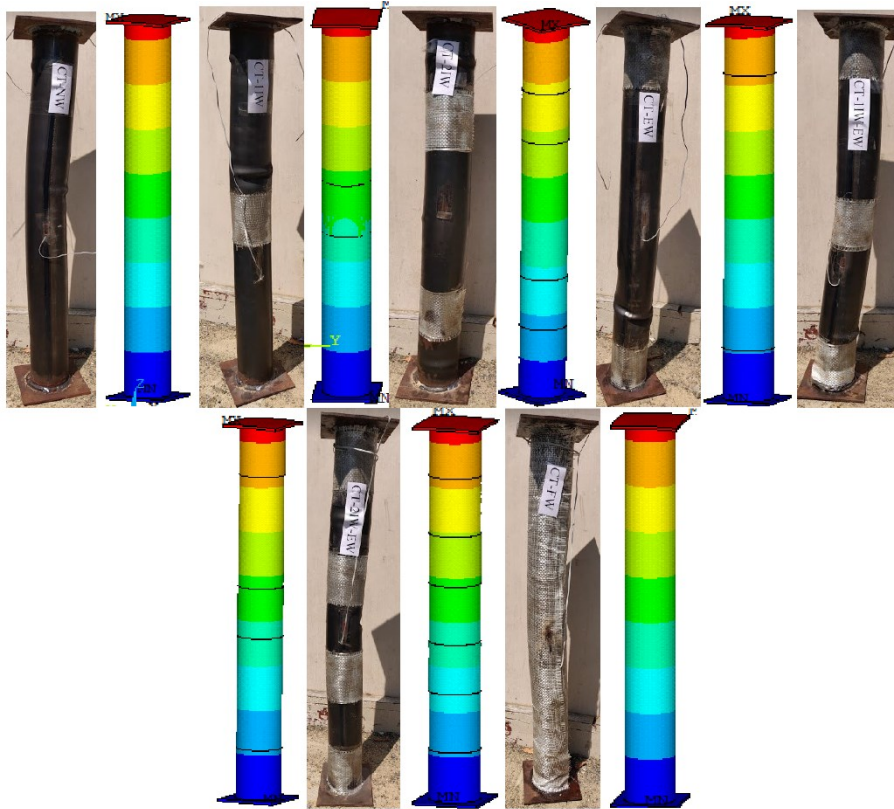


(b)

Fig. 11. Specimens after test



(a) Square Column with GFRP strip



(b) Circular Column with GFRP strip

Fig. 12. Deformed shape of the fibre strengthened specimens

Table 3. Summary of the experimental and FEM results

Specimen ID	$P_{EXP}$ (kN)	$P_{ANSYS}$ (kN)	$\frac{P_{ANSYS}}{P_{EXP}}$	$\Delta_{EXP}$ (mm)	$\Delta_{ANSYS}$ (mm)	$\frac{\Delta_{ANSYS}}{\Delta_{EXP}}$	Failure Mode
ST - NW	155	160	1.03	2.87	2.59	0.90	L
ST - 1IW	190	195	1.03	2.97	2.27	0.89	L
ST - 2IW	190	197	1.04	2.50	2.25	0.90	L
ST - EW	200	205	1.03	3.35	3.01	0.90	L
ST - 1IW - EW	190	199	1.05	3.30	2.94	0.89	L
ST - 2IW - EW	190	201	1.06	2.35	2.22	0.94	L
ST - FW	190	205	1.08	2.60	2.17	0.83	L
Mean			1.044			0.895	
Std Deviation			0.020			0.032	
COV			1.871			3.601	
CT - NW	150	160	1.07	6.40	5.81	0.91	F + L
CT - 1IW	152	162	1.07	5.00	4.85	0.97	F + L
CT - 2IW	155	165	1.06	5.60	4.35	0.83	L
CT - EW	157	160	1.02	6.45	5.27	0.82	L
CT - 1IW - EW	160	164	1.03	6.25	5.38	0.92	F + L
CT - 2IW - EW	160	166	1.04	5.80	4.78	0.92	F + L
CT - FW	160	171	1.07	4.77	3.97	0.91	F + L
Mean			1.050			0.896	
Std Deviation			0.022			0.054	
COV			2.067			6.030	

F = Flexural Buckling; L = Local Buckling

The test ultimate load values ( $P_{EXP}$ ) were quite close to the ultimate load values ( $P_{ANSYS}$ ) obtained for the finite element analysis as shown in Table. 3. The mean and standard deviation of the  $P_{ANSYS} / P_{EXP}$ , read as 1.044 & 0.02 for SHS and 1.050 & 0.022 for CHS. Similarly, the ratio of axial deflection observed between the test and FEM ( $\Delta_{ANSYS} / \Delta_{EXP}$ ) read the mean and standard deviation as 0.895 & 0.032 for SHS and 0.896 & 0.054 for CHS.

## 5 Conclusions

In this paper, the effect of strengthening the cold-formed steel square and circular column using GFRP strip were investigated both in the experimental and analytical studies. A series of fourteen tests of cold-formed steel tubular sections with externally bonded GFRP strips was conducted to study the strength and buckling behaviour of tubular member. The analytical study using ANSYS was carried out and validated using the experimental results. The effect of GFRP strips at different locations and their behaviour were compared. The conclusions derived from this study are as follows.

1. The square tubular columns and circular tubular columns fail by local and global buckling.
2. The GFRP strips at the ends with one or two intermediate strips delay the local buckling and they occur at one-third and one-fourth height of the column of the specimen with one intermediate and two intermediate strips along with the end strip respectively.
3. The percentage increase in the strength was 16 % for change of cross-section from circular to square tubes.

The square and circular column specimens with GFRP strip at ends can resist more load of 200 kN and 157 kN respectively.

4. The strength enhancement of the square and circular tubular columns was 24 % and 5 % respectively as compared to unwrapped columns.

5. The stiffness of the square and circular tubular column with end and the intermediate strip was more than the specimens with fully wrapped specimens, which gives confidence of using GFRP strips at specific location instead wrapping fully and it also reduces the amount of fiber usage.

6. The results indicate that the ultimate buckling resistance with intermediate and end GFRP strips is sensitive to the cross-sectional area of the tubular section that causes local and global buckling of the columns under axial compression.

7. Once the strain reaches beyond the ultimate tensile strain of the fibre, all the specimens mainly fail by GFRP rupture at the end strip both in square and circular cross-section. The rupturing of the fibre was not observed for the specimens with the intermediate strip.

8. The finite element model developed for the wrapped column specimen in the study, predicts the strength accurately with the mean and standard deviation of 1.047 and 0.020 respectively.

## Acknowledgment

The authors would like to thank the Management and Principal, Sri Sivasubramaniya, Nadar College of Engineering, Chennai, India.

## References

- [1] Bambach, M. R., Jama, H. H., & Elchalakani, M. (2009) Axial capacity and design of thin – walled steel SHS strengthened with CFRP. *Thin-Walled Struct* 47(10):1112-1121.
- [2] Fernando, D., Yu, T., Teng, J. G., & Zhao, X. L. (2009) CFRP strengthening of rectangular steel tubes subjected to end bearing loads: Effect of adhesive properties and finite element modelling. *Thin-Walled Struct* 47(10):1020-1028.
- [3] Jiao, H., & Zhao, X. L. (2004) CFRP strengthened butt – welded very high strength (VHS) circular steel tubes. *Thin-Walled Struct* 42(7), 963-978.
- [4] Fawzia, S., Al-Mahaidi, R., Zhao, X. L., & Rizkalla, S., (2007) Strengthening of circular hollow tubular sections using high modulus CFRP sheets. *Constr Build Mat* 21(4):839-845.
- [5] Jimmy Haedir, S., & Xiao-Ling Zhao., (2011) Design of Short CFRP-reinforced steel tubular columns. *J Constr Steel Res* 67(3):497-509.
- [6] Zhao, X.L., & Zhang Lei, (2007) State-of-the-art review on FRP strengthened steel structures. *Eng Struct*, 29(11):1808-1823.
- [7] Hongyuan Tang., Canjun Wang & Ruijiao Wang, (2016) Enhancing Stability of Thin- Walled short steel channel using CFRP under eccentric compression. *Int J Polymer Science*, 2016(2790385):1-11.
- [8] Teng, J.G., Yu, T., & Fernando, D., (2012) Strengthening of steel structures with fiber-reinforced polymer composites. *J Constr Steel Res* 78(11):131-143.
- [9] Silvestre, N., Young, B., & Camotim, D. (2008) Non-linear behaviour and load-carrying capacity of CFRP-strengthened lipped channel steel columns. *Eng Struct*, 30(10):2613–2630.
- [10] Punitha Kumar A., & Senthil R (2016) Behaviour of CFRP strengthened CHS under axial static and axial cyclic loading. *KSCE J Civ Eng* 20(4):1493-1500.
- [11] Punitha Kumar A., & Senthil R (2016) Axial Behaviour of CFRP-Strengthening circular steel hollow sections. *Arab J Sci Tech* 41(4):3841-3850.
- [12] Jai –Woo Park, Hee-Jin Yeom & Jung-Han Yoo (2013) Axial loading tests and FEM analysis of slender square hollow section (SHS) stub columns strengthened with carbon fiber reinforced polymers. *Arab J Sci Tech* 13(4):731-743.
- [13] Amr Shaat & Amir Z. Fam (2009) Slender steel columns strengthened using high-modulus CFRP plates for buckling control. *J Comp Constr* 13(1):2-12.
- [14] Masoumeh Karimian, Kambiz Narmashiri, Mehdi Shahraki & Omid Yousefi (2017) Slender steel columns strengthened using high-modulus CFRP plates for buckling control. *J Constr Steel Res* 138(11):555-564.
- [15] Dabaon, M., Ellobody, E., & Ramzy, K. (2015) Experimental investigation of built-up cold-formed steel section battened columns. *Thin-Walled Struct* 92:137–145.
- [16] Davison, B., & Owens, G. W. (Eds.). (2011) *Steel designers' manual*. New York: Wiley.
- [17] Nuno Silvestre., Dinar Camotim & Ben Young, (2009) On the use of the EC3 and AISI specifications to estimate the ultimate load of CFRP-strengthened cold-formed steel lipped channel columns. *Thin-Walled Struct* 47(10): 1102-1111.

## Građevinski materijali i konstrukcije Building Materials and Structures

journal homepage: [www.dimk.rs](http://www.dimk.rs)

doi: 10.5937/GRMK2104261Y UDK: 624.21 (73)

Original scientific paper



### Supply and Demand in Engineering and Management

Bojidar Yanev <sup>\*1)</sup><sup>1)</sup> Department of Civil Engineering & Engineering Mechanics Columbia University, New York

#### Article history

Received: 19 September 2021

Received in revised form: /

12 November 2021

Accepted: 19 November 2021

Available online: 30 December 2021

#### Keywords

bridge,  
demand,  
energy,  
money [\$],  
performance,  
resilience,  
robustness,  
supply

#### ABSTRACT

All successful infrastructure products and processes exemplify the collaboration of engineering and economics in space and time. In their respective domains, the two specialized professions optimize supply and demand (S / D) of energy and money. If their priorities diverge, structural and economic failures result. The various stages of a bridge lifecycle and the transitions between them are examined as vulnerable nodes and links where diverging constraints of supply and demand must be reconciled. Robustness, resilience and sustainability are considered as properties which, if sufficiently defined, can model realistically the cost-effective performance of the infrastructure under varying conditions over extended lifecycles.

#### 1 Introduction: supply / demand (S / D) in economics and engineering

The Industrial Revolution channeled the social transactions and acquisitions of intelligence, information, money and energy in increasingly specializing professions. Concurrent technological and economic schools of thought evolved as a result. In the dimensions of physics, natural information / energy and time / space are integrated. In the dimensions of economics, social ones are distinct. Economics and engineering process and produce tangible social assets, however they operate in social and natural time / space, respectively. Engineering harnesses natural information and energy into relatively more permanent products. The universally valid laws of thermodynamics underly all design of engineering products. Economics specializes in more dynamic processes in terms of money, whose value is local and transient. Engineered structures demonstrably supply strength superior to the service demands. Demands exceeding supplies energize social development. As a result, engineering solutions attain a higher level of determinacy in the natural environment than do those of economics in society. Von Neumann and Morgenstern [1] acknowledge: "Our knowledge of the relevant facts of economics is incomparably smaller than that commanded in physics at the time when mathematization of that subject was achieved". In Eq. 1 – a and – b the defining contrast between the two fields is reduced to the supply / demand (S / D) equilibria governing them:

$$\begin{aligned} \text{Economic processes: } S < D \text{ [\$]} & \quad (1-a) \\ \text{Engineering products: } S > D \text{ [Energy]} & \quad (1-b) \end{aligned}$$

The inequalities of Eq. 1–a and –b express opposite dynamics in incongruent dimensions. They reflect the varying unsatisfied demand inherent in all economic processes and the invariable satisfaction supplied by all engineered structures. Economics improves the process of supply S to meet the greater demand D. Engineering perfects the oversupply S in products creating future demand D. Economics maximizes by indeterminate negotiations under the restraint of money. Engineering optimizes by deterministic calculations under the constraint of energy. Both utilize the instruments, tools and methods of art and science. In both, reversing the governing inequalities of Eq. 1 produces failures. With luck, the claims of 're-engineering government' and 'economical structures' remain overreaching fantasies. Drucker's [2] statement is quantifiable in engineering dimensions: "Everything degenerates into work". Managers also agree that bottom lines crystalize in money.

Table 1 presents a comparison between the specialized domains of economics and engineering. The two systematically mingle and borrow from each other. The processes and products of the transportation infrastructure are optimized when they integrate. The inherently different restraints and constraints on the supply and demand in the two fields are briefly examined, in order to qualify and quantify the terms of their collaboration.

\* Corresponding author:  
E-mail address: [bojidaryanev1@gmail.com](mailto:bojidaryanev1@gmail.com)

Table 1. Economics and engineering

	Economics	Structural Engineering
Domain	Society	Nature
Instrument	Politics	Physics
Preferred models	Probability, Statistics	Determinism, Mechanics
Type of equilibrium	Dynamic, unstable	Static, stable
Method	Negotiation	Calculation
Dimensions \$,	Time	Energy, Space
Bounds	Adopted restraint	Imposed constraint
Supply / Demand	$S < D$	$S > D$
Outcome	Process Transaction	Product Acquisition

2 Supply and demand (S/D) in economic processes

Von Neumann and Morgenstern [1] begin by stipulating that “there exists at present no universal system of economic theory” and “if one should ever be developed, it will probably not be in our lifetime”. Hence, they obtain mathematically rigorous solutions for games representing “the endeavor of the individual to obtain a maximum utility, or in the case of the entrepreneur, a maximum of profit”. In that reduced domain demand exceeds the available supplies ( $S < D$ ) and players win / lose or minimize their losses / maximize benefits.

Social models assuming  $S \geq D$  reduce all non-negotiable constraints to optional restraints. If they were attainable technologically and psychologically, a stagnant indifference, analogous to entropic death might result. Hence, the various schools of economics differ primarily on the optimal  $S / D < 1$  ratio and on the constructive means to influence it. From Adam Smith (1723 – 1790), Anne Robert Jacques Turgot (1727 - 1781) and Henri de Saint-Simon (1760 – 1825) to Friedrich Hayek (1899 – 1992) and John Maynard Keynes (1883 – 1946), on to Milton Friedman (1912 – 2006) and John Kenneth Galbraith (1908 – 2006), complementary, contradictory, and conflicted views on the need for ground-up and / or top-down regulation of the economy have evolved and are still in progress. As Von Neumann and Morgenstern state [1], the empirical evidence amassed over centuries remains insufficiently homogeneous and much too subjective to be conclusive. A hopefully realistic expectation is that the top-down / ground-up regulation schools might integrate into an optimal dynamic hybrid. Thus far, the two agree that ‘social engineering’ of the type championed for example by Auguste Comte (1798 – 1857) and Karl Marx (1818 – 1883) is not that hybrid. As a by-product of that conclusion, reached over three centuries of free market research, engineering and economics have specialized in acquiring products in space, and transacting processes in time, respectively.

3 Supply and demand (S/D) in engineering products

In physics, as in economics, a unified theory remains elusive. Von Neumann and Morgenstern [1] point out that “It happens occasionally that a particular physical theory appears to provide the basis for a universal system, but in all instances up to the present time this appearance has not

lasted more than a decade at best.” As in Game Theory, engineering achieves its stated objectives by defining the limited domain over which they apply. Engineered products supply services exceeding known present and expected future demands in terms of quantifiable information and energy. A structure is built to resist greater loads than expected. A new transportation facility is designed to accommodate present and anticipated numbers of users. The material ‘oversupply’ is dimensioned in time and energy, under various names, such as ‘safety factor’, ‘reliability index’, and ‘performance index’. It is perpetually reviewed and refined. When the constraints are rigorously defined, the process becomes optimization.

During the 20<sup>th</sup> century physics gained critically important intelligence about the transactions and acquisitions of information and energy in the natural world. The  $S / D$  relationship in engineering evolved accordingly, as documented in the many editions of the Bridge Design Specifications by the American Association of State Highway Transportation Officials (AASHTO). The Allowable Stress Design (ASD) evolved to Load Factor Design (LFD), and (thus far), to Load and Resistance Factor Design (LRFD), now in its 8<sup>th</sup> edition [3]. The relationship between the demand of loads  $Q$  and the supply of structural resistance  $R$  is stated in Eq. 2–a, –b, and –c, and illustrated in Fig. 1:

ASD (1928):  $R \geq S.F. Q$  (2–a)

LFD (1960s):  $\phi R \geq \sum \gamma_i Q_i$  (2–b)

LRFD (1994):  $\phi R \geq \sum \eta_i \gamma_i Q_i$  (2–c)

where:  $R$  – structural resistance;  
 $Q_i$  – demand of load  $i$ ;  
 $S.F.$  – safety factor;  
 $\phi$  – resistance factor;  
 $\gamma_i$  – factor of load  $i$ ;  
 $\eta_i$  – modifier of load  $i$ .

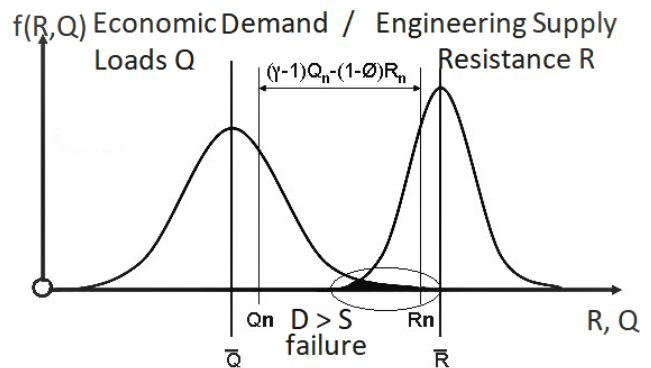


Figure 1. Distribution of load demand  $Q$  and structural resistance  $R$ , recommended by AASHTO LRFD Bridge Design Specifications

The parameters of Eq. 2 are physically quantifiable. However, they also qualify socially evolving views. Engineering supplies resistance  $R$ , constrained by material properties, to meet the demands the economically restrained design loads  $Q$ .

Equation 2 and Fig. 1 are fundamentally deterministic, but they acknowledge the different uncertainties in the socially restrained demand  $D$  for service loads and the naturally constrained supply of structural resistance  $R$ . Material strength and reliability are consistently improving. So are the quality and quantity of information about all pertinent variables. Thus, the supply  $S$  of engineering

resistance  $R$  approaches the demand  $D$  of the loads  $Q$  (as ever from above). Both however, are prone to different uncertainties, which in turn are treated by widely diverse probabilistic models. The entailed professional challenges are addressed for example in Yanev [4]. Higher quality and reduced quantity of materials have produced tallest towers, longest bridges, largest aircraft, and further-venturing spacecraft. The concurrent trends in lifespans and implied safety margins might benefit from a more far-sighted economic assessment, again recognizing the probabilistic and deterministic constraints of its modeling.

**4 Supply and demand ( $S/D$ ) in economics / engineering management**

Drucker [2] wrestled with the vagueness of the management process as follows:

"Management is a practice rather than a science. In this, it is comparable to medicine, law, and engineering. It is not knowledge but performance. Furthermore, it is not the application of common sense, or leadership, let alone financial manipulation. Its practice is based both on knowledge and on responsibility."

The economics and engineering 'knowledge and responsibility' in Drucker's rumination differ. Long-term, both should tend towards maximizing social benefits, however under the opposed constraints of  $S < D$  [\$] and  $S > D$  [energy], respectively, short-term priorities diverge. Economics and engineering do not anticipate convergence to  $S = D$  but they approach that equality by a lower and an upper bound path, respectively.

As financial restraints govern most contemporary management, decisions related to the infrastructure at the highest levels are taken 'top-down' by economists, lawyers and ultimately, politicians, whereas engineers deliver assets 'ground-up'. Figures 2-a and -b illustrate the evolving engineering and management chain of supply and demand. Figure 2-a depicts a bi-lateral relationship between comprehensively resourceful manager and competent builder. From the pyramids, the Code of Hammurabi (1730 - 1685 B.C.), and the Roman aqueducts to some modern 'signature' structures, such exclusive interactions have supplied outstanding products, respecting natural constraints, and selective about social demands. Between 1928 and 1964 the fortuitous collaboration of master manager Robert Moses (1888 - 1981) and master designer Othmar Ammann (1879 - 1966) produced the unique network

of record – breaking spans in New York City. The demands for preserving that network today compete with other services for restrained funding supplies.

Figure 2 – b depicts a typical modern democratic chain of infrastructure management responsibilities. The levels of responsibility, the competences, the constraints, and their dimensions are different throughout the various stages of the process. The  $S/D$  restraints on money and constraints of energy are implicit. As the number of links and nodes increases, so do the potentially vulnerable transitions where  $S/D$  dimensions change and priorities reverse. Economics adjusted to the scientific and technological advances, by shifting its priorities from static acquisitions to dynamic transactions, dimensioned in time, energy, and money. Ground-up at the bottom of the chain in Fig. 2 – b, structural engineering supplies products exceeding the performance demands.

The accelerated pace of social transactions has affected the longevity of structural acquisitions. Whereas old bridges have lasted for centuries, AASHTO currently recommends a useful life of 75 years, and contemporary bridge decks often serve only 30 years. The trend reduces the supply of services by the engineered product but expands demands in the economic process. Therefore, infrastructure management must reconcile ostensibly opposed economic and engineering views and dimensions. Particularly sensitive are the stages involving the disparate sets of actors, with their incongruent dimensions of supply / demand.

In a letter to the author, dated 10/6/1993 President Bill Clinton wrote:

"I agree with you that America must address the problems of its vast network of bridges and highways if we are to remain a strong nation during the next century."

However, on 10/23/1993, Chief Highway Administrator (later Secretary of Transportation) Rodney Slater specified the restraints as follows:

"Needs typically exceed the means available to address them. ... Clearly if funds were unlimited, we would do more."

No profession can compete with engineering in the design and construction of the infrastructure. In management however, engineering must collaborate with economics. The first step in meeting that demand is to model the products constrained in space and energy also as processes restrained in time and money. Bridge management initiated that transition in the U.S. and worldwide during the 1990s. It is reflected for example in [5-8]. Yanev [9] expands the static snapshot of a bridge management operation shown in Fig. 3-a to the dynamic presentation of a bridge lifecycle shown

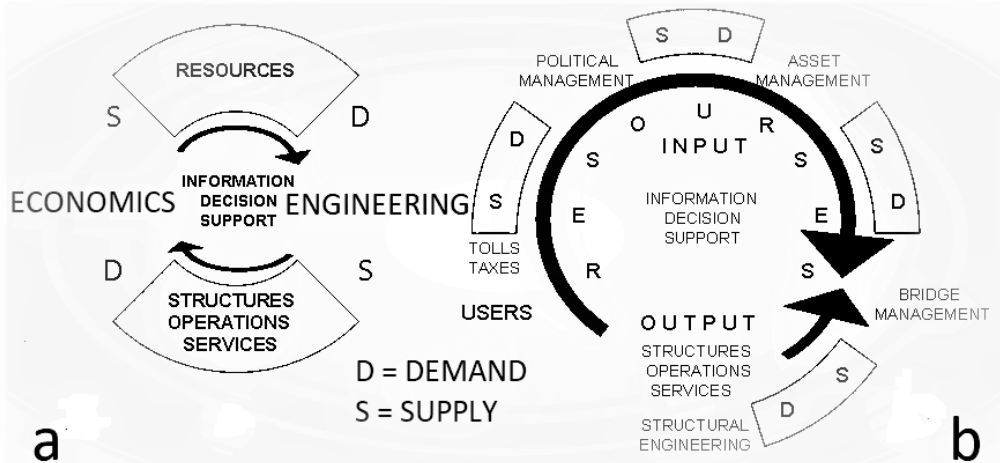


Figure 2. Supply and demand at different levels of management and engineering

in Fig. 3–b. The intelligence, information, money and energy, demanded and supplied at each stage of the lifecycle differ, satisfying different *S / D* ratios, obtained and measured by different means. In a typical transportation network, all stages are concurrent, demanding complementarity and collaboration of the diverse competences.

*Lifecycle costs: present worth (PW) versus annualizing*

Economics and engineering tend to assess future supply and demand by the present worth (*PW*) and annualizing methods, respectively. The *PW* of future costs and benefits is a function of a selected discount rate *i*, according to Eq. 3–a and –b.

$$i = (1 + cc) (1 + fr) (1 + pi) - 1 \tag{3-a}$$

where: *cc* = 'real' opportunity-cost of capital

*fr* = required premium for financial risk associated with the considered investments  
*pi* = anticipated rate of price inflation

Neglecting the higher order terms is justified by their relatively small values and reduces Eq. 3–a to the following:

$$i = cc + fr + pi \tag{3-b}$$

The present worth of an amount *A* occurring *N* years into the future is reduced by the factor  $1/(1+i)^N$ . The aggregate present worth of amounts *a* occurring annually during *N* years from the present is equal to:

$$a \sum_{n=1}^N 1/(1+i)^n = a (1 + 1/i) [1 - 1/(1+i)^N] \tag{4-a}$$

$$\lim_{N \rightarrow \infty} a \sum_{n=1}^N 1/(1+i)^n = a (1 + 1/i) \tag{4-b}$$

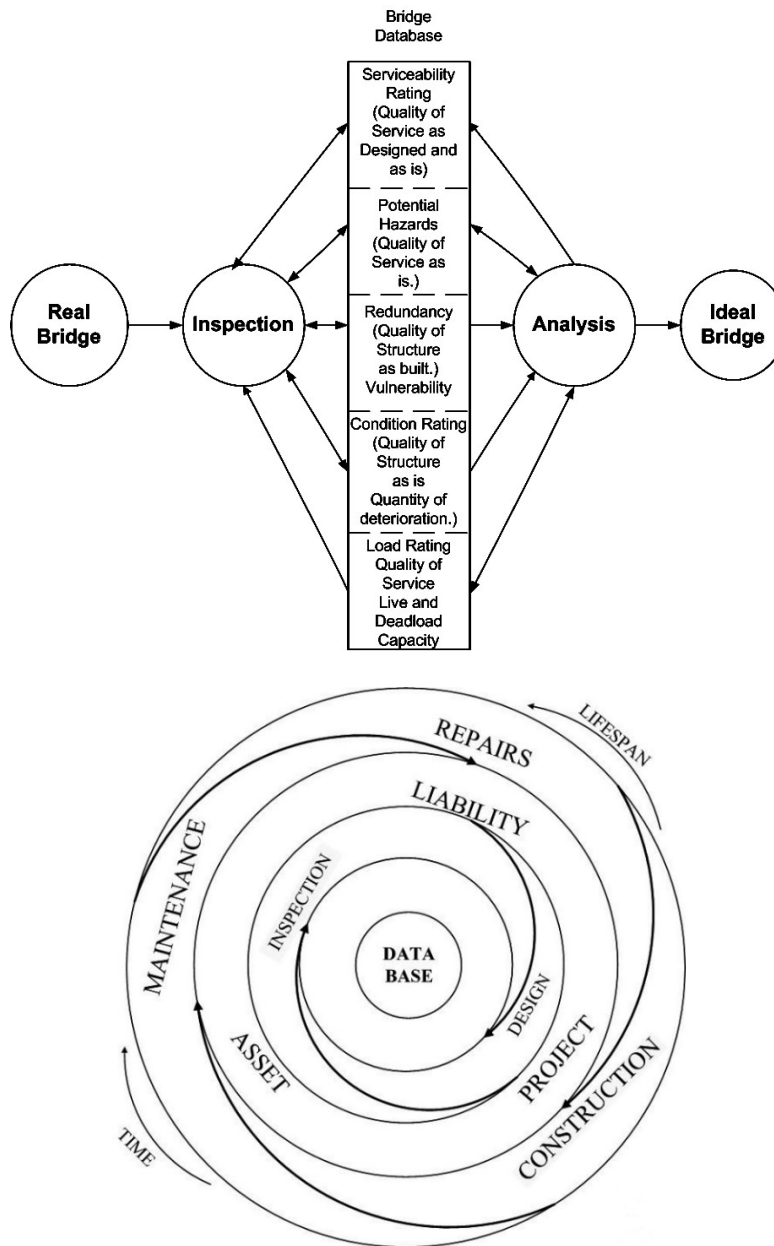


Figure 3. The Bridge Management lifecycle: a: Cross section, b: Plan

Hence,  $i$  determines a finite discounted present worth of the infinite series ( $a, a, a, \dots$ ). The ratio of the discounted sums of a finite  $N$  and  $n$  tending to infinity is equal to:

$$a(1 + 1/i) [1 - 1/(1 + i)^N] / a(1 + 1/i) = [1 - 1/(1 + i)^N] \quad (5)$$

Given a discount rate  $i$ , a period of  $N$  years can be selected such that the neglected remainder of the infinite sum would not exceed an acceptable error  $\epsilon$ , as follows:

$$N = -\ln \epsilon / \ln(1 + i) \quad (6)$$

Yanev [9] shows that, at a discount rate  $i = 4\%$  and a period  $N = 75$  years (the bridge useful life recommended by AASHTO), the remainder of the infinite sum is 5%. The truncated 'attention span' of the  $PW$  method moved Leeming [10] to conclude:

"Future maintenance costs are regarded as visionary while capital costs are real. ... If maintenance of our bridge stock is to remain a fixed percentage of the total governmental expenditure on construction, then there is an argument for a zero-discount rate in calculating the net present value of maintenance."

Annualizing distributes all lifecycle costs equally over the structural life. Whereas economics considers infrastructure assets over a limited time, new engineering facilities permanently alter geographic space. Hence, annual maintenance costs can be expressed as a relatively constant percentage of the renewal cost, changing proportionally over the years. If services are tolled, the annual maintenance can be expressed as a percentage of the revenue. For infrastructure facilities requiring periodic maintenance and replacements, De Gramo et al. [11] recommend *perpetuity*, e.g. a uniform series of indefinitely running payments.

In order to provide for annualized payments  $X$ , a principal  $P$  must be set aside at annual interest  $in\%$  (interest  $\neq$  discount rate), such that  $P in = X$ . If the payments are not annual but arise at  $k$  periods, the relationship becomes:

$$X = P [(1 + in)^k - 1] \quad (7)$$

where:  $P =$  the capitalized value of  $X$ .

Under the diverse engineering and economic assessments of future and even present supply and demand in the domains of money and energy, particularly sensitive are the transitions from one lifecycle stage to the next, when the  $S / D$  parameters and their ratios change. Brief descriptions of each follow.

#### 4.1 Design and selection

Codified design supplies structural resistance in acceptable excess over the demands of standard load combinations or states. Barring the rare error, the constraint of  $S > D$  stipulated in Eq. 2 is satisfied in terms of forces  $R > Q$ . For bridges of average size, forces are applied statically or pseudo-statically. The dynamic demands of the service life are acknowledged for example in fatigue and seismic provisions, and in some serviceability recommendations (including displacements). Redundancy and ductility, allowing load redistribution on the global (structural) and local (element) levels are encouraged.

Performance-based design has become a broadly defined subject, ranging over heterogeneous engineering and economic parameters. This is elaborated for example in [12-15]. The perpetually elaborated demands of a performance-based design by far exceed the laconic form of Eq. 2.

Design selection is one of two critical moments in the structural lifecycle which are briefer than the commonly recognized 'stages', and hence, do not appear explicitly in Fig. 3 – b. Assuming that all design alternatives satisfy  $S > D$  in terms of  $R > Q$ , structural costs are restrained by the supply of money, e.g.,  $S < D$  in terms of  $\$ < \$$ . Lower first costs are strongly favored, even if they might correspond to higher lifecycle costs. The  $PW$  method enhances this effect.

Given adequate funding supply, lifecycle costing considerations can justify higher first costs. An owner can require a larger  $S / D$  ratio, serviceability, inspectability, maintainability, or other design enhancements.

Peer review is targeted by cost-cutting, whereas Value Engineering has emerged as a process of reconciliation between the two opposed constraints of first cost and lifecycle performance. It has an incentive to produce multiple recommendations reducing the demand of first costs. An owner may implement few or none of them.

Despite the extensive commentary of AASHTO LRFD (2017 and earlier editions), structures supplying  $R > Q$  can perform below the long-term and even the short-term demand. Purvis [16] and Yanev [17] are among many arguing that expansion joints fail to satisfy the demand for  $R > Q$  in the domain of forces under normal traffic over relatively short periods. Joints are not considered as essential links in the transfer of live loads and hence, are not designed to resist the impact forces of even moderate service. They fracture, but are not fracture – critical and hence, their under-performance affects resilience and sustainability over long service periods more than it does robustness under brief extreme events. If robustness and resilience were qualified and quantified sufficiently for direct reference in design specifications, they could serve as the criteria of lifecycle needs.

#### 4.2 Construction

The constructors and owners manage energy and money in space and time under different and even opposite constraints. Projects materialize after the supply and demand of these constraints are successfully negotiated. In roughly 80% to 90% of the cases, construction is awarded to the lowest bidder, reflecting the strong economic constraint of first costs. The time constraint is negotiated in terms of contractual incentive / disincentive. Both owner and builder have incentive to minimize the time and space of construction. However, the supply / demand of projects and assets differ. The constructor's incentive is to minimize construction time and cost. The asset manager's incentive is to maximize service and time at minimum cost. As a result, the 'knowledge and responsibilities' in Drucker's [2] preceding quote diverge. Quality assurance of the process (QA) and quality control of the product (QC) traditionally ensure that all contract specifications are met, however both are conducted on a spot-check and sample basis. Under diverging constraints, QA and QC can reduce to spot-checks optimized by risk assessment.

The design / build method reduces the project demand for time by merging the two stages. Once again, design and construction prioritize  $S / D$  differently. Design transacts abstract intelligence and information, whereas construction acquires real money and energy. As the capabilities of analysis and construction are expanding, so are the design options. Ultimately, the design / build method is likelier to restrain the intelligence and information of design to the money and energy constraints of construction.

### 4.3 Delivery and Service

Project delivery, as design selection, is a brief but critical moment in the bridge lifecycle, not explicit in Fig. 3. Both the constructors and the future users have incentives to open the structure to service. As a result, the transition from constructed project to asset in service is plagued by haste and incomplete assessment. All construction constraints of space, time and money may be satisfied at delivery without guaranteeing the owner's ability to deliver service over the structural lifecycle. According to certain management practices large infrastructure projects are inspected 10 years after completion. Divergences from the designed performance are attributed to the responsible parties, including owners, designers and builders. A more volatile economy precludes such practice. When, after 40 years of service, the I-35 bridge over the Mississippi at Minneapolis collapsed on Aug. 1, 2007, the designing consultants were no longer active. The critically important design calculations and construction drawings were unavailable.

Whereas the Federal Highway Administration mandates biennial bridge inspections, it only recommends preservation and serviceability, as in AASHTO 2010 [18] and FHWA 2011 [19]. Some recommendations may translate into performance – based design specifications, however with a considerable time-lag.

So long as FHWA funded construction but not maintenance, the supply of service declined and the demand for construction grew. After the policy was rescinded, the funding could meet more diverse demands, within the same restrained supply. If the total deck area  $A$  of a bridge network and its condition rating  $R$  are relatively constant from year to year, Eq. 8 should reflect the equilibrium between the demand of the annual deterioration  $r$  and the improvement, supplied by reconstruction and repair.

$$(A - A_{rec}) r = A_{rec} \Delta R_{rec} + A_{rep} \Delta R_{rep} \quad (8)$$

where:

- $A$  - the deck area of the bridge network
- $A_{rec}$  - deck area under reconstruction
- $A_{rep}$  - deck area under repair
- $\Delta R_{rec}$  - average annual change of  $R$  of  $A_{rec}$
- $\Delta R_{rep}$  - average annual change of  $R$  of  $A_{rep}$
- $R$  - bridge condition
- $r$  - rate of bridge deterioration in annual increments (=  $\partial R / \partial t$ )

A cost-effective maintenance should reduce the rate of deterioration  $r$ , and hence, the demand for costlier reconstruction and repair. Yanev [9] points out that maintenance and preservation supply unquantifiable benefits over indeterminate lifecycles, whereas their funding demands are immediate and compete with the more attractive capital condition upgrades. The supply / demand ( $S / D$ ) of service and of structural preservation are easier to 'monetize' at toll structures. By incorporating maintenance into the more general preservation, FHWA 2011 [19] allows the qualifying activities to be planned as discrete projects with quantifiable costs / benefits.

The demands of probable random extreme events are more effective than those of predictably determinate regular maintenance in supporting bridge serviceability demands. Robustness has emerged as a measure of structural performance under unique loading demands over limited time. Resilience and sustainability expand that demand over the recovery and the ensuing lifecycle.

### 5 Supply and demand $S / D$ in masterpieces and 'signature' structures

The Renaissance separated art and science, predating, and prefiguring the separation of economics and engineering in the Industrial Age. The French language refers to large infrastructure assets as *ouvrages d'art*. A structural masterpiece exceeds lifecycle service demands within economic constraints to such a degree that it becomes a 'signature' of the professional art and science. According to Billington [20] the two fundamental ideas of structural art are efficiency and economy (of both process and product). The author argues that the products of structural artists, such as Eiffel, Roebling, and Freyssinet continually meet service demands, while their process minimized first costs. The Brooklyn, Golden Gate, and George Washington bridges, and the Eiffel Tower have become signatures of their creators and of their localities. If structural masterpieces have established their standing over millennia, 'signature' structures deliver instant gratification. In a reversal, the demand for a 'signature' structure can precede its ability to supply the service within the governing constraints.

Demands for 'signature' structures relax funding restraints. The advanced analysis and construction capabilities can foster the illusion that the energy constraints in terms of  $R > Q$  are similarly relaxed. In such instances, the long view of supply / demand in terms robustness, resilience and sustainability introduces a sobering restraint.

'Signature' structures have resulted from individual visions, as well as from popular demand (as in the case of the San Francisco – Oakland East Bay Bridge). President François Mitterand's Grands Travaux burnished his pharaonic image, but over time joined older Paris signatures. At the Viaduct de Millau Lord Norman Foster and Michel Virlogeux designed, and Eiffage constructed a masterpiece, such that  $R > Q$ . Fifteen years later the structure bears the signature of its authors and of the region.

### 6 Supply and demand ( $S / D$ ) in structural failures

Engineering commonly attributes structural failures to a demand of loads equaling or exceeding the supply of resistance in terms of forces ( $R \leq Q$ ). However, most failures can be traced to multiple coinciding supplies falling short of demands ( $S < D$ ) in the dimensions of time and money. The investigation following the failure of the Silver Bridge at Point Pleasant in 1967 found critical deficiencies in all stages of its lifecycle, including design, construction, maintenance, and inspection. One assessment of the collapse in 1994 of the Seongsu Bridge over the Han River in Seoul, found the structure "poorly designed, built, and used". Multiple causes were identified after the failures at the Charles de Gaulle airport in France in 2004 and suspected at the I-35 bridge over the Mississippi in Minnesota in 2007. At each lifecycle stage the  $S / D$  relationships imply and reflect different vulnerabilities in the process and the product.

#### 6.1 Design and construction

A restrained supply of money is unlikely to cause deliberate design or construction error however, it can constrain time and thus render the process vulnerable. Since the quantities supplied and demanded in construction exceed those for design, that is when a misplaced  $S < D$  ratio is likelier to affect the  $R > Q$  ratio adversely. Since QC and QA can add to the cost and delay delivery, their demands

can be viewed as counter-productive and targeted for 'streamlining'.

## 6.2 Service

It is impossible to estimate how many service failures have been prevented as a result of the bridge management efforts following the Silver Bridge failure, not only in the USA, but worldwide. The main contribution is due to the funding of the National Bridge Inventory (NBI) and the biennial inspections of vehicular bridges. The push for funding of bridge lifecycle extension has been less effective. Among the reasons may be the institutional inertia restraining all 'expense' funding to  $S < D$ . The funding of large (possibly 'signature') projects is popular, but the continuing preservation of assets is 'streamlined' and eliminated. Thus, each stage of the lifecycle inherits pending demands from the preceding ones and expands them to the next one. Concurrently, it is argued that biennial inspections should be relaxed to a 'risk-based' schedule at the discretion of the owner.

## 6.3 Management

If failures are expressed as  $S \geq D$  and  $S \leq D$  by economics and engineering, respectively, they are bound to occur when the processes and products managed by the two domains unduly influence each other. Hence, all failures are failures of management. Just as structural failures are likelier at links transferring loads between elements, so are management failures likelier at transfers of responsibilities. Figure 2 – b illustrates the proliferation of such links. Engineering design delivers redundant products. Economic management 'streamlines' processes by eliminating 'duplication of effort'. As time and money are negotiable restraints in economics and absolute constraints in engineering, most management failures can be traced to unreconciled economic and engineering supply of and demand for time and money.

## 7 Supply and demand ( $S/D$ ) for robustness, resilience, and sustainability

Robustness, resilience, and sustainability are relatively new qualifiers (and hopefully, quantifiers) of structural performance during regular service and extreme events. Their many and still slightly vague definitions reveal an attempt to reconcile the diverse  $S/D$  restraints and constraints governing the various stages of structural lifecycles. For structures designed to supply  $R > Q$ , robustness and resilience gain significance when 'adverse' conditions threaten to reverse that inequality. Bruneau and Reinhorn [21] define resilience as "the ability to prepare and plan for, absorb, recover from, and more successfully adapt to adverse events". Robustness is defined as the ability of a structure or network with an impaired resistance to redistribute its supply to meet the load demand in constrained time, for example during 'extreme events'. Thus, robustness can be dimensioned in space and energy, and resilience – in time and money. The two properties are correlated with structural redundancy and ductility and can be extended from structural design to network management. A resilient network comprises robust assets. A sustainable asset must be a network of robust and resiliently linked elements. In Fig. 4 robustness and resilience are superposed

over the codified strength and stability governing performance-based structural design. The figure illustrates the following stages:

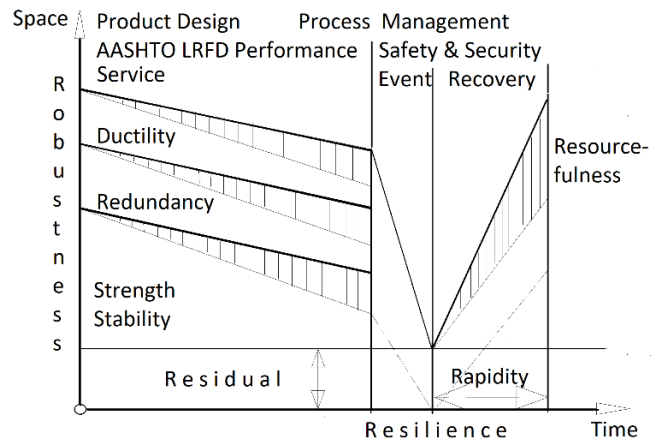


Figure 4. Robustness, resilience, and the structural performance properties currently designed according to specifications

- Performance – based design according to AASHTO 2017 [3] supplies structural strength, stability, ductility, and redundancy to exceed rigorously codified demands, including regular service loads, environmental conditions and 'extreme events'.

- 'Normal' service conditions gradually reduce the as-built levels of the structural properties. The rate of decline is drawn as a range, rather than a line, to represent the implicit uncertainties and variability, as discussed for example in Yanev [4].

- 'Extreme demands' of brief durations reduce the structural supply to an uncertain new level. Any residual supply of structural resistance is a measure of its robustness. The time during which the impaired structure can supply some level of service is a measure of its resilience.

- The rapidity with which the supply of service can be restored to meet and exceed acceptable demand levels is a measure of resourcefulness.

With some qualifications, the reasoning can be extended to networks. If a network's sustainability is quantified by its annualized lifecycle supplies and demands, robustness and resilience can be shown to improve it, in both engineering and economic terms.

## 8 Conclusions

Under the dynamic social restraints and more permanent natural constraints, the different managers of bridge economics and engineering optimize (or more often prioritize) the supplies  $S$  and demands  $D$  of different resources, over different time – horizons. The resources of energy and money tend to, but do not reach,  $S = D$  by upper- and lower-bound routes. At various stages of their activities, both economics and engineering may apply ratios of  $S/D > 1$  and  $S/D < 1$  to different parameters under different restraints and constraints. Engineering designs the relatively stable parameters of products such that  $R > Q$ , but once it adopts time and money as governing constraints (as for example during construction), it too seeks to minimize the supply of services and costs. Thus, engineers and economists may tend to demand and to supply more and less than the necessary funding. Therefore, it must be

recognized whether these ratios are as intended, or due to mismanagement. Economics expects future supplies to meet current demands. Present engineering supplies exceed projected future demands. In all structural achievements economics and engineering have reconciled that difference. They must do so perpetually, as rigorous optimization is not possible. The alternative is failure.

Billington [20] points out that masterpieces create the false impression of courting risks, because they meet demands with minimum supply of material, time and money. In the meanwhile, insufficient supply is blamed for failures. Upon closer examination of an engineered masterpiece, it appears that  $R > Q$  is a hard constraint in the domain of ultimate forces, but  $S < D$  has been an optimized restraint of the initial resources.

In a market democracy the overriding political management supplies services to voters. Consequently, it is highly risk-averse over its short-term mandate, but has limited long-term incentive and competence in economics, let alone engineering. As a result,  $S/D$  optimization can narrow down to risk minimization. Qualifying management and inspections as 'risk-based' signals not a reduction of risk by increasing supply, but a reduction of supply, while trying to control risk. The risk of supplying only the means demanded by hazard mitigation, common in the early days of bridge management, can creep back into it.

From their origin in assessing structural performance under extreme events, robustness, resilience and sustainability are expanding to integrated qualifiers and, potentially, quantifiers of transportation networks in economic and engineering terms. Moreover, they are applicable to management itself, with its nodes and linkages, as illustrated in Fig. 2–b. Sustained robustness over extended periods within the restraints and constraints of the available supplies amounts to resilience. Such a definition expands the design responsibility from the performance of the product under specified loads to the benefits of the process within the social fabric over the time of service. Restraints of money and constraints of energy reconcile. In this expanded view, sustainable design and management can be qualified and quantified for consideration in political debate. Thus far, the design, construction and preservation of robust, resilient and sustainable bridges are recommended. Forthcoming bridge design specifications are addressing this subject in more concrete terms.

The optimal supply and demand of the hard-fought 1.3 trillion \$US (2021) for upgrading the nation's 'hard' infrastructure will require rigorous and authoritative engineering end economic collaboration along the described terms.

## References

- [1] Von Neumann, John and Oskar Morgenstern, *Theory of Games and Economic Behavior*, John Wiley & Sons, Inc., New York, N.Y., 1945.
- [2] Drucker, Peter F., *Management*, Harper & Row, Publishers, New York, N.Y., 1973.
- [3] AASHTO, LTRFD Bridge Design Specifications, 8<sup>th</sup> Edition, American Association of State Highway Transportation Officials, 2017.
- [4] Yanev, Bojidar, *Probability and Determinism in Bridge Management*, *Building Materials and Structures* 62(2019), 3-14. ISSN 2217-8139.
- [5] Purvis, Ron, *Life-Cycle Cost Analysis for Protection and Rehabilitation of Concrete Bridges Relative to Reinforcement Corrosion*, NCHRP Report 377, National Cooperative Highway Research Project, Strategic Highway Research Program, National Research Council, Washington, D.C., 1994.
- [6] Hudson, Ron, R. Haas and W. Uddin, *Infrastructure Management*, McGraw-Hill, New York, N.Y., 1997.
- [7] Hawke, Hugh, BLCCA (Bridge Life-Cycle Cost Analysis), National Cooperative Research Project, NCHRP Report 483, Washington, D.C., 2003.
- [8] Brühwiler, Eugen and B. Adey, *Improving the consideration of life-cycle costs in bridge decision-making in Switzerland*, *Structure and Infrastructure Engineering*, Vol. 1, No. 2, Taylor & Francis Group, Ltd., Abington, U.K., 2005, pp. 145 - 157.
- [9] Yanev, Bojidar, *Bridge Management*, John Wiley, Inc., Newark, N.J., 2007.
- [10] Leeming, M. B. 1993, *The Application of Life-Cycle Costing to Bridges*, *Bridge Management 2*, Harding, J. E., G. A. R. Parke and M. J. Ryall, editors, Thomas Telford, London, UK, 1993, pp. 574-583.
- [11] De Gramo, E. P., J. R. Canada and W. G. Sullivan, *Engineering Economy*, Macmillan Publishing Co., New York, N.Y., 1979.
- [12] Wilson, David C., *Value Engineering Applications in Transportation*, NCHRP Synthesis 352, Transportation Research Board, National Research Council, Washington, D.C., 2005.
- [13] Bell, Michael E. and T. J. McGuire, *Macroeconomic Analysis of the Linkages Between Transportation Investments and Economic Performance*, NCHRP Project 2-17 (3), Transportation Research Board, National Research Council, Washington, D.C., 1994.
- [14] Frangopol, Dan, editor, *Optimal Performance of Civil Infrastructure Systems*, ASCE, SEI, Reston, VA, 1998.
- [15] Furuta, H. et al., *Performance Measures for Bridge Management*, *Proceedings of the International Workshop on Structural Health Monitoring of Bridges*, Sept. 1-2, 2003, pp. 181-186, Kitami Institute of Technology, Japan Society of Civil Engineering, Kitami, Japan.
- [16] Purvis, Ron, *Bridge Deck Joint Performance*, NCHRP Synthesis 319, National Cooperative Highway Research Council, Transportation Research Board, Washington, D.C., 2003.
- [17] Yanev, Bojidar, *Joints: the weak link in bridge structures and life cycles*, *Smart Structures and Systems*, Vol. 15, No. 3, 2015.
- [18] AASHTO, 2010, *Bridge Element Inspection Manual*, American Association of State Highway and Transportation Officials, 2010.
- [19] FHWA, 2011, *Bridge Preservation Guide*, Office of the Infrastructure, Federal Highway Administration, FHWA-HIF-11042, Washington, D.C., 2011.
- [20] Billington, David, *The Tower and the Bridge*, Basic Books, Inc., 1983.
- [21] Bruneau, Michel and A. Reinhorn, *Overview of the Resilience Concept*, *Proceedings of the 8th U.S. National Conference on Earthquake Engineering*, San Francisco, CA, April 18-22, 2006.



## Kula Belgrade – Part 1 - Specific topics of structural design

Nemanja Miljković<sup>\*1)</sup>, Mladen Milićević<sup>1)</sup>, Svetlana Ristić<sup>1)</sup>, Darko Popović<sup>1)</sup>, Vanja Alendar<sup>1)</sup>

<sup>1)</sup> Company DNEC d.o.o. Belgrade, Serbia

### Article history

Received: 13 November 2021

Received in revised form:

18 November 2021

Accepted: 24 November 2021

Available online: 30 December 2021

### Keywords

Tall building,  
Transfer structure,  
Piles,  
Composite structural members,  
PT structural members,  
Non-linear beam analysis,  
Abaqus software

### ABSTRACT

Kula Belgrade is the tallest building within Belgrade Waterfront project, located at the right bank of the Sava river. It is envisaged as the future landmark of Belgrade and pivotal point of Belgrade Waterfront development. It consists of 168m high - 42 storey tower, podium and eccentric basement. It is one of the rare towers in the world in which the bottom and the top parts are mutually rotated by 90° in plan and where such transition is achieved through 7 floors. Such configuration imposed significant demands to structure. The paper addresses design of structure, which has been divided in two stages – piles and structure above the piles. Former was provided by SOM company from Chicago, USA; latter by AECOM company from UAE, both as per American International Building Code. DNEC company from Belgrade was a member of Joint Venture of local companies in charge for nostrification of design and permitting process. Check of design was conducted per Eurocodes. During the construction stage, DNEC was in role of Engineer but was also actively involved in structural value engineering process in which the composite structural members (reinforced concrete with embedded steel) of transition zone were converted to reinforced concrete or post-tensioned members. Link beams of main core that comprised embedded steel plates were redesigned as RC beams, but due to the openings in web their adequacy was checked by non-linear analysis in Abaqus software.

## 1 Introduction

Kula Belgrade is the tallest building within Belgrade Waterfront (BW) project, located on plot 19.1, at the right bank of the Sava river. It is envisaged as the future landmark of Belgrade and pivotal point of BW development. Accordingly, the Investor „BW Kula“, Ltd. has engaged prominent architectural company Skidmore, Owings and Merrill LLT (SOM), Chicago, USA as an Author.

In accordance with the Lex Specialis law, design process was divided in two stages: Stage I – Foundation design and Stage II – Design of Kula.

Structural Consultant in stage I was SOM's Structural department. Their geotechnical Consultant was Terracon from Chicago. Design of structure and foundations was based on International Building Code (USA norms).

Joint venture (JV) of local companies Energoprojekt Urbanizam & Arhitektura, Energoprojekt Entel and DNEC was in role of Local Consultant in charge for nostrification of design and permitting process. Based on initial meetings with Republic Revision Committee it was decided that the check of the structure is conducted as per Eurocodes which were not Serbian official code at a time, but were expected to become official by the end of the project. Responsible Engineer for foundation design was Professor Miloš Lazović.

Geotech report [1] was provided by CIP Institute from Belgrade. Design of piles was completed in 2016 and Novkol company constructed all piles by 2017 under the supervision of MACE company.

Structural Consultant in stage II was AECOM company from Abu Dhabi. JV of local companies had the same role as in stage I. In cases where DNEC's checks as per Eurocodes found insufficiencies of structural members, they were strengthened to comply with Eurocodes. In cases where it was estimated that the structure was over-dimensioned in AECOM's design, no changes were made in order to keep AECOM's liability on packages submitted to Client.

Design was completed by the end of 2018 and construction started in February 2019, by JV of companies Millennium team from Serbia and Pizzarotti company from Italy (PZMT). Engineer's role as per FIDIC was assigned to DNEC.

Contractor has conducted structural value engineering (VE) exercise during the construction stage. His consultant was BG&E company from London, UK. Officially, DNEC was approver of VE design, but practically DNEC worked together with BG&E on this package.

By the time of the writing of this text (Oct. 2021) the main structural works are completed, while facade, MEP and architectural works are still in progress.

\* Corresponding author:

E-mail address: [nemanja.miljkovic@dneccom](mailto:nemanja.miljkovic@dneccom)

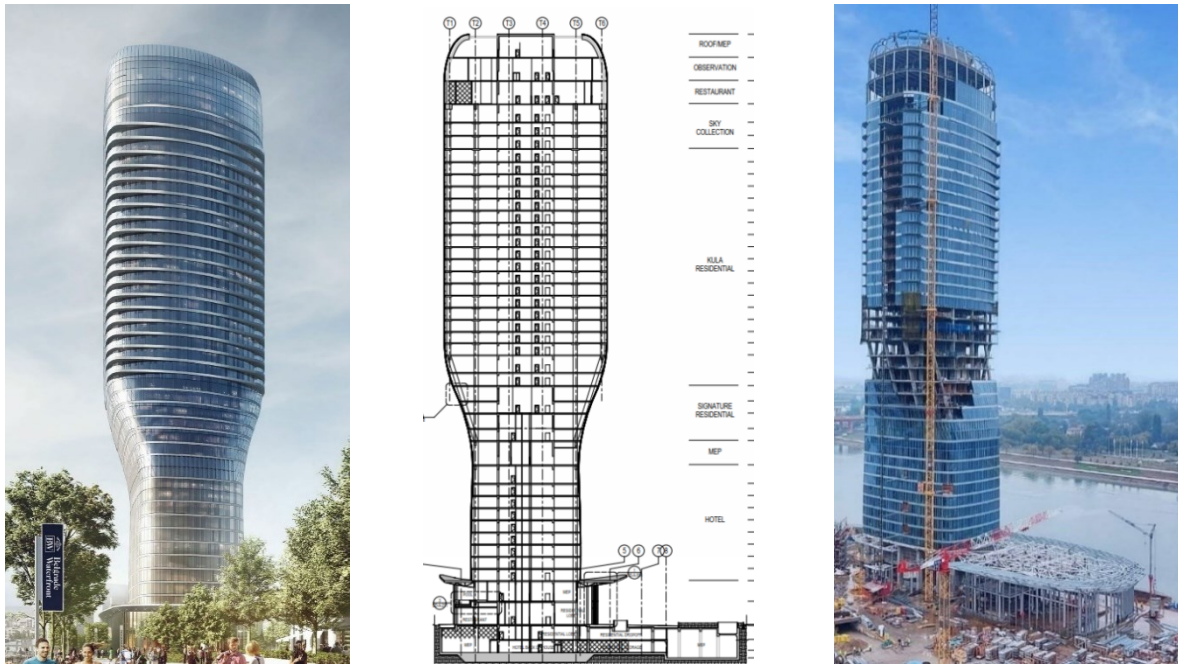


Figure 1. Kula Belgrade– render (left), vertical section (middle), progress of works in Oct 2021 (right)

## 2 About kula

Kula Belgrade is 168 m high, 42-level building located on the right bank of the Sava river, separated from it only by embankment. It consists of tower of mixed use, podium and basement.

Bottom of the tower is allocated for five-star hotel with 119 rooms. MEP level divides hotel part from upper residential part of the building, which comprises 220 branded apartments. It is one of the rare towers in the world in which the bottom and the top parts are mutually rotated by 90° in plan and where such transition is achieved through 7 floors. Typical storey height is 3.5m and maximum one 6.6m.

Podium is 13m high one-storey structure connected to the tower on its North side. Overall dimensions in plan are approximately 50 x 50 m.

There is a two-level basement (mezzanine and B1), each with storey height of 3.5m. It has irregular shape in a form of a circle segment with 150 m long straight going parallel with the river. Maximum dimension in perpendicular direction is approximately 100m. It comprises parking, loading dock, drop off area and back of house (service) areas. Columns' grid is 8.5 x 8.5 m. Ground floor is divided into paved and landscaped areas. Basement is enclosed by the boundary wall which retains not only the soil but also the underground water.

Structure is integral with no expansion joints between the tower and podium and basement.

At the South side of the plot, Kula is connected to the adjacent Galerija shopping mall, by the 40 m long footbridge, designed by Arhipro company. Structurally, it is a simple beam that spans between the two buildings without intermediate supports. Supporting on Kula's side is enabled by RC beam on Level 03.

## 3 Key input parameters for structural design

### 3.1 Geotech report and pile testing

Based on Geotech report [1] and its amendment [2] typical soil profile consisted of:

- Infill „n“: Silty clayey materials, rarely sand and debris. Thickness of layer is 1-2 m.
- Still water facies „am“: Clays, silty muddy and sporadically sandy clay. Thickness of layer is 1-2 m.
- Floodplain facies „ap“: Clayey silt and clayey sandy silt. Thickness of layer is 10-12 m.
- Riverbed facies „ak“: Sand and gravel. Thickness of layer is 8-10 m.
- Marl „L“: Marly clay, marl and marlstones. Thickness of layer is 13-15 m.
- Limestones „K“: Reef organic limestone in upper layers, more compacted Urgonian limestone in lower ones.

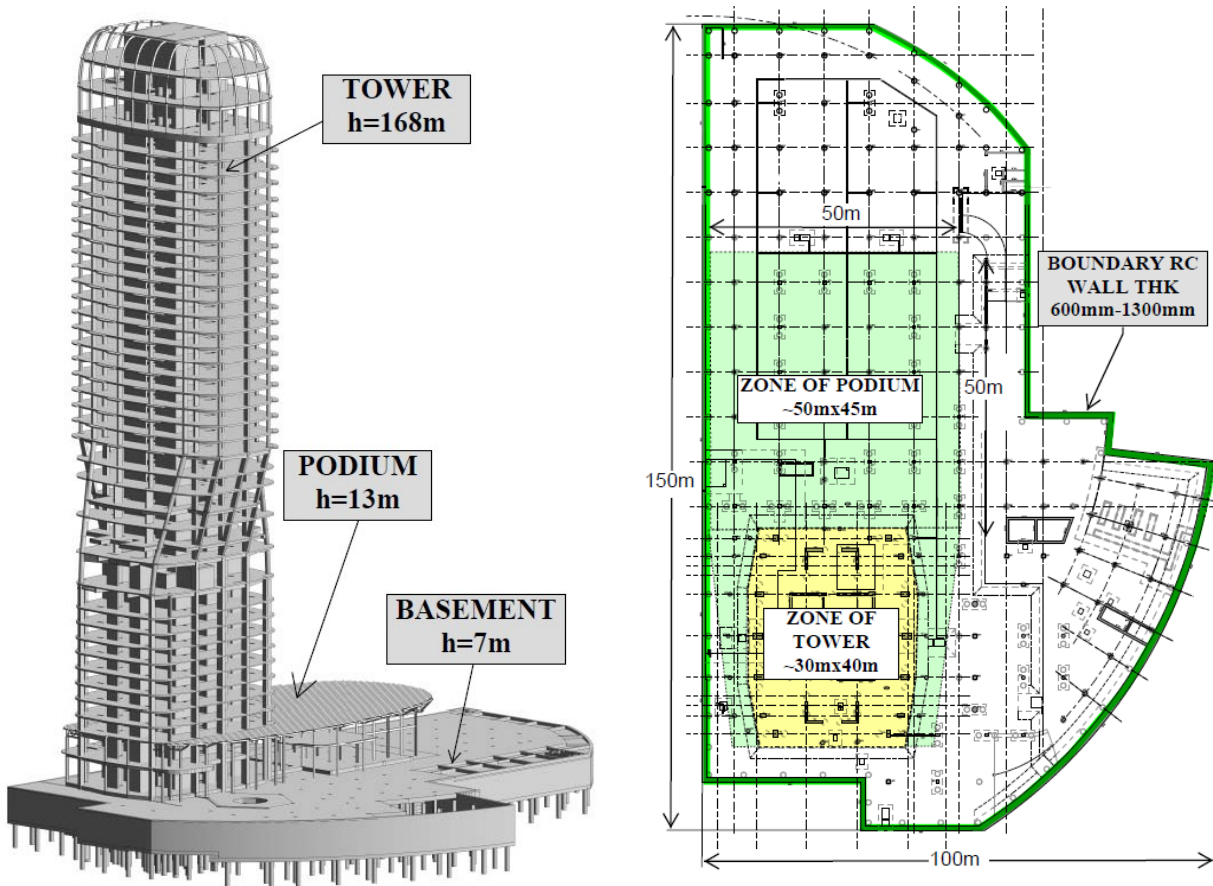


Figure 2. Kula Belgrade – functional units

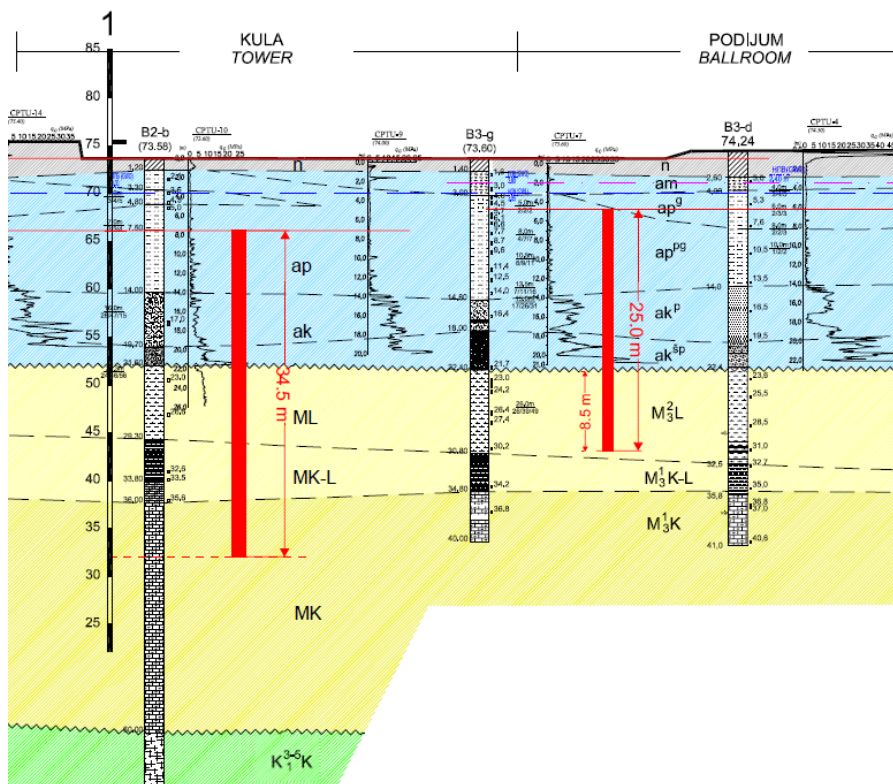


Figure 3. Typical soil profile with drawn piles Ø1200mm (left) and Ø1000mm (right)

Due to poor mechanical properties of upper layers, deep foundation in form of piled raft was recommended foundation option. Geotech report provided estimation of piles capacities of 23.6/5 MN for Ø1200/1000 mm piles anticipated for tower/basement areas, respectively. Capacity was confirmed by comprehensive pile testing program which included:

- Testing of two Ø1200 mm test piles by O-cell method
- Testing of two Ø1000 mm test piles by static test with anchor piles
- Cross hole integrity testing at 100% piles Ø=1200 mm and 20% of piles Ø=1000 mm
- Dynamic testing at 20% piles Ø=1200 mm and 5% of piles Ø=1000 mm
- PIT testing at 100% of constructed piles.
- Geotech report defined the design of water table at +74.0 meters above see level (MASL).

### 3.2 The report on the specific elastic response spectrum of local soil

Seismic action for analysis of Kula structure was defined by seismic micro-zoning report [3], based on seismological and geophysical testing conducted on Kula site. Key findings of this report are summarized in below bullets and elastic spectrum of accelerations.

- Reference Peak Ground Acceleration on Type A ground .....  $a_{gR}=0.06g$
- Importance Factor (EC8, T 4.3 Structure category III).....  $\gamma_I=1.2$
- Design acceleration .....  $a_g=1.2 \cdot 0.06g=0.072$
- Ground type ..... Type S2
- Factor for local soil .....  $S_s=2.3$

- Dumping ratio (concrete structure) .....  $\zeta=5\%$
- Lower period limit of the constant spectral acceleration branch. ....  $T_b=0.18\text{ s}$
- Upper period limit of the constant spectral acceleration branch.....  $T_c=0.42\text{ s}$
- Value defining the beginning of the constant displacement response range of the spectrum .....  $T_d=1.5\text{ s}$

### 3.3 Wind tunnel report

Canadian company RWDI conducted wind testing and provided Wind tunnel testing (WTT) report for the design of Kula structure [4].

Basic parameters:

- Designed wind speed (Maximum mean ten-minute wind speed, on height of 10 m, for recurrence period of 50 years) ..  $V_{m,50,10}=22.0\text{ m/s}$
- Terrain category..... III
- Orography factor.....  $C_o(z)=1$
- Turbulence factor. ....  $K1=1$
- Structural factor .....  $C_s \cdot C_d=1$
- Air density .....  $\rho_0=1.25$
- Windward side exposure coefficient .....  $C_p=0.8$
- Leeward side exposure coefficient .....  $C_p=0.7$

Based on comparison of wind forces, calculated per Eurocode and WTT report it was observed that the ratio of coded to test value was approximately 3/1, which suggested that Kula's shape is highly aerodynamic. However, the wind load reduction was limited to 20% based on recommendations provided in ASCE 7-10 – 31.4.3 [5], so the design of main structure was conducted with 80% of the coded wind load.

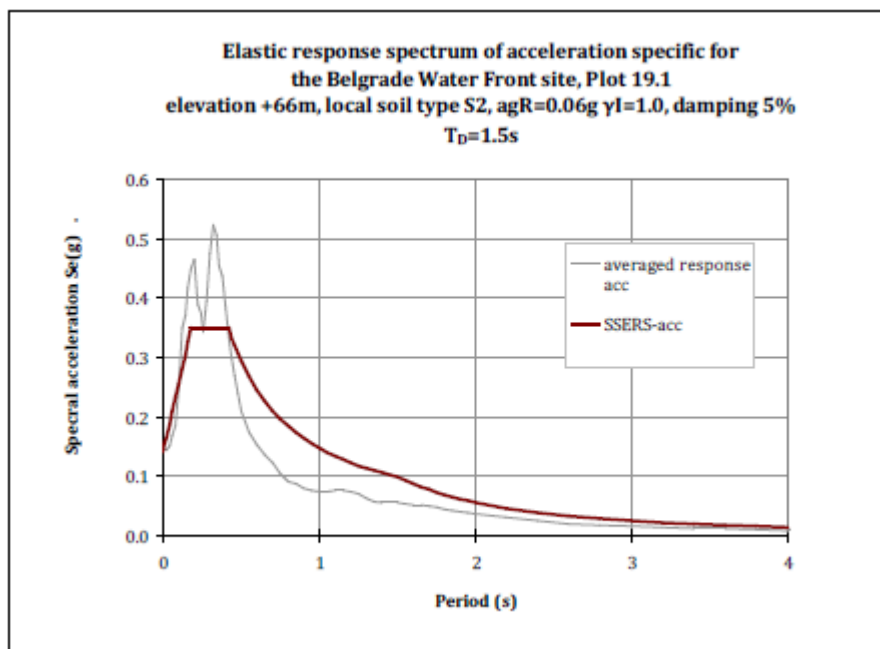


Figure 4. Elastic response spectrum of acceleration specific for Kula location (BW plot 19.1)

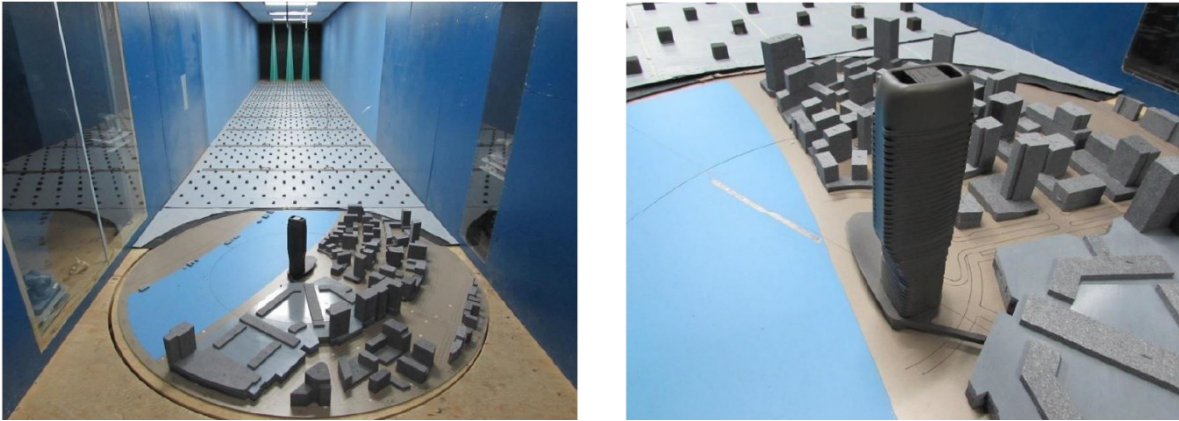


Figure 5. Wind Tunnel Testing

### 3.4 Materials

Concrete grades were adopted in range from C32/40 for ground floor (GF) and basement mezzanine (B1M) slab, C40/50 for raft, basement wall and superstructure slabs, up to C50/60 for core walls and as high as C60/70 for columns in order to minimize their cross-section dimensions and impact on architecture.

Reinforcement was uniformly adopted for all structural members as B500C.

Structural steel was uniformly adopted as S355 for all steel structural members.

## 4 Kula structure as per original solution

### 4.1 The tower structure

Structural concept was defined by SOM's structural team in the first stage of design. It was later taken over and developed to detail design level by AECOM. Both teams used IBC code while DNEC conducted checks as per Eurocodes.

Structural slabs were adopted as two-way reinforced concrete (RC) slabs. Thickness of the typical slab was 200 mm with 450 mm thick drop panels at columns. Concrete grade was C40/50.

Columns were designed as RC columns. Dimensions range from 1100 x 1700 mm at basement levels to 400 x 1200 mm on top floors. Concrete grade was C60/70. They were treated as secondary structural members in seismic analysis.

Lateral stability of the structure is provided by core walls. Dimensions of the main core are 17 x 17 m in plan and it runs from the raft to the top. It is backed up by two satellite cores adopted in lower levels. Thickness of walls is typically 500 mm up to Level 28 and 400 mm above this level. Concrete grade was C50/60.

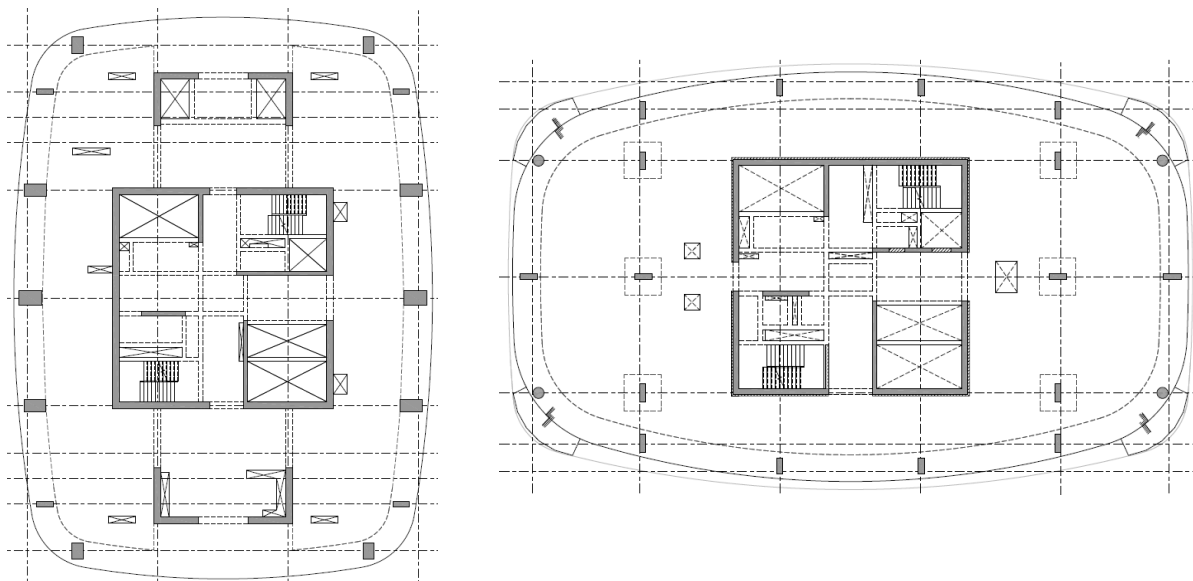


Figure 6. General arrangement (GA) plans of typical Hotel and Residential level as per original design

4.2 The transfer structure

Slabs gradually change their shape in the transition zone of the building, between Level 12 and Level 20. Below Level 12 they are elongated in direction parallel to the river, while above Level 20 they are elongated in perpendicular direction. Columns are vertical in bottom part of the building. Then the columns in the corners of the plan turn into sloping columns at Level 12, 14 and then they turn again on Level 20 to vertical part of level. Each of six central columns (located on the East and West side of hotel floor) branch at Level 14-15 in two columns (see Figure 7). The ones closer to the core keep verticality all the way, while the outer ones slope from Level 15 to Level 20 where they turn to become vertical up to the top of the building. These kinks in columns geometry originate turn forces in range of 5-10 MN, which tend to split the building so the special “transfer” structure was design to resist these forces.

Transfer structure consisted of Transfer beams on Level 12, 14 and 20, which were adopted as composite beams, with embedded steel plates in mid of section and reinforced concrete around them. Former part was originated by column kinks to take the turn forces, while latter part took local loads from floors and provided fire resistance to the entire section. Embedded steel plates were adopted within core walls in their full lengths to allow for continuity in plan, thus forming horizontal ties starting from column-beam joint at one end, running through the transfer beam, core wall, another transfer beam, terminating at symmetrical column beam joint on other end of plan. Columns in transition zone were adopted as composite columns. Their capacity and stiffness were enhanced by embedded steel profiles in transition zone.

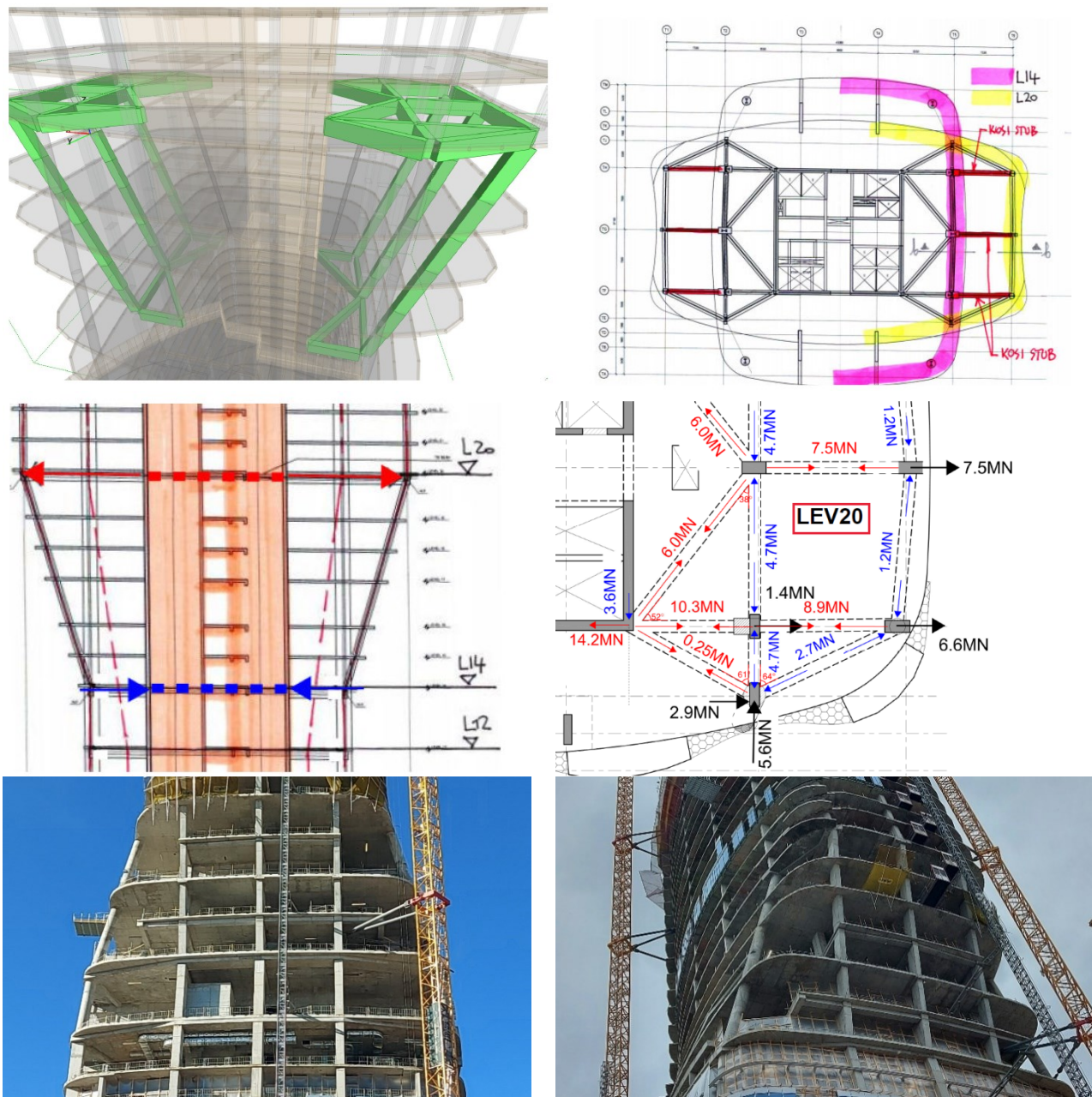


Figure 7. Transfer structure illustration of geometry and turn forces

SOM's idea behind such solution was to design embedded steel structure so it could sustain the weight of the upper structure, thus enabling the start of construction of floors above Level 20 as soon as the transfer steel structure alone would be erected, while the construction of RC parts of columns, beams and floors at transition levels would be done simultaneously with construction of upper floors.

#### 4.3 The podium structure

Podium structure was designed as steel structure. It consists of roof trusses, two composite slabs (at Level 02 and MEP well) and steel columns. Lateral stability is provided by anchoring of roof structure to the concrete tower structure and by frame action of columns and horizontals, so the vertical bracings were omitted. Steel grade is S355.

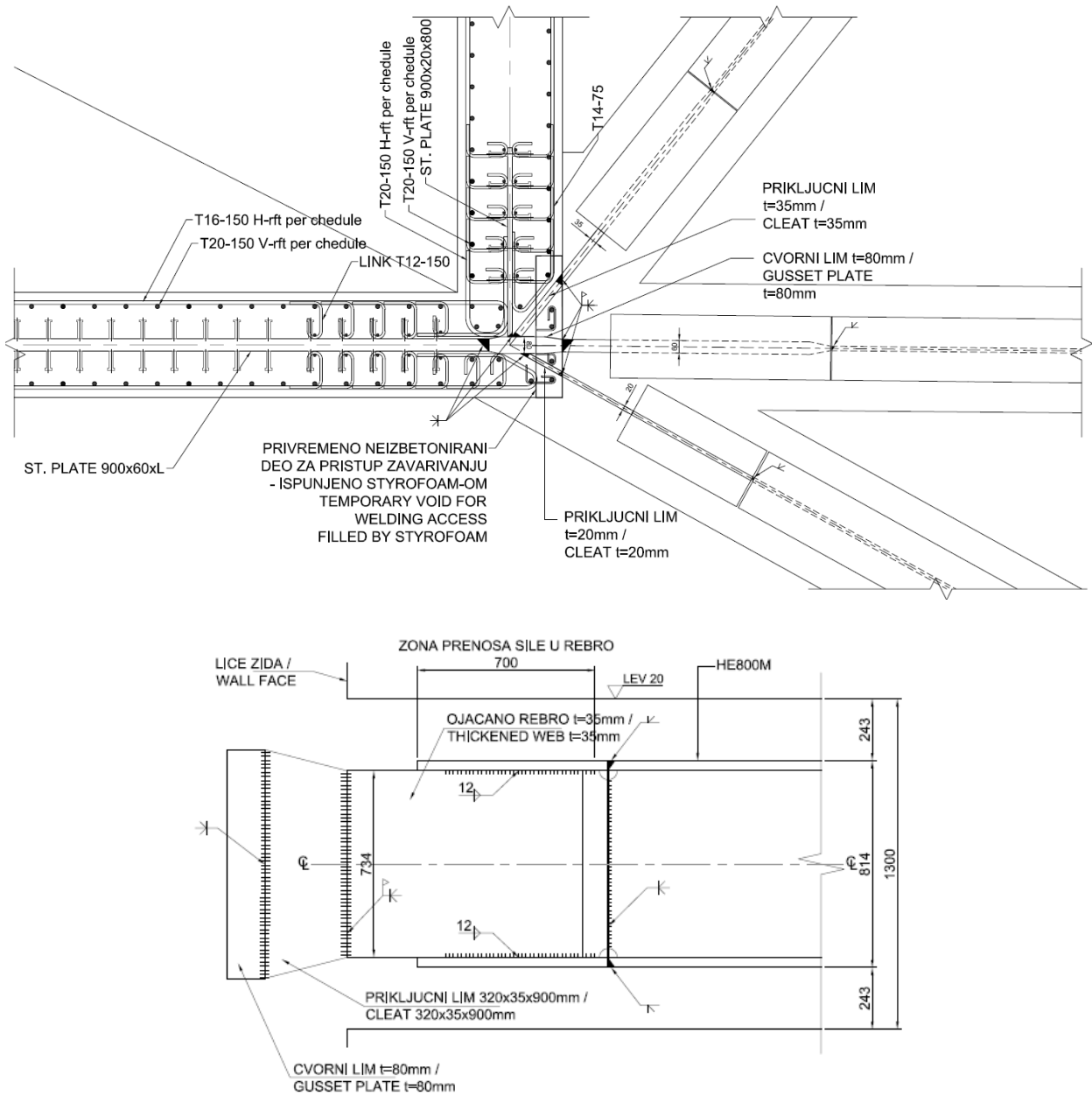


Figure 8. Transfer structure-joint detail at core corner – plan view (upper detail) and vertical section (lower detail)

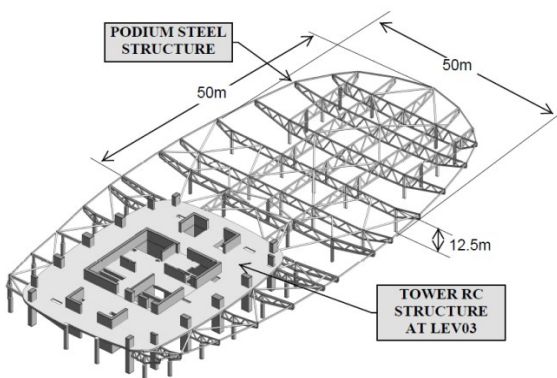


Figure 9. Podium Roof Steel Structure

#### 4.4 The basement structure

Ground floor slab was adopted as two-way RC slab with RC beams in orthogonal directions. Typical beam size is 600 x 1000 mm, while the slab is 300 mm thick. It is heavily loaded by pavers and landscape build-ups but also with traffic load both in construction and service stage. Design concrete grade was C32/40.

Basement mezzanine slab is of mixed type. In the zone of the parking lot, it is 250 mm flat slab with 450 mm thick drop panels, whereas in the zone of the tower and around it is similar to ground floor slab – two-way slab with beams and same concrete grade.

Vertical loads are transferred by two storey RC columns 600 x 600 mm made of C40/50.

The perimeter of the structure is protected from soil and water pressures by RC wall. Depending on end conditions its thickness varies from 600 mm in case of two-way continuous

member to 1300 mm in case of 10 m high cantilever in zone of ramps. Concrete grade was C40/50.

#### 4.5 Foundations

Due to poor geotechnical properties of upper soil layers, adopted foundation solution is piled raft. The tower is founded on 62 bored piles with diameter of  $\varnothing 1200$  mm and length of 30.0-35.0 m. The reason for non-uniform length of tower piles was in non-uniform thickness of tower raft, which ranged from 2800 mm to 6800 mm in the zone of elevators shafts, while the toe level of tower piles was constant at +32MASL, or approximately 8-9 m deep into the reef organic limestone layer.

Basement structure is founded on 208 bored piles at 800 mm thick piled raft with diameter of  $\varnothing 1000$  mm and constant length of 25 m. Bases of piles are in Limestone/Marl for tower/basement piles, respectively.



Figure 10. Basement structure under Construction

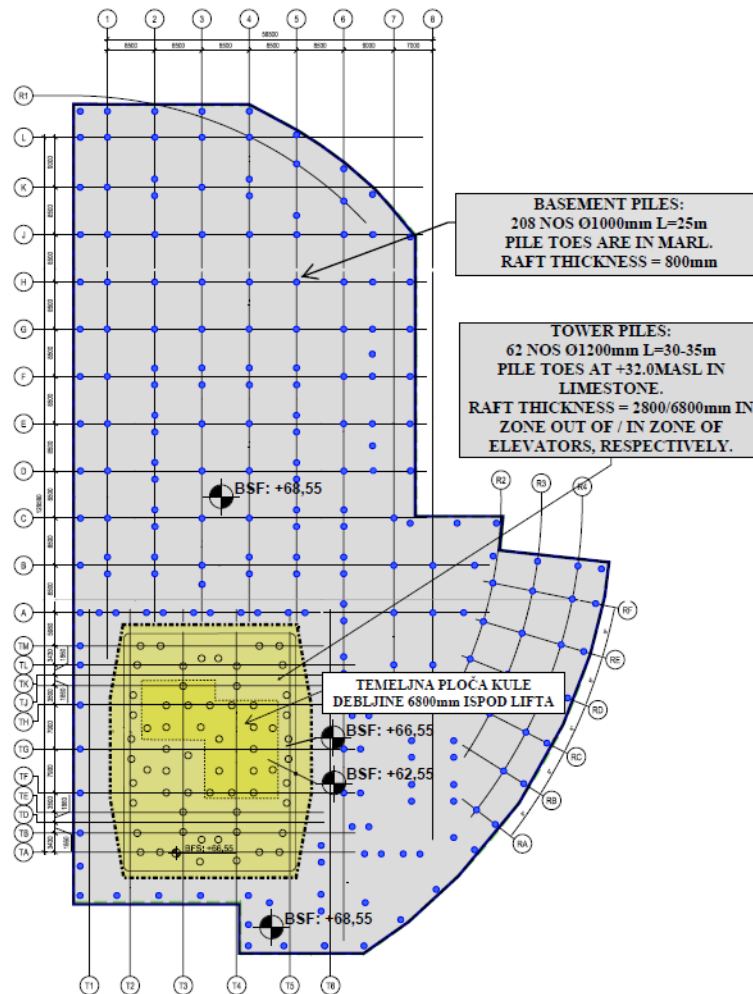


Figure 11. Piles layout

Axial capacities of piles are 23.6/5 MN, while maximum design forces reach 21/4.5 MN for Ø1200/Ø1000 mm piles, respectively.

Design water table at +74MASL resulted with uplift pressures in range of 75 kN/m<sup>2</sup> to 115 kN/m<sup>2</sup>, under the Tower and 55 kN/m<sup>2</sup> to 78 kN/m<sup>2</sup> at Basement structure, where the piles acted as ties with tension capacities of 3 MN.

All actions in horizontal direction were assigned to piles alone. Capacity of tower piles is sufficient to resist the seismic force from the tower, while all together they take full seismic force from Tower, Podium and Basement. Due to eccentricity between the centres of mass and stiffness, raft tends to rotate in its plane, so the utmost rows of basement piles are subjected to horizontal forces to which they cannot respond elastically. However, these piles are not subjected to high axial loads - they are ductile and may respond elasto-plastically. Therefore, the adequacy of piles for horizontal actions was confirmed by iterative non-linear analysis. As an extreme case such analyses included the accidental case when top 5 m of soil strata is completely lost so the piles have no lateral support in this zone and the structure may be regarded as “pile dwelling house”.

## 5 Kula structure as per value engineering (VE) solution

While the construction of Kula was still in early stage, Contractor has decided to conduct a VE exercise. Basement levels were omitted as they were under construction at a time, while the following items were redesigned in tower structure:

- Embedded steel sections were removed from columns
- Composite transfer beams were redesigned to post-tensioned (PT) beams
- Slabs were redesigned from RC to PT slabs
- Embedded steel plates were removed from core walls and their reinforcement was optimized

### 5.1 VE of transfer structure

The main goal set by Contractor was to eliminate the embedded steel sections from beams and columns as well as the steel plates from core walls in order to simplify and speed up construction process. However, it was in the early stage of VE exercise when it was noticed that the differential settlements doubled in comparison with those in the original design. Comparative analysis has shown that this was originated by the removal of embedded steel sections from columns, which were subjected to high axial pressures as they were designed as secondary structural members and

accordingly had not limited normalized axial force (axial load ratio). Same parameter was limited to 0.4 in the core walls, as per Eurocode 1998 [6] requirement for DCM, to allow for their ductility. Therefore, it was the combination of big difference in core walls - columns stresses and reduction in stiffness of columns that made differential settlements to become an important item in VE design. Such finding was surprising at the first glance, since the differential settlements are usually insignificant in 40 storey buildings. However, having in mind previously mentioned branching of columns and the fact that six pairs of columns take the loads from 28 floors (Level 42 to 15) and transfer them to six single columns below Level 15, Kula may be regarded as 70 storeys building in terms of the axial loads at the base of six main columns.

In order to mitigate the effects of differential settlements BG&E and DNEC decided to reduce the thickness of transfer beams, especially in bays adjacent to the core, so the beams

of 600 x 1300 mm were replaced by 1600 x 700 mm and 2000 x 700 mm in outer spans, and 1600 x 450 mm and 2000 x 450 mm in spans adjacent to core. Furthermore, layout of transfer beams was significantly rearranged on Level 020, as shown in Figure 12. Three beams highlighted in yellow in the Figure 12 were adopted as PT beams while other beams in plan were designed as RC beams.

Each of Level 20 PT beams comprised two multistrand tendons with 22 strands,  $\varnothing 15.2$  mm, made of low relaxation steel grade 1860 MPa. Ducts were grouted after the stressing so the tendons were bonded to beams.

Due to geometrical issues with beams at slab corners, the force in tendons was not fully developed at the point of the action of kink force. Accordingly, U-shaped reinforcement bars had been designed in quantity sufficient to fully cater the kink force up to a point where tendons would overtake it.

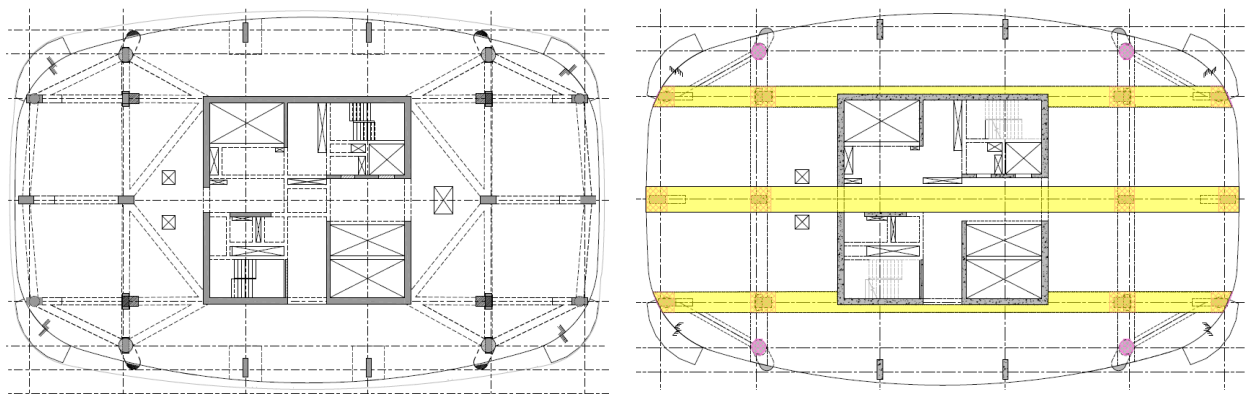


Figure 12. GA plan on Level 20 – from original design (left) and VE design (right)

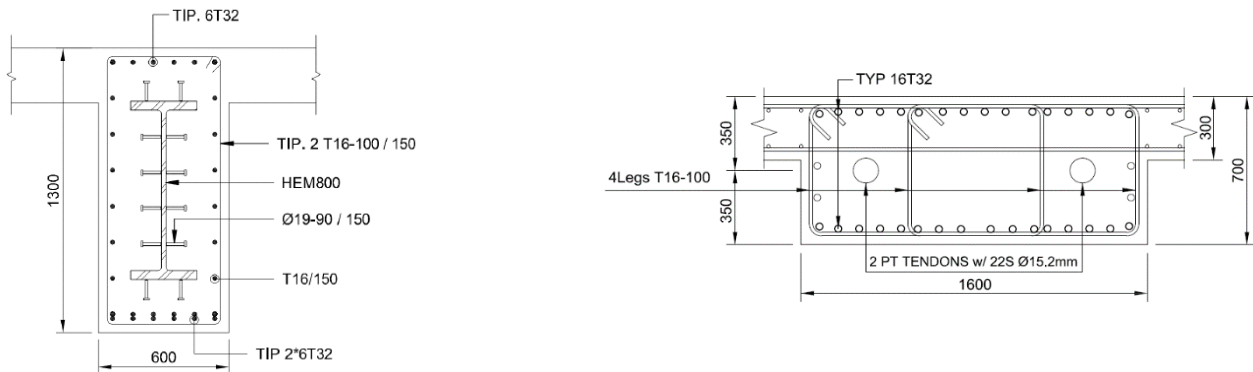


Figure 13. Transfer beams on Level 20 – cross sections from original design (left) and VE design (right)

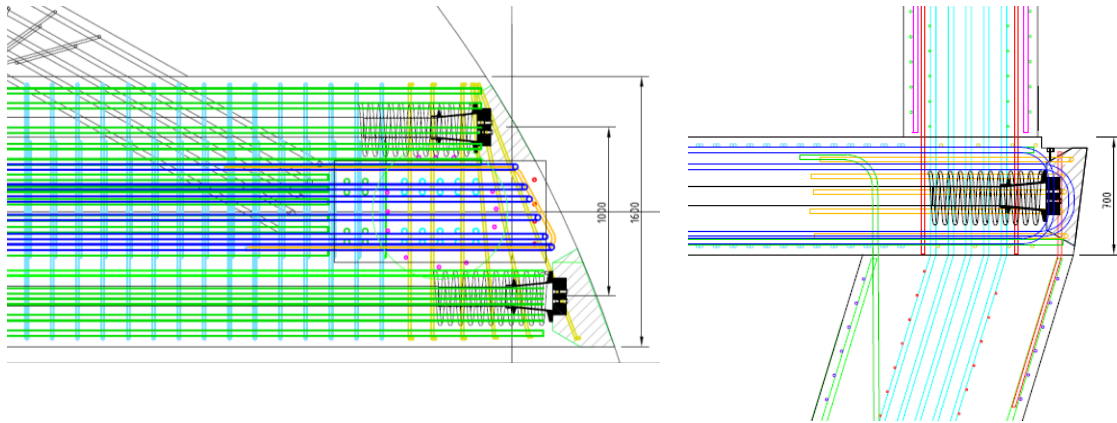


Figure 14. Transfer structure Level 20 – Node at façade in plan (left) and vertical section (right)

## 5.2 VE of slabs

Basic thickness of slabs was kept the same as in original design (200 mm) but perimeter beams were removed both in hotel and residential levels, and in residential levels replaced by 400 mm drop panels. However, the biggest change was conversion from RC to PT slab. High strength strands,  $\text{Ø}12.7$  mm, made of low relaxation steel grade 1860 MPa were placed in flat ducts with 3 to 5 slots to form the flat tendons suitable for slabs. Ducts were grouted after the stressing so the tendons were bonded to slab.

Design conducted as per Eurocode 2 [7] and Technical Report 43 [8] resulted in non-conventional layout as there were no pronounced distributed versus banded arrangement in two orthogonal directions. Instead, tendons in both directions appear more as distributed with spacing in range of 6-10 times slab thickness.

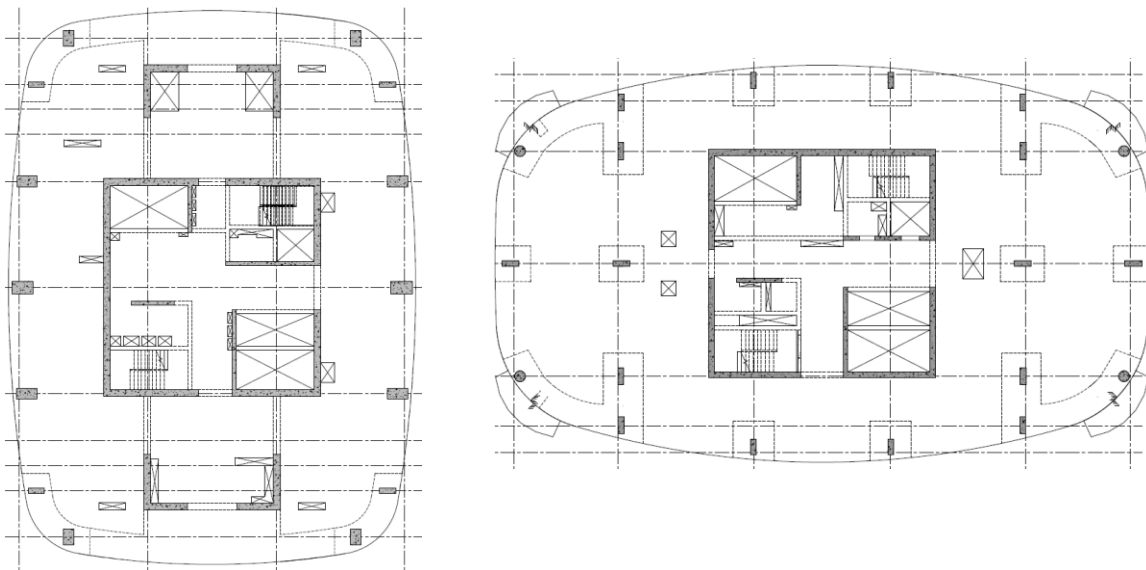


Figure 15. GA plans of typical Hotel and Residential level as per VE design



Figure 16. Reinforcement and PT works in progress

Previously mentioned issue of differential settlements greatly affected the design of PT slabs, too - mostly in the aspect of punching but also crack control. Local FEM models for slab analysis simulated the case of columns settlement – as illustrated in Figure 17. Typically, the East and West edges of slabs above Level 30 were lowered approximately by 40 mm with respect to the core. Bending moments originated by imposed displacements were combined with those from other load cases and used for punching checks. Punching resistance was provided by the increase of longitudinal reinforcement in tension zone and by shear stud reinforcement.

5.4 VE of core walls

Apart from embedded steel plates at transfer levels that were removed by VE of transfer structure, core walls of the original design comprised another type of embedded steel and that was steel plate in link beams. Namely, each link beam in main core, satellite cores, but also coupling beams between the cores comprised embedded steel plate. Thickness of the plates was typically 40 and 50 mm, while the depth ranged from 750 mm in case of typical storey, up to 8500 mm in case of link beam above the big opening in East core wall at Level 2.

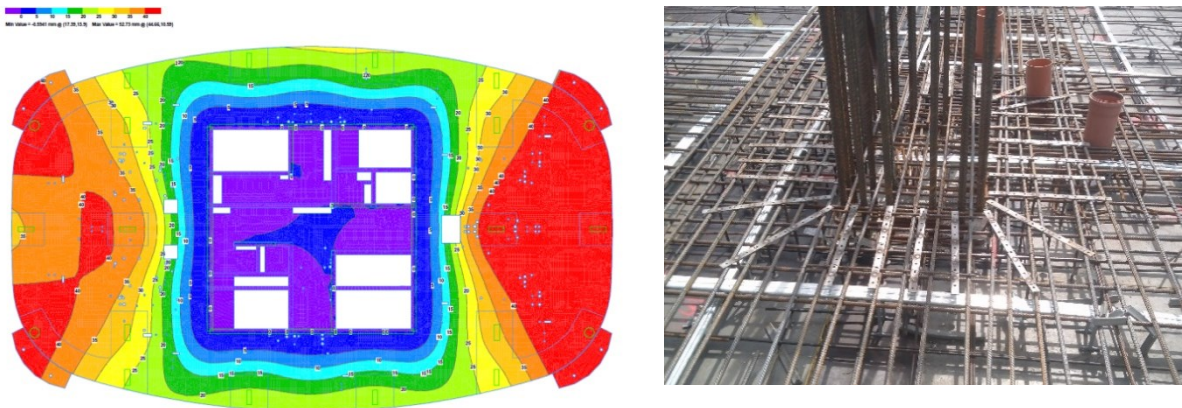


Figure 17. Simulation of differential settlements in FEM model (left) and Stud shear on rails installed in slab (right)

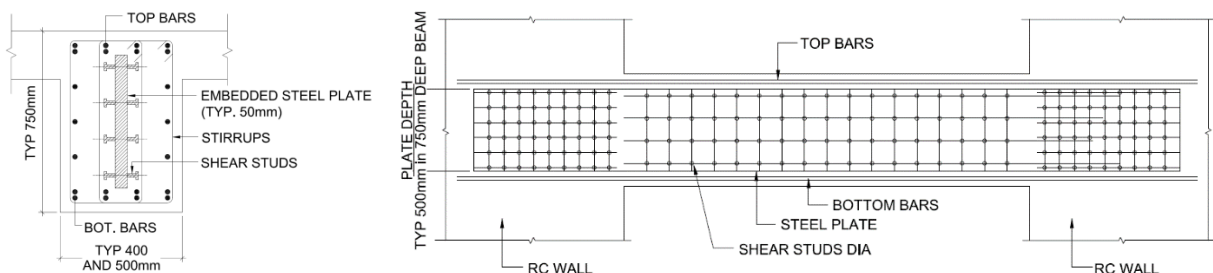


Figure 18. Link beam solution from original design – Composite link beam

During the VE stage, not only that link beams were converted from composite to RC beams, but they were also required to include web openings to allow for final MEP routing. Solution was to minimize the quantity of flexural reinforcement and accordingly shear demand obtained by capacity design and to detail shear reinforcement so it

provided maximum possible shear capacity and ductility to the beam. Shear reinforcement was adopted as a combination of closed hoops (stirrups) and diagonal rebar which formed diamond shaped framing around the openings. Cross ties were adopted to confine the trimmer bars placed above and below the openings.

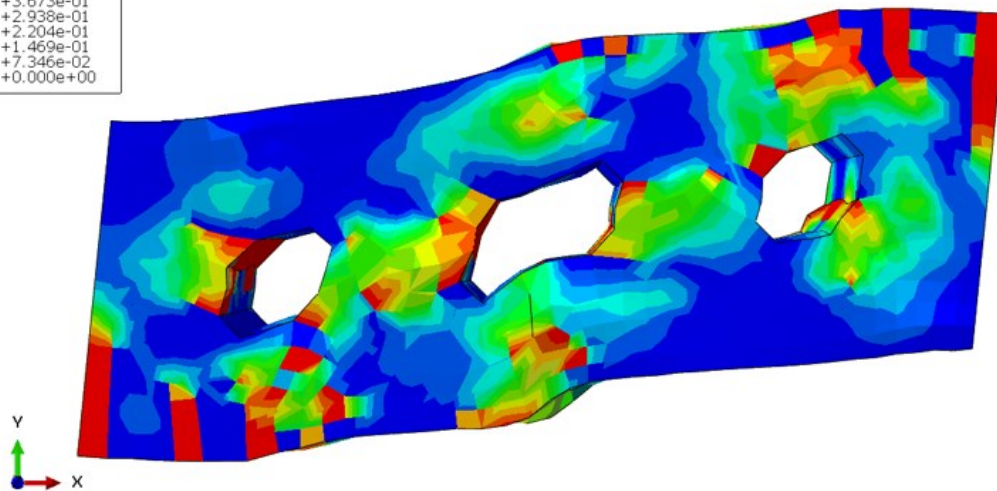
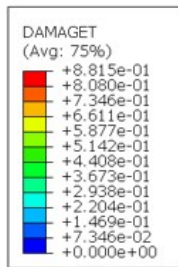
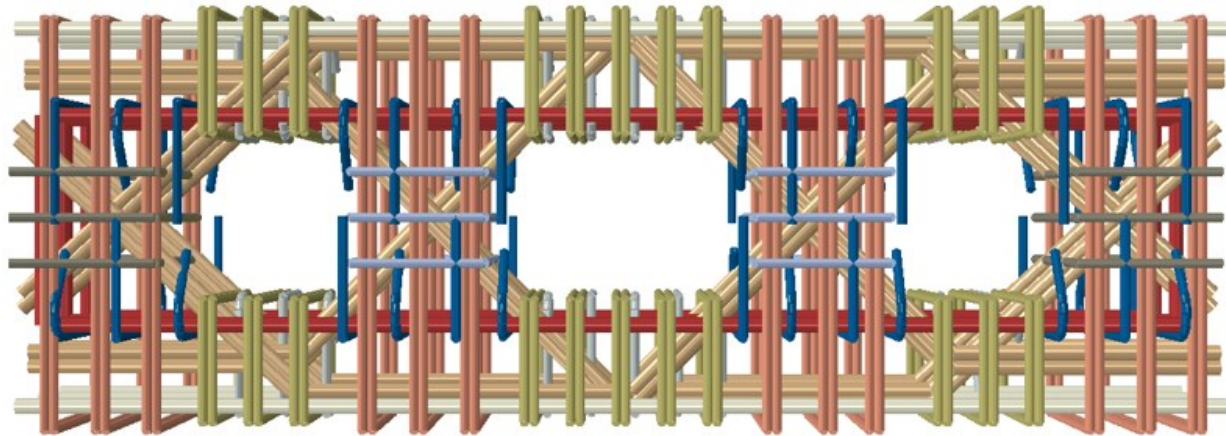


Figure 19. Model of Link Beam in Abaqus, Version 2017 (above), deformed shape with tensile damage distribution at 9 mm of displacement and 0.0075 rad of rotation (mid) and prefabrication of link beam rebar cage on ground for later erection and installation into core wall (below)

The checking of achieved level of capacity and ductility was done by non-linear analysis executed in Abaqus software by Faculty of Civil Engineering at Belgrade University [9]. Micro modelling approach was implemented, so each reinforcement bar and stirrup were modelled with its own shape. Concrete part was modelled, too. Nonlinear stress-strain and stress-displacement relations were defined for the behaviour of concrete, while bilinear plastic behaviour was applied for reinforcement material definition. Rotations and displacements at the left and right ends of the beam were assigned as loading that simulates the earthquake loading transferred from the walls to the coupling beam. Analysis has shown that the plastic behaviour occurred at the ends of the beam and it remained there. Brittle damage of concrete was avoided, while reinforcement activation led to the ductile behaviour of specimen, so it was concluded that the adopted link beam solution was adequate.

### 5.5 Overview of ve process

Although the significant saving was achieved by removal of embedded steel sections from transfer structural members, the overall savings was somewhat reduced due to the increase of reinforcement added for punching resistance and to control the cracking. However, the VE process may be regarded as successful as it resulted in simpler, thus faster construction of transfer levels and core walls and also faster construction of superstructure slabs, which Contractor achieved to cast in 2-3 days cycles at typical levels.

## 6 About the 2<sup>nd</sup> part of the article

While this part of the article addressed the specifics of design process, the second part will present the key items related to Kula construction including: enabling works, the execution and testing of piles, concreting of raft (part below the tower – approximately 4750 m<sup>3</sup> of concrete was cast in one turn), works on transfer structure, etc.

### References

- [1] Geotech report – Book 1 and Book 2 (Laboratory testing) – CIP Institute Belgrade, December 2015.
- [2] Geotech report – amendment – CIP Institute Belgrade, April 2016.
- [3] Slavica Radovanović, Seismic study - Report on results of defining specific elastic response spectrum of local soil at the Belgrade Waterfront location. Plot 19.1, February 2016.
- [4] Wind tunnel testing report, RWDI, Canada, April 2016.
- [5] ASCE Standard 7-10, Minimum design loads for buildings and other structures, ASCE/SEI, 2010
- [6] Eurocode 8 - EN 1998-1-1:2004 and SRPS EN 1998-1/NA, December 2018
- [7] Eurocode 2 – EN 1992-1-1:2004 and SRPS EN 1992-1-1/NA, November 2015
- [8] Technical report 43 - Post tensioned concrete floors – Concrete Society, Second Edition, 2005.
- [9] Marko Marinković, Non-linear analysis of RC coupling beam Rev00. 01.06.2020.

## INSTRUCTIONS FOR AUTHORS

### Acceptance and types of contributions

The Building Materials and Structures journal will publish unpublished papers, articles and conference reports with modifications in the field of Civil Engineering and similar areas (Geodesy and Architecture). The following types of contributions will be published: original scientific papers, preliminary reports, review papers, professional papers, objects describe / presentations and experiences (case studies), as well as discussions on published papers.

Original scientific paper is the primary source of scientific information and new ideas and insights as a result of original research using appropriate scientific methods. The achieved results are presented briefly, but in a way to enable proficient readers to assess the results of experimental or theoretical numerical analyses, so that the research can be repeated and yield with the same or results within the limits of tolerable deviations, as stated in the paper.

Preliminary report contains the first short notifications on the results of research but without detailed explanation, i.e. it is shorter than the original scientific paper.

Review paper is a scientific work that presents the state of science in a particular area as a result of analysis, review and comments, and conclusions of published papers, on which the necessary data are presented clearly and critically, including the own papers. Any reference units used in the analysis of the topic are indicated, as well as papers that may contribute to the results of further research. If the reference data are methodically systematized, but not analyzed and discussed, such review papers are classified as technical papers.

Technical paper is a useful contribution which outlines the known insights that contribute to the dissemination of knowledge and adaptation of the results of original research to the needs of theory and practice.

Other contributions are presentations of objects, i.e. their structures and experiences (examples) in the construction and application of various materials (case studies).

In order to speed up the acceptance of papers for publication, authors need to take into account the Instructions for the preparation of papers which can be found in the text below.

### Instructions for writing manuscripts

The manuscript should be typed one-sided on A-4 sheets with margins of 31 mm (top and bottom) and 20 mm (left and right) in Word, font Arial 12 pt. The entire paper should be submitted also in electronic format to e-mail address provided here, or on CD. The author is obliged to keep one copy of the manuscript.

As of issue 1/2010, in line with the decision of the Management Board of the Society and the Board of Editors, papers with positive reviews, accepted for publication, will be published in Serbian and English, and in English for foreign authors (except for authors coming from the Serbian and Croatian speaking area).

Each page should be numbered, and the optimal length of the paper in one language is about 16 pages (30.000 characters) including pictures, images, tables and references. Larger scale works require the approval of the Board of Editors.

The title should describe the content of the paper using a few words (preferably eight, and up to eleven). Ab-

brevisions and formulas should be omitted in the title. The name and surname of the author should be provided after the title of the paper, while authors' title and position, as well as affiliation in the footnote. The author should provide his/her phone number, e-mail address and mailing address.

The abstract (summary) of about 150-250 words in Serbian and English should be followed by key words (up to seven). This is a concise presentation of the entire article and provides the readers with insight into the essential elements of the paper.

The manuscript is divided into chapters and sub-chapters, which are hierarchically numbered with Arabic numerals. The paper consists of introduction and content with results, analysis and conclusions. The paper ends with the list of references. All dimensional units must be presented in international SI measurement units. The formulas and equations should be written carefully taking into account the indexes and exponents. Symbols in formulas should be defined in the order they appear, or alternatively, symbols may be explained in a specific list in the appendix. Illustrations (tables, charts, diagrams and photos) should be in black and white, in a format that enables them to remain clear and legible when downscaled for printing: one to two columns (8 cm or 16.5 cm) in height, and maximum of 24.5 cm high, i.e. the size of the letters and numbers should be at least 1.5 mm. Original drawings should be of high quality and fully prepared for copying. They also can be high-quality, sharp and contrasting photo-copies. Photos should be in black and white, on quality paper with sharp contours, which enable clear reproduction.

The list of references provided at the end of the paper should contain only papers mentioned in the text. The cited papers should be presented in alphabetical order of the authors' first name. References in the text should be numbered with Arabic numerals in square brackets, as provided in the list of references, e.g. [1]. Each citation in the text must be contained in the list of references and vice versa, each entry from the list of references must be cited in the text.

Entries in the list of references contain the author's last name and initials of his first name, followed by the full title of the cited article, the name of the journal, year of publication and the initial and final pages cited (from - to). If the doi code exists it is necessary to enter it in the references. For books, the title should be followed by the name of the editor (if any), the number of issue, the first and last pages of the book's chapter or part, the name of the publisher and the place of publication, if there are several cities, only the first in the order should be provided. When the cited information is not taken from the original work, but found in some other source, the citation should be added, "cited after ..."

Authors are responsible for the content presented and must themselves provide any necessary consent for specific information and illustrations used in the work to be published.

If the manuscript is accepted for publication, the authors shall implement all the corrections and improvements to the text and illustrations as instructed by the Editor.

Writings and illustrations contained in published papers will not be returned. All explanations and instructions can be obtained from the Board of Editors.

Contributions can be submitted to the following e-mails: [sneska@imk.grf.bg.ac.rs](mailto:sneska@imk.grf.bg.ac.rs) or [miram@uns.ac.rs](mailto:miram@uns.ac.rs)  
Website of the Society and the journal: [www.dimk.rs](http://www.dimk.rs)



Financial support



**MINISTRY OF EDUCATION, SCIENCE AND  
TECHNOLOGICAL DEVELOPMENT OF  
REPUBLIC OF SERBIA**



**UNIVERSITY OF BELGRADE FACULTY OF  
CIVIL ENGINEERING**



**INSTITUTE FOR TESTING OF MATERIALS-  
IMS INSTITUTE, BELGRADE**



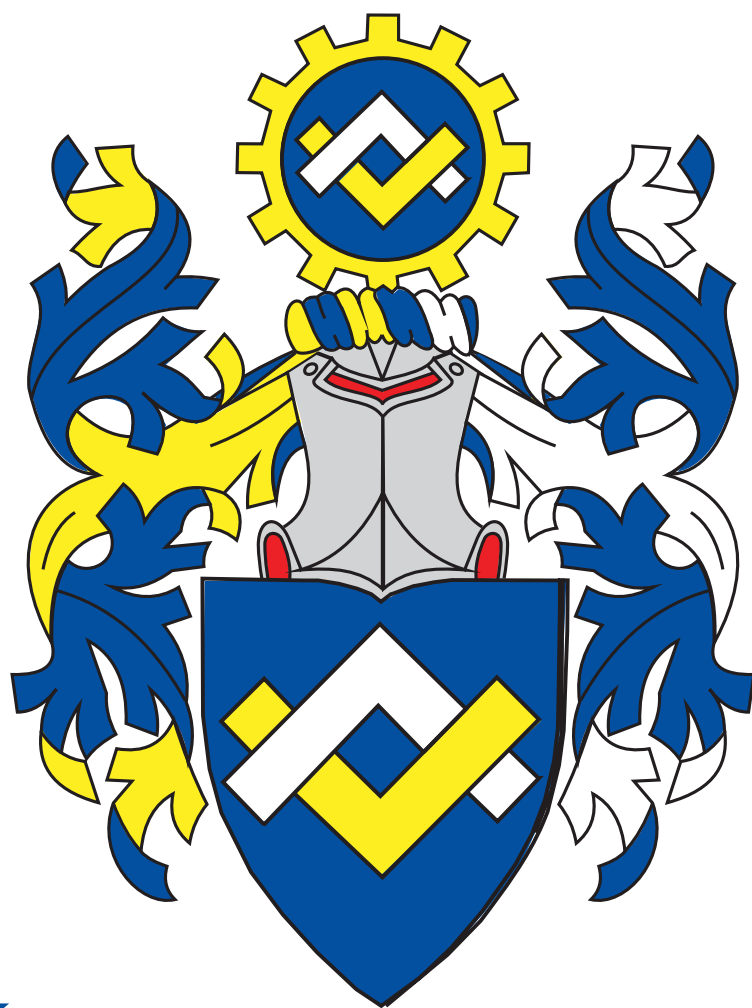
**FACULTY OF TECHNICAL SCIENCES,  
UNIVERSITY OF NOVI SAD, DEPARTMENT  
OF CIVIL ENGINEERING**



**ИНЖЕЊЕРСКА  
КОМОРА  
СРБИЈЕ**

**SERBIAN CHAMBER OF ENGINEERS**





**INŽENJERSKA  
KOMORA  
SRBIJE**



Oplatna tehnika.

# Vaš pouzdan partner

za brzu, bezbednu i ekonomičnu gradnju!

**Doka Serb** je srpski ogranak austrijske kompanije **Doka GmbH**, jednog od svetskih lidera na polju inovacija, proizvodnje i distribucije oplatnih sistema za sve oblasti građevinarstva. Delatnost kompanije Doka Serb jeste isporuka oplatnih sistema i komponentni za primenu u visokogradnji i niskogradnji, pružanje usluga konsaltinga, izrade tehničkih planova i asistencije na gradilištu.

## Panelna oplata za ploče Dokadek 30 – Evolucija u sistemima oplata za ploče

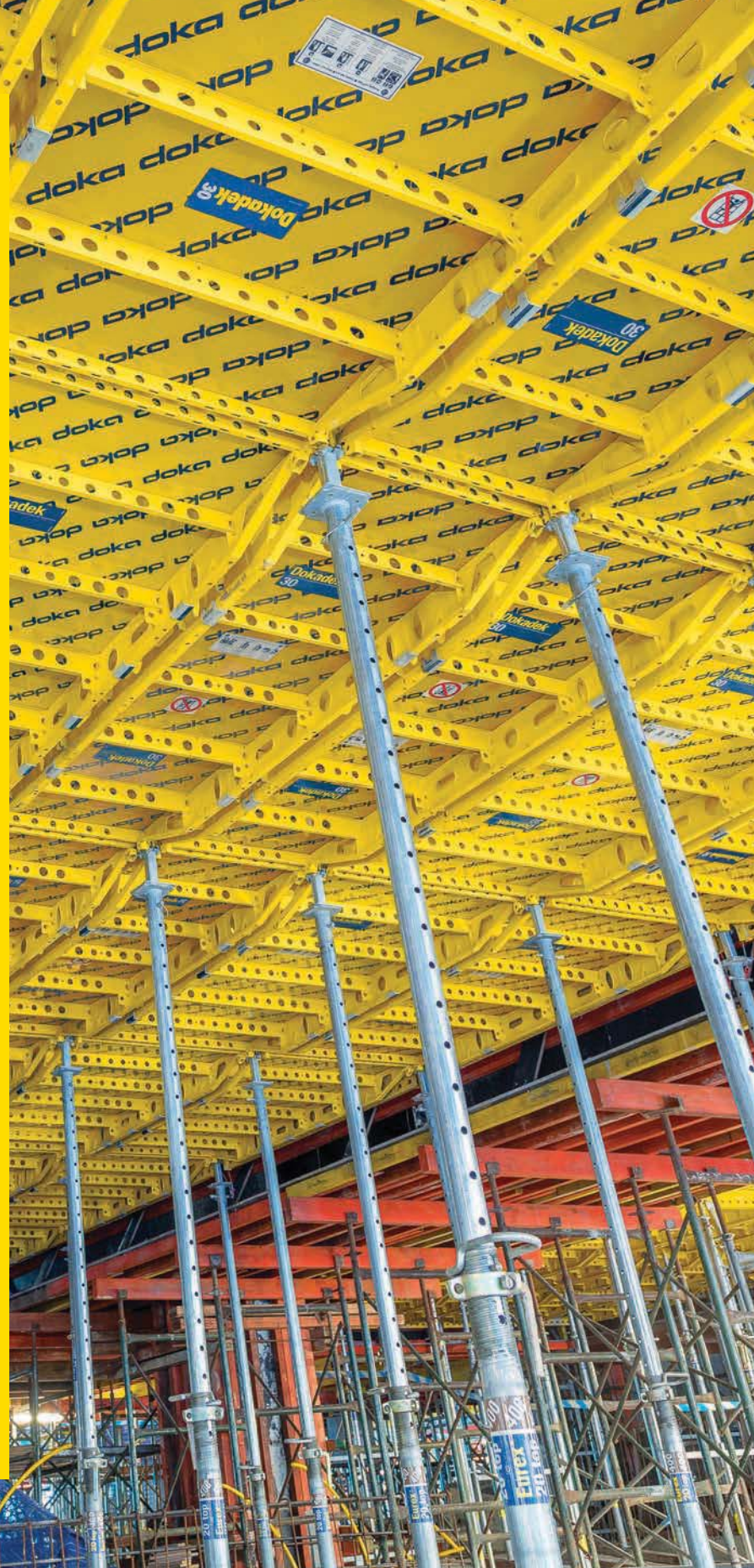
Dokadek 30 je ručna oplata lake čelične konstrukcije, bez nosača sa plastificiranim ramovima, koji su prekriveni kompozitnim drveno-plastičnim panelom površine do 3 m<sup>2</sup>.

### Izuzetno brzo, bezbedno i lako postavljanje oplata

- Mali broj delova sistema i pregledna logistika uz samo dve veličine panela (2,44 x 1,22 m i 2,44 x 0,81 m)
- Dovoljan 2-člani tim za jednostavnu i brzu montažu elemenata sa tla bez merdevina i bez kрана
- Sistemski određen položaj i broj podupirača i panela, unapred definisan redosled postupaka
- Prilagođavanje svim osnovama zahvaljujući optimalnom uklapanju sa Dokaflex-om
- Specijalni dizajn sprečava odizanje panela pod uticajem vetra
- Horizontalno premeštanje do 12 m<sup>2</sup> Dokadek 30 pomoću DekDrive

Više informacija o sistemu naći ćete na našem sajtu [www.doka.rs](http://www.doka.rs)

**Doka Serb d.o.o.** | Svetogorska 4, 22310 Šimanovci | Srbija | T +381 22 400 100  
F +381 22 400 124 | [serb@doka.com](mailto:serb@doka.com) | [www.doka.rs](http://www.doka.rs)



# ZAŠTITNI PREMAZI ZA BETONE

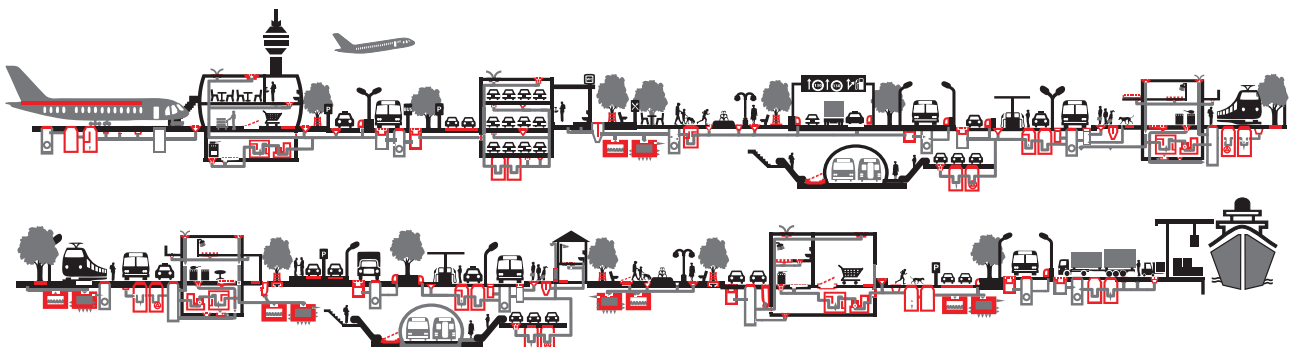


## PROIZVODNI PROGRAM

- |                                |   |                               |
|--------------------------------|---|-------------------------------|
| Aditivi za betone i maltere    | ● | Zaštitni premazi              |
| Smese za zalivanje             | ● | Protivpožarni materijali      |
| Reparacija betona              | ● | Građevinska lepila            |
| Industrijski i sportski podovi | ● | Smese za izravnavanje         |
| Kitovi                         | ● | Dekorativni premazi i malteri |
| Hidroizolacije                 | ● | Proizvodi za građevinarstvo   |

[www.ading.rs](http://www.ading.rs)

# ACO. The future of drainage.



aco.rs

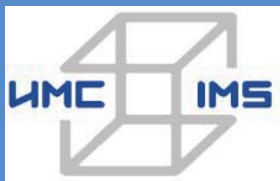


***Institut za ispitivanje materijala IMS, sa tradicijom od 1929. godine, predstavlja najstariju naučno-istraživačku instituciju u Srbiji. Osnovna ideja prilikom osnivanja bila je potreba za jedinstvenom institucijom koja bi se osim istraživanja bavila i kontrolom građevinske industrije.***

Delatnost Instituta IMS obuhvata laboratorijska ispitivanja građevinskih materijala, sertifikaciju proizvoda, nadzor nad izvođenjem radova i ispitivanje različitih tipova konstrukcija, izradu projektne dokumentacije, kao i naučno - istraživački rad u svim oblastima građevinarstva.

Poslovni centri Instituta IMS :

- Centar za puteve i geotehniku
- Centar za materijale
- Centar za metale i energetiku
- Centar za konstrukcije i prednaprezanje



**INSTITUT IMS a.d.**

Bulevar vojvode Mišića 43

11 000 Beograd

Tel: 011-2651-949

Faks: 011-3692-772

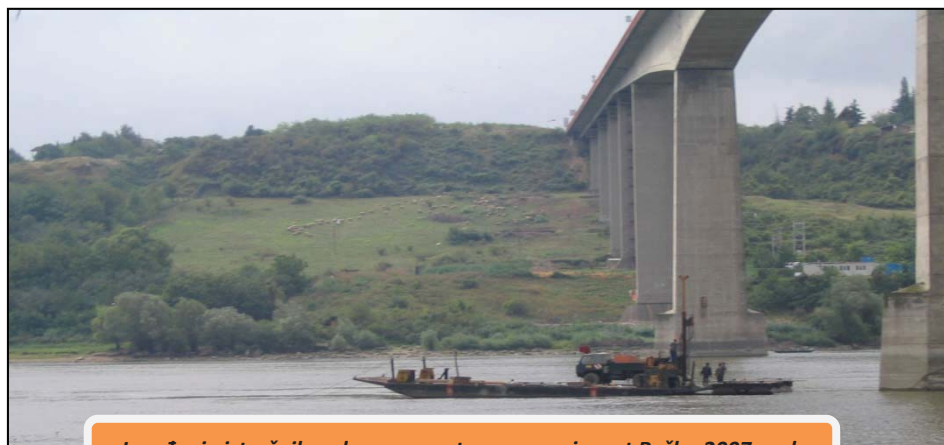
[office@institutims.rs](mailto:office@institutims.rs)

[www.institutims.rs](http://www.institutims.rs)

Institut IMS sertifikovao je sistem kvaliteta prema zahtevima standarda SRPS ISO 9001:2001. Svoju kompetentnost je potvrdio najvećim obimom akreditacije kod Akreditacionog tela Srbije (ATS) i Sertifikacionog tela.

Kadrovsku strukturu Instituta IMS čine doktori nauka, diplomirani inženjeri sa licencama Inženjerske komore Srbije i stručni tehnički kadar. Inženjeri Instituta IMS aktivno učestvuju na naučno-stručnim skupovima u zemlji i inostranstvu.

Institut IMS kontinuirano unapređuje kvalitet poslovanja na svim nivoima, kako u okviru terenskih i laboratorijskih ispitivanja, tako i na izradi projektno-tehničke dokumentacije s ciljem uspešne realizacije postavljenih zadataka.



***Izvođenje istražnih radova sa pontona za novi most Beška, 2007.god.***

### Geotehnička istraživanja i ispitivanja – in situ

Od terenskih istražnih radova izdvajamo izvođenje istražnih bušotina (IB), standardnih penetracionih opita (SPT), statičkih penetracionih opita (CPT i CPTU), opita dilatometarskom sondom (DMT i SDMT), ispitivanja vodopropustljivosti tla različitim terenskim metodama (VDP), ugradnja pijezometara i dr.

Terenske metode ispitivanja šipova zauzimaju značajno mesto u našoj delatnosti, a na tržištu se izdvajamo kao lideri u toj oblasti u protekloj deceniji.

### Ispitivanje šipova

**SLT metoda (Static load test)** ispitivanje nosivosti šipova statičkim opterećenjem;

**DLT metoda (Dynamic load test)** ispitivanje nosivosti šipova dinamičkim opterećenjem;

**PDA metoda (Pile driving analysis)** omogućava praćenje i optimizaciju procesa pobijanja prefabrikovanih betonskih i čeličnih šipova u tlo;

**PIT (SIT) metoda (Pile(Sonic) integrity testing)** koristi se za ispitivanje integriteta izvedenih šipova (dužine, prekida, suženja ili proširenja).



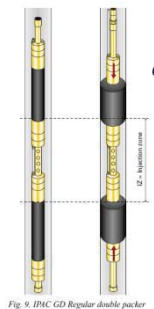
**DLT-dinamičko ispitivanje šipova**



**CPT/CPTU opiti**



**Aktivno klizište**



**oprema za ispitivanje vodopropusnosti stena pod pritiskom do 10 bar-a metodom LIŽONA**

### Laboratorija za puteve i geotehniku

Laboratorija za puteve i geotehniku akreditovana je kod Akreditacionog tela Srbije – ATS prema SRPS ISO/IEC 17025:2006. U njoj se vrše ispitivanja tla (identifikaciono–klasifikaciona ispitivanja, fizičko–mehanička modelska ispitivanja), kamenog agregata i brašna, bitumena i bitumenskih emulzija, asfaltnih mešavina. U okviru laboratorijskih ispitivanja na terenu vrši se kontrola kvaliteta ugrađenog materijala i izvedenih radova ( prethodna, tekuća, kontrolna ispitivanja i izvođenja opita in situ ).

### Projektovanje puteva i sanacija klizišta

U okviru projektovanja značajno mesto u radu zauzimaju geotehnička istraživanja terena i projekti sanacije klizišta - nestabilnih kosina useka i nasipa puteva i prirodno nestabilnih padina . Značajna su i projekovanja svih vrsta fundiranja specijalnih geotehničkih konstrukcija. Ističe se i iskustvo u oblasti putarstva, na projektovanju novih, rehabilitacija i rekonstrukcija postojećih puteva svih rangova sa pratećim objektima i dimenzionisanjem kolovoznih konstrukcija.

### Nadzor

Naši inženjeri imaju veliko iskustvo u kontroli i proveru kvaliteta izvođenja svih vrsta radova, kontroli građevinske dokumentacije i praćenju radova u skladu sa njom, kao i rešavanju novonastalih situacija tokom izvođenja radova.

# Najlepši krov u komšiluku



Continental Plus Natura je premium crep u natur segmentu! Dobro poznatog oblika, trajan i veoma otporan, a povrh svega pristupačan, naprosto oduzima dah svima. Čak i vašim komšijama!

Continental Plus Natura crep potražite kod ovlašćenih Tondach partnera.

## PUT INŽENJERING



Put inženjering d.o.o punih 25 godina radi kao specijalizovano preduzeće za izgradnju infrastrukture u niskogradnji i visokogradnji, kao i proizvodnjom kamenog agregata i betona. Preduzeće se bavi i transportom, uslugama građevinske mehanizacije i specijalne opreme.

Koristeći inovativne tehnike i kvalitetan građevinski materijal iz sopstvenih resursa, spremni smo da odgovorimo na mnoge zahteve naših klijenata iz oblasti niskogradnje.



Osnovna prednost prefabrikovane konstrukcije jeste brzina kojom konstrukcija može biti projektovana, proizvedena, transportovana i namontirana.



Izvodimo hidrograđevinske radove u izgradnji kanalizacionih mreža za odvođenje atmosferskih, otpadnih i upotrebljenih voda, izvođenjem hidrograđevinskih radova u okviru regulacije rečnih tokova, kao i izvođenjem hidrotehničkih objekata.



Površinski kop udaljen je 35 km od Niša. Savremene drobilice, postrojenje za separaciju i sejalice efikasno usitnjavaju i razdvajaju kamene agregate po veličinama. Tehnički kapacitet trenutne primarne drobilice je 300 t/h.



Za spravljanje betona koristimo drobljeni krečnjački agregat sa našeg kamenoloma, deklariranih frakcija, kontrolisane vlažnosti. Kompletan proces proizvodnje i kontrole kvaliteta vršimo prema važećim standardima.



Obradu armature vršimo brzo, stručno i kvalitetno, sa kompjuterskom preciznošću i dimenzijama po projektu.



Naša kompanija u oblasti visokogradnje primenjuje sistem prefabrikovanih betonskih elemenata koji u odnosu na klasičnu gradnju ima brojne prednosti.



Prednapregnute šuplje ploče su konstruktivni elementi visokog kvaliteta, proizvedeni u fabrički kontrolisanim uslovima.



Izrađujemo betonske "New Jersey profile" koji se u svetu koriste za preusmeravanje saobraćaja i zaštitu pešaka u toku izgradnje puta, kao i Betonblock sistem betonskih blokova.



Uslugu transporta vršimo automikserima, kapaciteta bubnja od 7 m<sup>3</sup> do 10 m<sup>3</sup> betonske mase. Za ugradnju betona posedujemo auto-pumpu za beton, radnog učinka 150 m<sup>3</sup>/h, sa dužinom strele od 36 m.



Kao generalni izvođač radova, vršimo koordinaciju svih učesnika na projektu, planiranje, praćenje i nabavku materijala, kontrolu kvaliteta izvedenih radova, poštujući zadate vremenske rokove i finansijski okvir investitora.



Osnovi princip našeg poslovanja zasniva se na individualnom pristupu svakom klijentu i pronalaženje najoptimalnijeg rešenja za njegove transportne i logističke potrebe.



Usluge građevinske mehanizacije vršimo tehnički ispravnim mašinama, sa potrebnim sertifikatima kako za rukovoce građevinskim mašinama tako i za same mašine.



Raspoložemo opremom i mašinama za sve zemljane radove, kipere i dampere za rad u teškim terenskim uslovima, automiksere i pumpe za beton, autodizalice, podizne platforme.



Sakupljanje i privremeno skladištenje otpada vršimo našim specijalizovanim vozilima i deponujemo na našu lokaciju sa odgovarajućom dozvolom. Kapacitet mašine je 250 t/h građevinskog neopasnog otpada.



### NIŠ

Krnjaževačka bb, 18000 Niš - Srbija  
+381 18 215 355  
office@putinzenjering.com

### BEOGRAD

Jugoslovenska 2a, 11250 Beograd - Železnik  
+381 11 25 81 111  
beograd@putinzenjering.com





## MATEST "IT TECH" KONTROLNA JEDINICA



### JEDNA TEHNOLOGIJA MNOGO REŠENJA

IT Touch Technology je Matestov najnoviji koncept koji ima za cilj da ponudi inovativna i user-friendly tehnologiju za kontrolu i upravljanje najmodernijom opremom u domenu testiranja građevinskih materijala

Ova tehnologija je srž Matestove kontrolne jedinice, software baziran na Windows platformi i touch screen sistem koji je modularan, fleksibilan i obavlja mnoge opcije

- IT TECH pokriva | INOVATIVNOST
- | INTERNET KONEKCIJA
- | INTERFEJS SA IKONICAMA
- | INDUSTRIJALNA TEHNOLOGIJA

### SISTEM JEDNOG RAZMIŠLJANJA

### JEDNOM SHVATIŠ - SVE TESTIRAŠ



#### NAPREDNA TEHNOLOGIJA ISPITIVANJA ASFALTA

- | GYROTRONIC - Gyrotory Compactor
- | ARC - Electromechanical Asphalt Roller Compactor
- | ASC - Asphalt Shear Box Compactor
- | SMARTTRACKER™ - Multiwheels Hamburg Wheel Tracker, DRY + WET test environment
- | SOFTMATIC - Automatic Digital Ring & Ball Apparatus
- | Ductilometers with data acquisition system

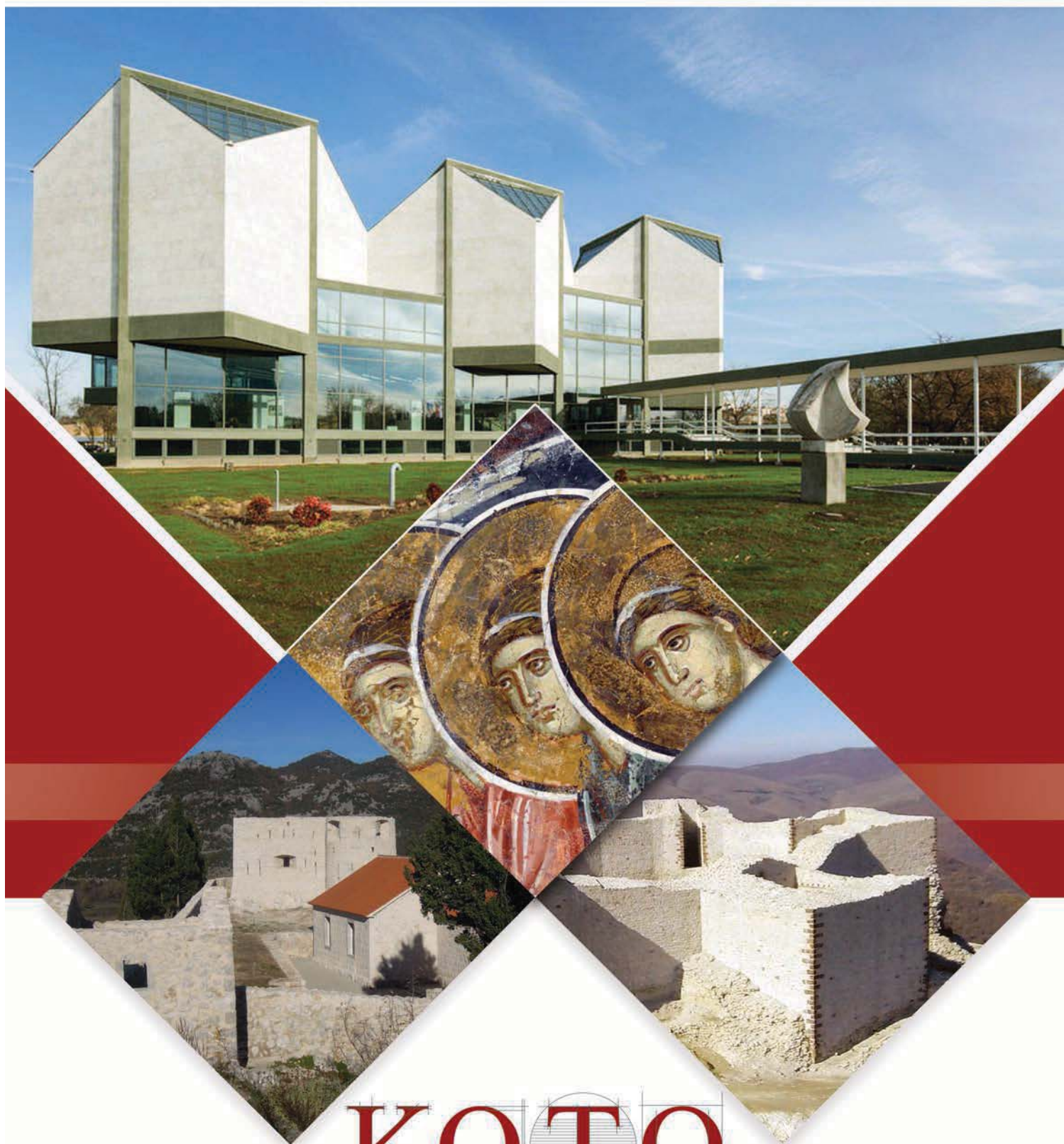
#### MULTIFUNKCIONALNI RAMOVI ZA TESTIRANJE

- | CBR/Marshall digital machines
- | Universal multispeed load frames
- | UNITRONIC 50kN or 200kN Universal multipurpose compression/flexural and tensile frames

#### OPREMA ZA GEOMEHANIČKO ISPITIVANJE

- | EDOTRONIC - Automatic Consolidation Apparatus
- | SHEARLAB - AUTOSHEARLAB - SHEARTRONIC
- Direct / Residual shear testing systems
- | Triaxial Load Frame 50kN

**MIXMATIC** - Automatic Programmable Mortar Mixer



# KOTO

[www.koto.rs](http://www.koto.rs) | [office@koto.rs](mailto:office@koto.rs) | 011 309 7410 | Vojvode Stepe br. 466, Beograd